Constructing *Ab initio* and Empirical Potential Energy Surfaces for Water

A Thesis submitted for the Degree

of

Doctor of Philosophy of the University of London

by

J Sophie Kain

June 2001

Department of Physics & Astronomy

University College London

University of London

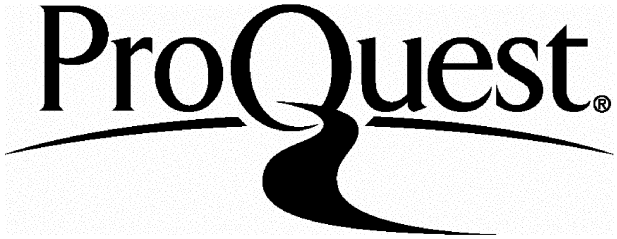

Abstract

The infrared spectrum of water is possibly one of the most well studied and yet portions of it are still poorly understood. Recently, significant advances have been made in assigning water spectra using variational nuclear motion calculations. The major factor determining the accuracy of ro-vibrational spectra of water is the accuracy of the underlying Potential Energy Surface. Even the most accurate *ab initio* Potential Energy Surface does not reproduce the Born-Oppenheimer surface to sufficient accuracy for spectroscopic studies. Furthermore, effects beyond this model such as the adiabatic correction, the relativistic correction and the non-adiabatic correction have to be considered.

This thesis includes a discussion on how the relativistic correction was calculated, for the water molecule, from first-order perturbation theory. The relativistic correction improved vibrational stretching motion while making the prediction of the bending modes far worse. For rotational motion the relativistic effect had an increasing effect with increasing K_a.

A further alteration to the *ab initio* calculations is introduced by adjusting the barrier to linearity in the water potential. This alteration to the barrier was considered in order to compensate for the lack of convergence of quantum chemical calculations of the Born-Oppenheimer surface. This barrier attempts to represent the change in the potential from linear to equilibrium. We show the improvements this has on calculated energy levels by comparison with the HITRAN database [5].

This then led the way to the improved spectroscopic potential presented here in this thesis. This new spectroscopic potential reduces the overall standard deviation significantly for vibrational and rotational energy levels.

Contents

1 Introduction **14**

1.1 The importance of water spectra 14

1.1.1 Water in our environment 14

1.1.2 Water in the universe 16

1.2 Calculations on the water molecule 17

1.2.1 Born-Oppenheimer Approximation (BO) 17

1.3 Rotational and Vibrational Motion of the water molecule 23

1.3.1 Vibrational motion 23

1.3.2 Rotational motion 26

1.3.3 Quantum Numbers 28

1.4 Potential Energy Surfaces (PES) 28

1.4.1 Partridge and Schwenke *ab initio* and empirical Potential Energy Surfaces 34

2 Solving the Schrödinger Equation for Nuclear motion **37**

2.1 Sutcliffe and Tennyson Molecular Hamiltonian 39

2.2 Perturbation Theory 44

2.3 Variational Calculations 46

2.3.1 Comparison of Variational Calculations and Perturbation Theory . . 49

2.4 Finite Basis Representation 49

2.5 Finite Basis Representation (FBR) Hamiltonian 50

2.6 Discrete Variable Representation 51
2.7 Basis Functions 52
2.8 The Hamiltonian for Discrete Variable Representation (DVR) 53
2.9 Discrete Variable Representation (DVR) for Water 55
2.10 Computational Methods: the DVR3D Program Suite 57
2.10.1 DIPOLE Surface 59
2.10.2 SPECTRA 61
2.10.3 XPECT3 61
2.10.4 Hellmann-Feynman Theorem 61
2.10.5 Optimised Basis Sets for the DVR3d program suite 62

3 Spectroscopy **66**
3.1 Assignment of the Sunspot Spectra 67
3.2 Previous Experimental Work 70
3.2.1 Calculated Line-lists 71

4 The Relativistic Correction **79**
4.1 Electronic Structure Calculations 79
4.2 Least-Squares Fitting 80
4.3 Nuclear Motion Calculations 84
4.4 Comparison with the Relativistic Surface by Quiney *et al* 89
4.5 Discussion and Conclusion 89

5 The Barrier to linearity **106**
5.1 Introduction 106
5.2 Calculations 109
5.3 Discussion and Conclusion 114

6 Empirical Potential Energy Surface (PES) **127**
6.1 Calculations 127

6.2 Conclusions 133

6.3 Publications on the work in this Thesis 160

A Program structure of the modified DVR3D program suite for fitting calculations **161**

A.1 Modifications to **DVR3D** 163

A.2 Modifications to **ROTLEV3B** 164

A.3 **XPECT3** - Program Use 164

A.3.1 Card input for **XPECT3** 164

A.4 **FIT** - Program Use 166

A.4.1 Card input for **FIT** 167

B Fortran routines for FIT and LSQFIT **169**

B.1 Program **FIT** 169

B.2 Program **LSQFIT** 174

List of Tables

1.1 Symmetry point group C_{2v} 23

1.2 Quantum Numbers used in this thesis for $H_2^{16}O$ 29

1.3 The four symmetry blocks used for computational purposes. 30

1.4 Improvement in the prediction of the fundamentals with improved *ab initio* PES's since 1974. Zobov *et al* ś [175] predictions for the fundamentals are based on the work presented in chapter 5. 33

1.5 Improvement in the overall standard deviation of the vibrational energy levels for the best empirical PES's since 1972 34

2.1 A table to show the parameters used for calculations in this thesis, using the DVR3D program suite 65

3.1 Experimental data for $H_2^{16}O$ since 1996 72

3.1 continued. 73

3.1 continued. 74

3.1 continued. 75

3.1 continued. 76

3.2 Empirical and *ab initio* line-lists 77

3.2 continued. 78

4.1 Coefficients in Eq. (2) for the relativistic correction surface of $H_2^{16}O$ for the linear set of variables. 92

4.1 continued. 93

4.2 Coefficients in Eq. (2) for the relativistic correction surface of $H_2^{16}O$ for the Jensen set of variables. 94
4.2 continued. 95
4.2 continued. 96
4.3 Band origins, in cm^{-1}, for $H_2^{16}O$. Results calculated using Born-Oppenheimer (BO), Born-Oppenheimer Diagonal Correction (ΔV^{ad}) and with the relativistic correction (ΔV_{rel}), are given as observed − calculated. 97
4.3 continued. 98
4.3 continued. 99
4.3 continued. 100
4.4 Rotational term values, in cm^{-1}, for the vibrational ground state and (010) state of $H_2^{16}O$. Results calculated using Born-Oppenheimer (BO), Born-Oppenheimer Diagonal Correction (ΔV^{ad}) and with the relativistic correction (ΔV_{rel}), are given as observed − calculated. 101
4.4 continued 102
4.5 Band origins, in cm^{-1}, for 4 isotopomers of water calculated using (a)Born-Oppenheimer of Partridge and Schwenke, (b) with adiabatic c) with both the adiabatic correction and the relativistic correction 104
4.5 continued. 105

5.1 A comparison of predicted barriers to linearity for water ($H_2^{16}O$ when adiabatic effects are considered). 117
5.3 Band origins, in cm^{-1} , for the $H_2^{16}O$, even parity only. Results calculated using (a) Born-Oppenheimer of Partridge and Schwenke, (b) with adiabatic and relativistic corrections added and (c) with the addition of our final angular correction, given as observed − calculated. 118
5.3 continued. 119

5.2 Different functions, $\Delta V(\theta)$, used to correct the angular potential. Also given are the standard deviation of the vibrational modes, σ_{vib}, the standard deviation of the rotational levels, σ_{rot}, and the correction to the barrier height, ΔB. 120

5.4 Rotational term values, in cm^{-1}, for the vibrational ground state of $H_2{}^{16}O$. Results calculated using (a) Born-Oppenheimer of Partridge and Schwenke, (b) with adiabatic and relativistic corrections added and (c) with the addition of our final angular correction, given as observed − calculated. 121

5.4 continued. 122

5.5 Band origins, in cm^{-1} for 4 isotopomers in water calculated using (a)Born-Oppenheimer of Partridge and Schwenke, (b) with adiabatic and relativistic corrections added and (c) with the addition of our final angular correction, given as observed − calculated. 123

5.5 continued. 124

5.6 Band origins, in cm^{-1} for the $H_2^{16}O$, even parity only. Results calculated using Born-Oppenheimer of Partridge and Schwenke,with adiabatic and relativistic corrections added and the addition of our final angular correction, given as observed − calculated for nuclear, middle and atomic masses . . . 125

5.6 continued. 126

6.1 Vibrational energy levels from Tennyson *et al* [152] removed from the fitting procedure 134

6.2 Initial coefficients of $M_f^{(1)}$ for $H_2^{16}O$. Units are consistent with bond lengths in a_0 and bond angle in radians for energies in μE_h. 135

6.3 Band origins, in cm^{-1}, for $H_2^{16}O$. Results calculated as observed, (a) Values from Tennyson *et al* [152], minus calculated, (b) Partridge and Schwenke's empirical potential, (c) V_{emp} for this work 136

6.3 continued. 137

6.4 Final coefficients of $M_f^{(1)}$ for $H_2^{16}O$. Units are consistent with bond lengths in a_0 and bond angle in rads for energies in μE_h. 138

6.5 Band origins, in cm^{-1}, for the $H_2^{16}O$. Results calculated as observed, (a) Values from Tennyson *et al* [152], minus calculated, (b) *ab initio* potential V_{ai}, (c) Partridge and Schwenke's empirical potential, (d) V_{emp} for this work 139

6.5 continued. 140

6.5 continued. 141

6.6 A_1 symmetry for J=2, for the $H_2^{16}O$. Results calculated as observed, (a) Values from Tennyson *et al* [152], minus calculated, (b) Partridge and Schwenke's empirical potential, (c) V_{emp} for this work 142

6.6 continued. 143

6.6 continued. 144

6.6 continued. 145

6.7 Rotational term values for J=10, in cm^{-1}, for the fundamentals of $H_2^{16}O$. Results calculated as observed, (a) Values from Tennyson *et al* [152], minus calculated, (b) V_{ai} defined in this work (c) V_{emp} defined in this work 146

6.7 continued. 147

6.8 Band origins, in cm^{-1} for 2 symmetric isotopomers in water calculated using (a) V_{ai} in this work and (b) V_{emp} in this work. 148

List of Figures

1.1 Vibrational and rotational motions of the water molecule 25

1.2 A 2D representation of the *ab initio* potential energy surface by Partridge and Schwenke plotted as r_1=r_2 against θ 32

2.1 Generalised curvilinear internal co-ordinate system for internal degrees of freedom described by three co-ordinates (r_1, r_2, θ). The co-ordinates are given by r_1 = A_2 - P_1, r_2 = A_1 - P_2 and $\theta = A_1\hat{Q}A_2$ 39

2.2 Radau co-ordinates for water. **D** is the centre-of-mass of the two hydrogen atoms, **C** is the centre-of-mass of the molecule, and **P** is the canonical point satisfying the condition $\overline{PD}^2 = \overline{OD}.\overline{CD}$ 40

3.1 A sample portion of the sunspot absorption spectrum (upper trace) and laboratory emission spectrum (lower trace). The vertical scale belongs to the sunspot absorption spectrum. Unity corresponds to no absorption of sunlight, 0.96 to absorption of 4% of the light. The strength of the laboratory emission was not recorded on an absolute scale. Quantum number assignments, given as J_{K_a,K_c}(Upper) - J_{K_a,K_c}(Lower) for various vibrational states, are marked. The spectra illustrate the congested nature of the whole sunspot spectrum in the 10-20 μ m region (figure courtesy of Serena Viti [164]) 68

4.1 Variation of the Relativistic Correction for the linear set of variables as a function of bond angle, θ, and bond-lengths r_1=r_2. The plot is for symmetric stretches only. Contours are spaced by 20 cm^{-1} from -0.051992 E_h. 82

4.2 Variation of the Relativistic Correction for the Jensen set of variables as a function of bond angle, θ, and bond-lengths r_1=r_2. The plot is for symmetric stretches only. Contours are spaced by 20 cm^{-1} from -0.051992 E_h. 83

4.3 Vibrational calculations on Partridge and Schwenke's *ab initio* PES. A 3D representation of how Calcs - Obs varies, with quanta of stretch and quanta of bend for J=0. 84

4.4 Vibrational calculations on Partridge and Schwenke's *ab initio* PES augmented by the Adiabatic Correction. A 3D representation of how Calcs - Obs varies, with quanta of stretch and quanta of bend for J=0. 85

4.5 Vibrational calculations on Partridge and Schwenke's *ab initio* PES augmented by the Adiabatic Correction and the Relativistic Correction. A 3D representation of how Calcs - Obs varies, with quanta of stretch and quanta of bend for J=0. 86

4.6 A graph to show Obs-Calcs for J=20 with increasing K_a. Dotted line, PS *ab initio* ; dashed line, PS *ab initio* + adiabatic; solid line, PS *ab initio* + adiabatic + relativistic. 88

4.7 Variation of the Relativistic Correction a) Quiney *et al* b) the linear set of variables as a function of bond angle, θ, and bond-lengths r_1 and r_2. The plots are for symmetric stretches only. Contours are spaced by 20 cm^{-1} . . 90

5.1 Functions, $\Delta V(\theta)$, used to model the correction to the barrier height. Solid line, linear function; dashed line, quadratic function; long dashed line, cubic function; dot-dashed line, Gaussian function; dotted line, sine function. The dark solid line is the final function. x denotes errors estimated by extrapolation from their cc-pV5Z basis by Partridge and Schwenke. 110

5.2 Vibrational calculations on Partridge and Schwenke's *ab initio* PES augmented by the Adiabatic Correction, Relativistic Correction and Correction Function. A 3D representation of how Calcs-Obs varies, with quanta of stretch and quanta of bend for J=0. 113

5.3 A graph to show Obs - Calcs for J=20 with increasing K_a. Dotted line, *ab initio* ; dashed line,*ab initio* + adiabatic; solid line, *ab initio* + adiabatic + relativistic; long-dashed line, *ab initio* + adiabatic + relativistic + correction. 116

A.1 Structure and data flow for the modified **DVR3D** program suite for iterative empirical fitting. Scratch disk files used by individual modules are not shown. 162

Acknowledgements

I would like to thank

- Jonathan Tennyson for his invaluable counsel and support.
- Oleg Polyansky for his endless encouragement and enthusiasm.
- Atila Császár for providing the theoretical data points for the electronic relativistic correction.
- David Schwenke, for finding the initial minor errors in the relativistic correction paper.
- György Tarczay for useful discussions.
- Djedjiga Belmiloud and Serena Viti for providing figures 1.1.1 and 3.1 respectively.
- My family for keeping my head above "water". Most importantly my sister, Alison, for nourishing lunches and fashion tips.
- My office mates, who all deserve a mention for having to share an office with me, and putting up with my singing. Especially the boys, Daniel Saraga and Steve Owen, for giving me much needed insight into the male mind.
- Paul Dando for being a very patient computer expert and a very good friend.
- Adam Burnley, for his intelligence, humour and trawling through pages of this thesis.
- William Bryan, for being the wittiest person I have ever met and my own personal Windows expert.
- Kate Eardley for her charm, grace and support.

Finally, I would like to dedicate this thesis to my favourite person in the world, Ms Helen Coyle, who saved my sanity.

Chapter 1

Introduction

1.1 The importance of water spectra

1.1.1 Water in our environment

Water is ubiquitous, essential to all life; human, plant and animal and is studied in all areas of science. On going studies are being carried out on the spectroscopy of the water molecule. The data obtained is used in atmospheric modelling, combustion chemistry and astronomy. Many decades of studying spectra of water have vastly increased our knowledge on the structure of water and where it can be found in our universe.

An important reason to improve water calculations is the use of these calculations in models of the earth's atmosphere. Figure 1.1.1 shows the earth's energy budget. It shows that presently 25% more sunlight is absorbed than predicted by models of a cloud free environment [121], when measuring the difference between the flux at the top of the atmosphere and that at sea-level. This is known as the " blue skies anomaly ". At ground level this anomaly leads to a difference in solar heating of around 25-30 Wm^{-2} which is at least ten times larger than the prediction of the greenhouse effect and probably more. A key question is what is causing this discrepancy. One of the possible answers is that beyond the 70% of sunlight already known to be absorbed by water, it maybe, that the weak water lines in the near infrared and the visible all also absorb significant amounts

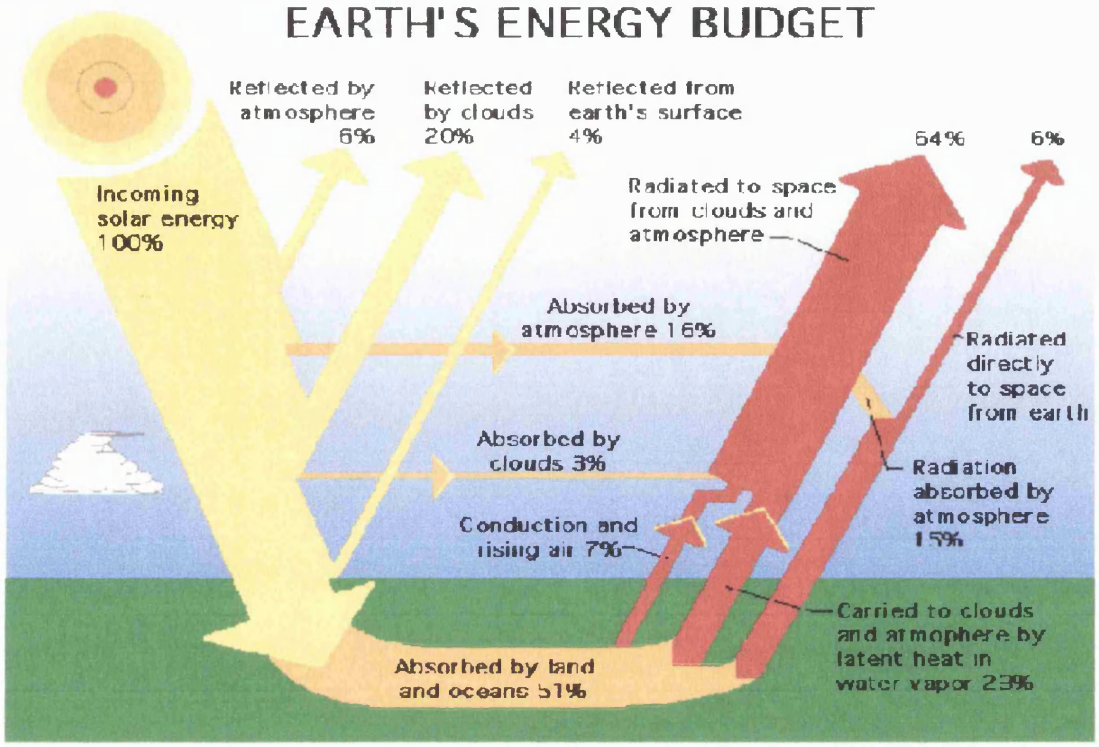

of sunlight. As yet the available data on weak water lines, mostly found in the HITRAN database [125, 126], is not sufficient to make these calculations. There are two reasons why there is a lack of data, firstly because experimental techniques are limited by the need for extremely long path lengths which is presently difficult to achieve. Secondly, theoretical calculations at the required accuracy are extremely complicated due to the complexity of water.

Water is the primary by-product of hydrocarbon combustion and the only product of burning Hydrogen in Oxygen. Data on water is therefore useful for modelling processes in flames and exhausts [99]. The transitions of water give spatial information on the distributions of water and also the local temperature, this can be used to optimise or monitor the internal combustion of engines.

Another important reason for studying the spectra of water is that hot water emissions from forest fires can be seen by aircraft [173]. This means that geo-stationary satellites , tuned to frequencies of hot water transitions, could be used for early detection of the movement of forest fires. In a similar way the location of ships, aircrafts and helicopter's can be established by tracking the hot water emission from their exhaust fumes [99].

A major problem involved in identifying and assigning data to water is the magnitude and complexity of data available. Theoretical methods have to be improved if water spectra are to be further analysed and assigned.

1.1.2 Water in the universe

Many scientists believe that water is the third most abundant molecule in the universe after hydrogen and carbon monoxide.

Allard *et al* in 1994 [1] showed that water is the most important source of infrared opacity in the spectra of oxygen rich late-type stars. Mira Variables [66] show strong infrared water bands. More recently in 1995 Tsuji and Ohnaka [158] showed that for brown dwarfs water is the most abundant molecule after H_2. In comets Mumma *et al* [98] showed that water is the primary " mother" molecule.

Water was also discovered in dark interstellar clouds [27] in 1969 on the basis of the maser transition 6_{16} to 5_{23}. Water masers can be thought to be collision pumped and are often associated with star forming regions [103]. Water in dark interstellar clouds and star forming regions was then studied by Cernicharo in 1994 [26] and Gensheimer *et al* [51] in 1996.

In general, observation of water is difficult from the Earth due to telluric absorption. In the infrared, however, highly excited transitions at high temperatures are shifted away from telluric absorption of cooler water and can therefore be observed. Now in the day and age of satellites the ISO satellite, which had infrared and far infrared spectrometers, has shown that cold water is present in our galaxy both in solid and gaseous form [128]. For example solid water ice can be seen in the massive star-forming region in Orion(IRc2) from the ISO satellite [160]. Water ice can also be seen in the outer solar system on bodies such as the moons of the giant planets [16].

A very important observation of water in the universe is the identification of water on sunspots on the sun. The idea that water could exist on our Sun was very popular with the media [47]. This area has seen many developments and is therefore discussed in full

in section 3.1.

1.2 Calculations on the water molecule

1.2.1 Born-Oppenheimer Approximation (BO)

To describe the movement of light particles i.e. electrons requires quantum mechanics. In the Schrödinger formulation the state of a many-particle system can be described by the wavefunction

$$\Psi(\underline{q}, t) = \Psi(q_1, q_2, q_3..., q_n, t) \tag{1.1}$$

where $q_1, q_2, q_3...q_n$ are the generalised co-ordinates of the particles at time t. The time dependent Schrödinger equation is then

$$i\hbar\frac{\partial\Psi}{\partial t} = \hat{H}\Psi \tag{1.2}$$

Where $\hat{H}$ is the Hamiltonian operator, the form of which for calculations in this thesis will be discussed in section 2.1. This equation is deceptively simple, however for a full set of variables in both electronic and nuclear motion it is impossible to solve analytically and needs to be simplified.

One simplification is to solve equation 1.2 for stationary states i.e $\Psi(q,t) = \psi(q)\phi(t)$. Here $\psi(\mathbf{q})$ is the spatial wavefunction and $\phi(t) = e^{-iEt/\hbar}$, the phase factor. In this way the time independent Schrödinger equation can be written in this way:

$$i\hbar\frac{\partial}{\partial t}\Psi(\mathbf{q})e^{\frac{-iEt}{\hbar}} = \hat{H}\Psi(\mathbf{q})e^{\frac{-iEt}{\hbar}}. \tag{1.3}$$

By differentiating we get the time independent Schödinger equation, writing $\Psi(\mathbf{q})$ as Ψ for convenience

$$\hat{H}\Psi = E\Psi. \tag{1.4}$$

A standard way of further simplifying the Schrödinger equation is with the Born-Oppenheimer approximation [12]. The basis of the approximation is that the nuclei are massive compared to the electron, so the electrons can be thought to instantly respond to the motion of the nuclei.

The Born-Oppenheimer approximation, therefore, separates the Schrödinger Equation into two parts, the first part describing the electronic wave function for a fixed nuclear geometry and the other the nuclear wave function. For this model the energy of the electronic wave function plays the role of a potential energy surface (PES) upon which the nuclei move.

So for the Born-Oppenheimer (BO) approximation the wavefunction can be written as

$$\Psi_{ne} = \Psi_e \Psi_n \tag{1.5}$$

and $\hat{H}$, for q_n nuclear and q_e electronic co-ordinates, can be written as,

$$\hat{H} = T_n(q_n) + \hat{H}_e(q_e, q_n). \tag{1.6}$$

T_n, $\hbar$=1 in atomic units, is given by

$$T_n = -\frac{1}{2}\sum_l \frac{\hbar^2}{M_l}\nabla_l^2 \tag{1.7}$$

The mass dependence, sign and summation is implicitly included in ∇_l^2. The chosen mass M_l of the atoms is discussed further in this section. H_e is

$$H_e(q_n)\Psi_i(q_n, q_e) = E_i(q_n)\Psi_i(q_n, q_e)\ i = 1, 2, ...\infty. \tag{1.8}$$

As $\hat{H}$ is hermitian

$$\int \Psi_i^* \hat{H} \Psi_j dq_e = \int \Psi_j \hat{H}^* \Psi_i^* dq_e \tag{1.9}$$

and solutions are chosen to be orthonormal and normalised. The total exact wavefunction can be written as an expansion of a complete set of electronic wave functions with

expansion coefficients written as a function of nuclear co-ordinates only:

$$\Psi_{tot}(q_n, q_e) = \sum_{i=1}^{\infty} \Psi_{ni}(q_n)\Psi_i(q_n, q_e). \tag{1.10}$$

If we then substitute these into equation 1.6 and equation $\hat{H}\Psi_{tot} = E_{tot}\Psi_{tot}$ then

$$\hat{H}\sum_{i=1}^{\infty} \Psi_{ni}(q_n)\Psi_i(q_n, q_e) = E_{tot}\sum_{i=1}^{\infty} \Psi_{ni}(q_n)\Psi_i(q_n, q_e) \tag{1.11}$$

or from equation 1.6

$$\sum_{i=1}^{\infty}(T_n + H_e)\Psi_{ni}(q_n)\Psi_i(q_n, q_e) = E_{tot}\sum_{i=1}^{\infty} \Psi_{ni}(q_n)\Psi_i(q_n, q_e). \tag{1.12}$$

If we then expand out this equation and write $\Psi_{ni}(q_n)\Psi_i(q_n, q_e)$ as $\Psi_{ni}\Psi_i$ for convenience and substitute in for T_n the equation becomes

$$\sum_{i=1}^{\infty}(-\frac{1}{2}\sum_{l}\frac{\hbar}{m_l}\bigtriangledown_l^2 + H_e)\Psi_{ni}\Psi_i = E_{tot}\sum_{i=1}^{\infty} \Psi_{ni}\Psi_i \tag{1.13}$$

$$\sum_{i=1}^{\infty} -\frac{1}{2}\sum_{l}\frac{\hbar}{m_l}\bigtriangledown_l^2 (\Psi_{ni}\Psi_i) + \Psi_{ni}H_e\Psi_i = E_{tot}\sum_{i=1}^{\infty} \Psi_{ni}\Psi_i \tag{1.14}$$

This can be written as,

$$\sum_{i=1}^{\infty} -\frac{1}{2}\sum_{l}\frac{\hbar}{m_l}\bigtriangledown_l [(\Psi_i \bigtriangledown_l \Psi_{ni}) + (\Psi_{ni} \bigtriangledown_l \Psi_i)] + \Psi_{ni}H_e\Psi_i = E_{tot}\sum_{i=1}^{\infty} \Psi_{ni}\Psi_i \tag{1.15}$$

$$\sum_{i=1}^{\infty} -\frac{1}{2}\sum_{l}\frac{\hbar}{m_l}(\Psi_i(\bigtriangledown_l^2\Psi_{ni}) + 2(\bigtriangledown_l\Psi_i)(\bigtriangledown_l\Psi_{ni}) + \Psi_{ni}(\bigtriangledown_l^2\Psi_i)) + \Psi_{ni}E_i\Psi_i = E_{tot}\sum_{i=1}^{\infty} \Psi_{ni}\Psi_i \tag{1.16}$$

H_e only acts on the electronic wavefunction and Ψ_i is an exact solution of the electronic Schrödinger equation. If we then multiply from the left by Ψ_j^* and using the orthonormality of Ψ_i and integrating over the electron co-ordinates. This becomes, using bra and ket notation,

$$-\frac{1}{2}\sum_l \frac{\hbar}{m_l}\nabla_l^2\Psi_{ni}+E_i\Psi_{ni}+\sum_{i=1}^{\infty}-\frac{1}{2}\sum_l \frac{\hbar}{m_l}(2\langle\Psi_j|\nabla_l|\Psi_i\rangle)(\nabla_l\Psi_{ni})+\langle\Psi_j|\nabla_l^2|\Psi_i\rangle\Psi_{ni}) = E_{tot}\Psi_{nj}. \tag{1.17}$$

In this equation the electronic wavefunction does not now show up in the first two terms. The summation contains terms which couple different electronic states. The adiabatic coupling effects are found when $i = j$ and the non-adiabatic terms when $i \neq j$. The non-adiabatic coupling elements are important for systems with more than one electronic surface. The details of this discussion on the Born-Oppenheimer approximation mainly follows Jensen [74].

In the adiabatic approximation the total wavefunction is restricted to a one electronic surface i.e. in equation 1.17 all the coupling elements are neglected and all the $i = j$ terms survive. Except for spatially degenerate wavefunctions the diagonal first order- non-spatial coupling element is zero, and so:

$$(-\frac{1}{2}\sum_l \frac{\hbar}{m_l}\nabla_l^2 + E_j - \frac{1}{2}\sum_l \frac{\hbar}{m_l}\langle\Psi_j|\nabla_l^2|\Psi_j\rangle)\Psi_{nj} = E_{tot}\Psi_{nj} \tag{1.18}$$

If we then substitute in for T_n

$$(T_n + E_j - \frac{1}{2}\sum_l \frac{\hbar}{m_l}\langle\Psi_j|\nabla_l^2|\Psi_j\rangle)\Psi_{nj} = E_{tot}\Psi_{nj} \tag{1.19}$$

and letting $U(q_n) = -\frac{1}{2}\sum_l \frac{\hbar}{m_l}\langle\Psi_j|\nabla_l^2|\Psi_j\rangle$ then

$$(T_n + E_j + U(q_n))\Psi_{nj}(q_n) = E_{tot}\Psi_{nj}(q_n) \tag{1.20}$$

$U(q_n)$ is the Born-Oppenheimer diagonal correction (BODC) which is found to be much smaller than $E_j(q_n)$ by a factor of the ratio of the electronic to nuclear mass ($\approx$ 1:1836). The diagonal correction is therefore usually very small and is generally ignored. However it has been shown that for water and for other light molecule species e.g. H_3^+ [37] this correction is significant if we want to achieve spectroscopic accuracy.

An elegant discussion of the adiabatic correction was given by Born and Huang [11] and updated by Handy and Lee [57].

In 1996 Zobov *et al* considered including the diagonal correction to the *ab initio* Born-Oppenheimer surface [176] . The adiabatic correction to the Partridge and Schwenke Born-Oppenheimer electronic energy surface [102] was found as a function of geometry using SCF (Self-Consistent Field) wavefunctions. These were calculated using the formulation by Handy *et al* [56] implemented in the CADPAC program suite [2, 37] using this expression where the sum is over all 3N nuclear co-ordinates.

$$U(q_n) = \Delta V^{ad} = \langle \Psi | - \frac{1}{2} \sum_l \frac{1}{M_l} \nabla_l^2 | \Psi \rangle \tag{1.21}$$

$$= \sum_l \frac{1}{2M_l} \langle \nabla_l \Psi | \nabla_l \Psi \rangle \tag{1.22}$$

They performed calculations for the 325 points used by Kedziora and Shavitt [79]. These calculations led to three mass-dependent BODC surfaces, one for each atom. The symmetry of the H atoms meant they used symmetrised displacement co-ordinates

$$S_1 = \frac{r_1 + r_2}{2} - r_e, \tag{1.23}$$

$$S_2 = \theta - \theta_e, \tag{1.24}$$

$$S_3 = \frac{r_1 - r_2}{2}. \tag{1.25}$$

r_e and θ_e are the values of r and θ at equilibrium. For isotopomers, XYO, the adiabatic correction becomes

$$\Delta^{ad}_{XYO} = \frac{1}{m_O} f^S_O(S_1, S_2, S_3) + (\frac{1}{m_X} + \frac{1}{m_Y}) f^S_H(S_1, S_2, S_3) + (\frac{1}{m_X} - \frac{1}{m_Y}) f^A_H(S_1, S_2, S_3) \tag{1.26}$$

These three surfaces (f_O^S, f_H^S, f_H^A) are expressed as a powers series in symmetrised displacement co-ordinates

$$f(S_1, S_2, S_3) = \sum_{i,j,k} c_{i,j,k} S_1^i S_2^j S_3^k \tag{1.27}$$

where symmetric functions, superscripted S, contain only even k and the asymmetric function, superscripted A, odd k. The asymmetric function is only applicable to HTO, HDO and DTO calculations.

Zobov *et al* 's results showed that the Born-Oppenheimer Diagonal Correction does not drastically effect the overall vibrational results and certainly does not show significant mass related effects necessary to reproduce the non-Born-Oppenheimer behaviour of the fundamentals.

Zobov *et al* presented electronic ground state rotational values for J=20. These results were more sensitive to the inclusion of Born-Oppenheimer Diagonal Correction than the vibrational levels, although the overall error is less. This adiabatic correction improves results for high K_a and makes the errors more uniform.

In this paper Zobov *et al* also explored the idea of changing the masses of the atoms involved. It would seem implicit that for the nuclear motion of the molecule, nuclear masses would be most appropriate. However use of atomic masses can partially account for the electrons instantly following the nuclei. Zobov *et al* [176] published results for nuclear, atomic and middle masses (a mass exactly half way between the atomic and nuclear mass, i.e. the mass of Hydrogen is taken to be 1.0075505 a.m.u. which is $\frac{1}{2}$(1.007825 + 1.007276) a.m.u.). These results were found not to be sensitive to the mass of oxygen. By far the best results were found using middle masses for both rotational and vibrational states. This change of mass partly accounts for non-adiabatic effects but certainly not to spectroscopic accuracy. Adjusting masses amounts to scaling the Kinetic Energy operators. More sophisticated analysis, such as techniques used by Bunker and Moss [20], suggest that to model these effects properly scaling factors which effect different parts of the Kinetic Energy operator and are symmetry dependent will be necessary, for further

Table 1.1: Symmetry point group C_{2v}

C_{2v}	E	$C_2(z)$	σ_{xz}	σ_{yz}		
A_1	+1	+1	+1	+1	t_z	x^2,y^2,z^2
A_2	+1	+1	-1	-1	R_z	xy
B_1	+1	-1	+1	-1	t_x,R_y	xz
B_2	+1	-1	-1	+1	t_y,R_x	yz

accuracy.

1.3 Rotational and Vibrational Motion of the water molecule

1.3.1 Vibrational motion

Ro-vibrational calculations for different molecules often consider the vibrational and rotational motion as independent, thereby treating them separately. If the two motions are treated as independent then the Coriolis forces must be included.

There are three vibrational normal modes in water: the symmetric stretch, the anti/asymmetric stretch and the bending modes, as shown in figure 1.1. These are given quantum assignments of ν_1 (symmetric stretch), ν_2 (bend) and ν_3 (antisymmetric/asymmetric stretch), with vibrational states written as (v_1, v_2, v_3). For example, the first excited state is the (010) bending mode. Symmetric and antisymmetric, in this case, refer to the fact that the water molecule does have some degree of symmetry. If we consider the line that bisects $H\hat{O}H$ it is possible to rotate the molecule by π and retain the same shape (although the two H atoms have been interchanged, which is equivalent to a reflection in the σ_{yz} plane, shown in figure 1.1). This axis is called the C_2 axis and water belongs to the C_{2v} group. The other properties of the C_{2v} group are summarised in table 1.1. ν_1 and ν_2 are referred to as symmetric, as they are totally symmetric with H interchange, A_1 symmetry, and ν_3 is referred to as antisymmetric; it transforms as B_2. Clearly, the actual motion of the water molecule is generally a combination of all types of vibrational motion (ν_1, ν_2, ν_3).

Although water vibrations cannot be treated as harmonic, harmonic notation is still

used to denote the vibrational states. One way of considering coupling between these states is by polyad.

A polyad is a group of states which are close in energy. This idea is based on the fact that one quantum of symmetric stretch is approximately equal to one quantum of asymmetric stretch which is approximately two quanta of bend. As an example, for n=3, the states belonging to the polyad conventionally denoted 3ν are

(3,0,0), (2,0,1),(1,0,2),(0,0,3),(2,2,0),(0,2,2),(1,4,0),(0,4,1) and (0,6,0).

In order to account for an odd number of quanta of the bending motion, the $n\nu + \delta$ polyad is introduced. This is given as the nν polyad plus an additional quantum of bend ($\delta = 1$), such that for the $3\nu + \delta$ polyad these states would be labelled

(3,1,0), (2,1,1),(1,1,2),(0,1,3),(2,3,0),(0,3,2),(1,5,0),(0,5,1) and (0,7,0).

For energy levels in the 4ν polyad and higher, water acts as a local mode molecule [21, 29]. The details of local mode theory are covered in [28, 54]. Local mode labels are (n, m)$^{\pm}\nu_2$, where n + m = ν_1 + ν_3 and the superscripted sign indicates whether the quanta in each local mode appears as a symmetric or antisymmetric combination. When n=m, only the symmetric combination is allowed and the superscripted sign is usually omitted.

The near-degeneracy of the local mode states (n,0)$^{+}$0 and (n,0)$^{-}$0 for n=4, 5, and 6 suggested to Carleer *et al* [22] in 1999 that normal mode labelling is increasingly difficult to support. Papers published more recently often give energy levels in both normal and local mode labelling.

If vibrations are assumed to be small in amplitude about the equilibrium position, they can be described using perturbation theory, starting with the un-coupled harmonic oscillator model. The entire motion can then be described if the equilibrium position and the four non-zero force constants are known, where the force constants are simply the 2nd derivatives of the PES at equilibrium, as follows:

For small amplitude motions, the potential energy surface can be approximated by a Taylor expansion around the equilibrium geometry. For $\mathbf{q} = (q_1, q_2, q_3 ... q_n)$ the generalised co-ordinates, V($\mathbf{q}$), can be written as

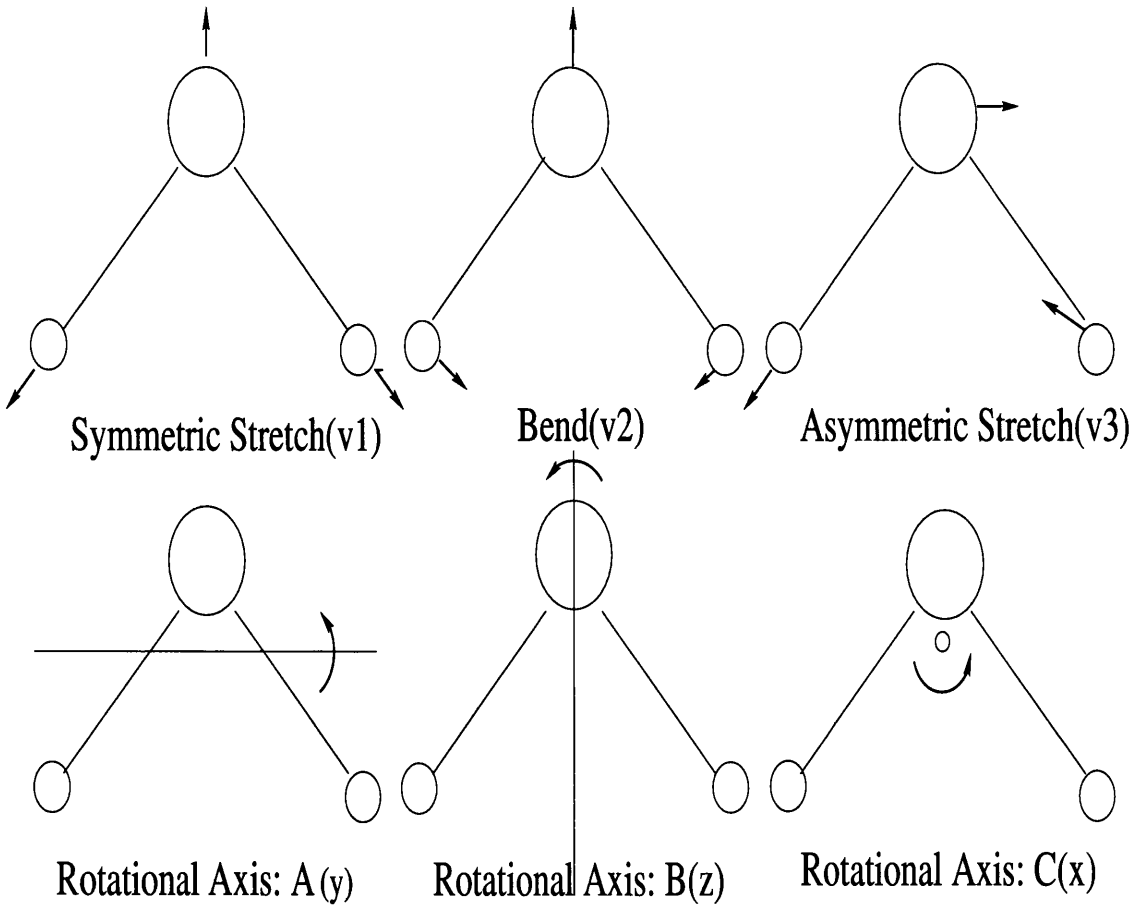

Figure 1.1: Vibrational and rotational motions of the water molecule

$$V(\mathbf{q}) \approx V(\mathbf{q}_o) + \frac{\partial V}{\partial \mathbf{q}^t}(\mathbf{q} - \mathbf{q}_o) + \frac{1}{2}(\mathbf{q} - \mathbf{q}_o)^t(\frac{\partial^2 V}{\partial \mathbf{q}^2})(\mathbf{q} - \mathbf{q}_o). \tag{1.28}$$

If $V(\mathbf{q}_o)$ is chosen to be zero, then $V(\mathbf{q})$ becomes

$$V(\mathbf{q}) = \frac{1}{2}(\mathbf{q} - \mathbf{q}_o)^t \frac{\partial^2 V}{\partial \mathbf{q}^2}|_{q=q_o}(\mathbf{q} - \mathbf{q}_o). \tag{1.29}$$

$\frac{\partial^2 V}{\partial \mathbf{q}^2}$ is a 3N x 3N matrix of the 2nd derivatives of the potential energy with respect to the co-ordinates called the force constants.

The nuclear Schrödinger equation then becomes

$$(-\sum_{i=1}^{3N} \frac{1}{2m_i}\frac{\partial^2}{\partial \mathbf{q}_i} + \frac{1}{2}(\mathbf{q} - \mathbf{q}_o)^t \frac{d^2 V}{d\mathbf{q}^2}(\mathbf{q} - \mathbf{q}_o))\Psi = E\Psi. \tag{1.30}$$

These assumptions are reasonably accurate for low excitation in water, however for very highly excited ro-vibrational states, which are available experimentally, none of the above assumptions hold true. Water is a "floppy" molecule which experiences large amplitude motion and would need a large basis set perturbation expansion. An alternative approach is discussed in section 2.3.

1.3.2 Rotational motion

A rigid body model is often used to describe rotational motion. Rotational motion for the water molecule is defined by the moments of inertia along the 3 principal axes in 3 dimensional space, as shown in figure 1.1. As water is an asymmetric top, the moments of inertia and the total rotor constants around the three axes are different.

By convention, the moments of inertia along each of the axes of the water molecule are defined by the rotational constants, (A, B, C) [86]

$$A = \frac{\hbar^2}{2I_A}; B = \frac{\hbar^2}{2I_B}; C = \frac{\hbar^2}{2I_C}. \tag{1.31}$$

For a prolate symmetric top $B = C$ and for an oblate symmetric top $B = A$. The range of B between A and C corresponds to different asymmetries. Water is between an

oblate and a prolate molecule with a permanent dipole along the B axis. Typical values of the rotational constants for the electronic ground state of water are A=27.88061 cm^{-1} , B=14.52161 cm^{-1} , C=9.27776 cm^{-1} [64].

From these rotational constants, the quantum mechanical rotational Hamiltonian for pure rotational motion for a rigid-rotor can be defined as

$$H_{rigid} = AJ_a^2 + BJ_b^2 + CJ_c^2 \tag{1.32}$$

where $J_{a,b,c}$ are the angular momentum components.

The essence of the "rigid-rotor approximation" is that A, B and C are considered constant. However, for water at high energies the behaviour is different from the rigid structure.

Bonds in atoms are not rigid and will vary with the speed of rotation; a phenomenon referred to as centrifugal distortion. Centrifugal distortion increases the rotational energy of the molecule, which in turn increases its rate of rotation. The centrifugal force is proportional to the square of the angular momentum, this force expands the bonds against their restoring forces. The energy associated with the centrifugal force must therefore be subtracted from the rigid-rotor energy.

In real systems another problem with the rigid-rotor model is that A, B and C depend on the moments of inertia of the system, which are themselves affected by the vibrational motion. Thus A, B and C are not constant for vibrational excitation.

For small displacements and low rotational energy, departure from the rigid-rotor model can be expressed simply by relaxing the assumption of rigidity. Rotational motion is considered to be a small shift from the rigid-rotor motion, i.e. small perturbations from the rigid-rotor Hamiltonian ($\hat{H}_0$). This perturbation theory method breaks down for high amplitudes and high rotational energy.

The permanent dipole moment of the water molecule points along the B axis, about which rotational motion is unstable. By convention, the overall rotation is defined by its projections along the A and C axes, the projection denoted by the quasi quantum numbers

K_a (prolate limit) and K_c (oblate limit). Here, K_a ranges from $0 \rightarrow J$ and K_c ranges from $J \rightarrow 0$ where $K_c = K_a \pm 1$. For each J there are 2J+1 non-degenerate levels, each denoted J_{K_a,K_c}.

The spectrum of an asymmetric top has many allowed transitions with no discernible structure, except that for high-level rotational excitation, many appear in degenerate pairs. This makes assigning both pure rotational and ro-vibrational spectra of water particularly challenging.

1.3.3 Quantum Numbers

Table 1.2 contains the definition of the quantum numbers used in this thesis. Table 1.3 shows how these quantum numbers relate to the symmetry blocks defined by the $C_{2\nu}$ group, to which water belongs, shown in table 1.1.

1.4 Potential Energy Surfaces (PES)

If we assume the Born-Oppenheimer approximation then the potential energy surface (PES) can be considered to be a hyper-space on which molecular dynamics take place. In theory the construction of the potential energy surface is straightforward. However, water is a many electron problem and a lot of nuclear configurations have to be considered for a realistic potential. These *ab initio* electronic structure calculations are theoretically and computationally difficult to perform up to the required spectroscopic accuracy.

Another way to determine a potential energy surface(PES) is empirically using experimentally/spectroscopically obtained data. The data is then fitted to an analytic functional form [99] and modified to minimise the differences between the levels calculated on the PES and the observed values.

These empirically determined surfaces are usually considerably more accurate within the region where experimental data is available, however as the errors on an empirically determined surface tend to be less uniform, these surfaces are less useful for higher energy levels. *Ab initio* calculations generally have more uniform errors and give a clearer picture

Table 1.2: Quantum Numbers used in this thesis for $H_2^{16}O$

Rigorous Quantum Numbers		
Quantum Number	Definition	Values
J	The rotational angular momentum	$J \geq 0$
p	Rotational parity $(-1)^{J+p}$ (reference [15]) $p = K_a + K_c$	0 (even) 1 (odd)
ortho	The symmetry of H interchange	$K_a + K_c + v_3$ odd
para	The symmetry of H interchange	$K_a + K_c + v_3$ even
q	Vibrational parity	0 (even value of v_3) 1 (odd value of v_3)
Non-rigorous Quantum Numbers		
v_i	v_i quanta of excitation in mode ν_i	v_1 symmetric stretch v_2 symmetric bend v_3 anti-symmetric stretch
K_a K_c	K_a is the projection of J on the A axis K_c is the projection of J on the C axis	$J \geq K_a \geq 0$ $J \geq K_c \geq 0$

Table 1.3: The four symmetry blocks used for computational purposes.

Sym. Block	DVR3D output	K_a	K_c	p	q	O/P
ν_3 even						
J even						
A_1	ee	even	even	0	0	P
A_2	eo	odd	even	0	1	O
B_1	fe	odd	odd	1	0	P
B_2	fo	even	odd	1	1	O
J odd						
A_1	ee	even	odd	0	0	O
A_2	eo	odd	odd	0	1	P
B_1	fe	odd	even	1	0	O
B_2	fo	even	even	1	1	P
ν_3 odd						
J even						
A_1	ee	odd	even	0	0	P
A_2	eo	even	even	0	1	O
B_1	fe	even	odd	1	0	P
B_2	fo	odd	odd	1	1	O
J odd						
A_1	ee	odd	odd	0	0	O
A_2	eo	even	odd	0	1	P
B_1	fe	even	even	1	0	O
B_2	fo	odd	even	1	1	P

of the interaction and orbital motion of the electron which gives an indication of where the remaining errors lie.

The popularity of water means that historically many potential energy surfaces are available, the very best of which is by Partridge and Schwenke [102]. The most accurate of the surfaces focus on the spectroscopic region yet have still to reach spectroscopic accuracy. The global potentials on water [67, 162] are a lot less accurate but will not be discussed in this thesis.

In table 1.4 we present a survey of the theoretical calculations of the vibrational fundamentals for the different *ab initio* potential energy surfaces since 1974. The main feature of this table is the vast improvement in the quality of the results in the last 25 years. This is mainly due to the improvement in the electronic structure calculations. However, Sexton and Handy [133] achieved vastly better *ab initio* predictions for the fundamentals using Kraemer *et al* ś [84] potential energy surface but switching to variational calculations as opposed to harmonic frequency and anharmonic frequency corrections. It should be kept in mind that even the best variational electronic structure calculations are many thousand wavenumbers above the true absolute energy. So the potential energy surface created is very near to the correct shape but parallel to the actual potential energy surface (PES).

Table 1.4 shows the improvement of the overall standard deviation of all the vibrational energy levels presented by different authors for various empirical potentials. The fundamentals alone, do not give a clear enough picture of the overall improvement as even ten years ago the calculated energy levels were close to the experimental levels. This table demonstrates that in the last 28 years the improvement in the calculations of the vibrational energy levels has improved by almost three orders of magnitude. This improvement is mainly due to the switch from perturbation theory calculations to variational calculations. The reason for further research is that even this level of accuracy is not sufficient for the assignment of all of the water spectra.

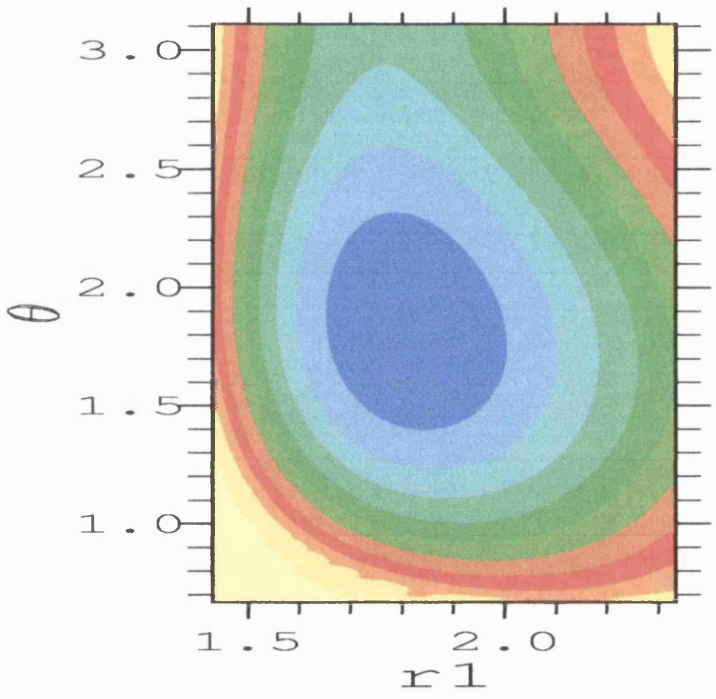

Figure 1.2: A 2D representation of the *ab initio* potential energy surface by Partridge and Schwenke plotted as r_1=r_2 against θ

Table 1.4: Improvement in the prediction of the fundamentals with improved *ab initio* PES's since 1974. Zobov *et al* ś [175] predictions for the fundamentals are based on the work presented in chapter 5.

Reference	Year	v_1	v_2	v_3
		1594.746	3657.053	3755.929
Bucknell and Handy [18]	1974	1728	4045	4139
Whitehead and Handy [172]	1976	1629	3720	3807
Rosenberg *et al* [124]	1976	1633	3689	3798
Hennig *et al* [63]	1978	1649	3619	3753
Bartlett *et al* [8]	1979	1610	3702	3789
Knowles *et al* [83]	1982	1645	3691	3794
Kraemer *et al* [84]	1982	1647	3662	3787
Kraemer *et al* [84]	1982	1613	3654	3757
Sexton and Handy [133]	1984	1623	3667	3752
Garing and McClatchey [49]	1984	1595	3657	3756
Martin *et al* [92]	1991	1595	3657	3756
Polyansky *et al* [116] (ZVPT)	1997	1596.5	3660.4	3758.3
Kedziora and Shavitt [79]	1997	1604.6	3650.5	3746.9
	1997	1603.6	3651.5	3747.5
Partridge and Schwenke [102]	1997	1597.4	3660.54	3758.18
Zobov *et al* [175]	2000	1594.85	3657.9	3756.3

Reference	Year	σ_{vib} cm^{-1}	No of Vib levels	Highest Energy
Hoy *et al* [70]	1972	214	25	13000
Carter and Handy [25]	1987	2.42	25	13000
Halonen and Carrington [55]	1988	5.35	54	18000
Jensen [75]	1989	3.22	55	18000
Polyansky *et al* [107] (PJT1)	1994	0.6	40	18000
Polyansky *et al* [109] (PJT2)	1996	0.94	63	25000
Partridge and Schwenke [102]	1997	0.24	30	18000
This work, vibrations only PES in chapter 6	2001	0.12	30	18000

Table 1.5: Improvement in the overall standard deviation of the vibrational energy levels for the best empirical PES's since 1972

1.4.1 Partridge and Schwenke *ab initio* and empirical Potential Energy Surfaces

In 1997 Partridge and Schwenke (PS) published their *ab initio* potential energy surface and dipole moment function for water [102]. PS employed correlation consistent polarised valence basis sets of Dunning [38], optimised to obtain the atomic correlation energy. The potential energy surface used the cc-pV5Z basis sets with a diffuse s, p and d on oxygen and s and p on hydrogen.

Within this publication they also empirically adjusted this potential for J $\leq$ 5 for $H_2^{16}O$. Using the equation for their *ab initio* data

$$V^{5Z}(r_1, r_2, \theta) = V^a(r_1) + V^a(r_2) + V^b(r_{HH}) + V^c(r_1, r_2, \theta) \tag{1.33}$$

where the r_i are the OH bond-lengths, θ is the HOH angle, r_{HH} the HH distance and

$$V^a(r) = Dexp[-2a(r - r_o) - 2Dexp[-a(r - r_o)] \tag{1.34}$$

$$V^b(r) = Aexp(-br) \tag{1.35}$$

$$V^c = c_{ooo} + exp{-}\beta[(r_1 - r_e)^2 + (r_2 - r_e)^2]$$

$$\times \sum_{ijk} c_{ijk}[(r_1 - r_e)/r_e]^i[(r_2 - r_e)/r_e]^j$$

$$\times[\cos\theta - \cos\theta_e]^k. \tag{1.36}$$

Parameters D, a, r_o, A, b and c_{ijk} were determined using a weighted least squares fit to the *ab initio* data compared with the HITRAN line-list of water energy levels. β was fixed to $2a_o^{-2}$ to give fast enough damping and r_e and θ_e remained fixed. Their final fit used $i + j \leq 8$ and $k \leq 14 - (i + j)$ for 245 different parameters, c_{ijk} fitted to some 355 data points. They then included the core correlation effects, by fitting the difference in energies between the CQZ calculations with and without correlating the core (relative to their minimums). This yielded the correction V^{core}, which takes the same form as V^c in equation 1.36, with $i + j + k \leq 6$ for 50 c_{ijk}. They used 371 points in this fit. A further basis set improvement was also computed by the difference between he CQZ and the 5Z calculations. Which gives the correction V^{basis}, fit the same way as V^{core} for 336 points. On average the core, contribution was found to be around twice that of the basis set correction. Including all these factors their overall empirically determined potential was given as

$$V^{emp} = c^{5Z}V^{5Z}(r_1, r_2, \theta) + c^{core}\Delta V^{core}(r_1, r_2, \theta) + c^{basis}\Delta V^{basis}(r_1, r_2, \theta) + \Delta V^{rest}(r_1, r_2, \theta) \tag{1.37}$$

where V^{rest} is represented in the same form as V^c in equation 1.36. The free parameters in this expression are therefore c^{5Z}, c^{core}, c^{basis} and c_{ijk} in ΔV^{rest}. The final values of these scaling parameters were found to be $c^{5Z} = 0.999678$, $c^{core} = 1.635$, $c^{basis} = -0.159$ and 21 different parameters, c_{ijk}, in ΔV^{rest} for the empirical potential. The *ab initio* values of these parameters are given as c^{5Z}=1, $c^{core} = c^{basis} = 0$.

These results were sufficiently accurate to be well matched with 99.9% of the experimental data in the HITRAN database, section 3.2, the standard deviations, σ, are given in table 1.4. In this paper they also published results using this potential for other isotopomers of water including, $H_2^{17}O$, $H_2^{18}O$, HDO, HTO, $D_2^{16}O$, $T_2^{16}O$ which used a mass dependent adiabatic correction, as introduced in Zobov *et al* [176]. Using this potential and the dipole moment function they produced a line-list which has over 300 million lines for $H_2^{16}O$.

Figure 1.2 shows a graphical representation of the *ab initio* potential energy surface of Partridge and Schwenke for values when r_1=r_2, r_1 from $1.4 \rightarrow 2.7$ and θ from $0.5 \rightarrow \pi$.

Chapter 2

Solving the Schrödinger Equation for Nuclear motion

There is no unique Hamiltonian for the nuclear motion of molecules. The centre-of-mass motion of a molecule gives a continuous spectrum, which has to be removed in order to study the rotation-vibration spectra. Finding suitable co-ordinates for the Hamiltonian is the first step of a rigorous treatment of ro-vibrational systems. The position of an N atom molecule can be described in 3N cartesian co-ordinates and if the centre-of-mass motion is removed then 3N-3 cartesian co-ordinates are left. These are generally referred to as the space-fixed co-ordinates. Space-fixed co-ordinates, however, do not distinguish between rotational and vibrational motion. This requires body-fixed co-ordinates.

The relationship between the space-fixed and the body-fixed co-ordinate system is given by the Euler angles (α, β, γ). These are the angles of orientation of the body-fixed axis in relation to the space-fixed axis. One advantage of the body-fixed co-ordinate system is that it allows the introduction of several de-coupling approximations. The properties of the Hamiltonian should remain the same for both the body-fixed and space-fixed co-ordinates and therefore conversion from one to the other has no significant effect, other than the possible introduction of singularities which will be discussed further.

A full description of the motion of a molecule requires 3N-6 (3N-5 for linear molecules)

internal co-ordinates characterising the molecular vibrational degrees of freedom. These internal co-ordinates represent the geometry of the molecule in the body-fixed frame with centre-of-mass **C**.

The translation motion of **C** is separable, but the rotational and vibrational motions are coupled via Coriolis effects and thus for water, a full molecular body-fixed nuclear motion Hamiltonian depends on 3N-3 co-ordinates (α, β, γ; q_i, i=1, 3N-6).

The body-fixed normal mode Hamiltonian is definitely preferable for small amplitude motion, although the choice of co-ordinates becomes less clear for large-amplitude motion, i.e. for water [4]. The definitions of normal and non-normal mode internal co-ordinates are discussed below.

The choice of the best internal co-ordinates very much depends on the molecule being considered, as shown by Bačić and Light and Zuniga *et al* [4, 179] . These authors suggest that the overall convergence rate and accuracy of the calculations depends very strongly on the initial choice of co-ordinates. The choice of co-ordinates is not implicit, but certain considerations are taken into account. Co-ordinates must span all of configuration space accessible to the molecules internal degrees of freedom, however large the amplitude motion. The co-ordinates should take advantage of the highest symmetry of the molecule. In order to make calculations simpler, the co-ordinates are preferably orthogonal, so that the number of cross terms in the kinetic energy operator is minimised. To make the Hamiltonian as separable as possible, the co-ordinates should minimise the mode-mode interaction. They should also be chosen to have singularities in physically unaccessible regions or singularities which can be overcome [150].

For a triatomic molecule, amongst the 3N-3 co-ordinates, 3 co-ordinates describe the orientation of the molecule with respect to the space-fixed co-ordinates. The other three internal co-ordinates must fully or partially meet these criteria.

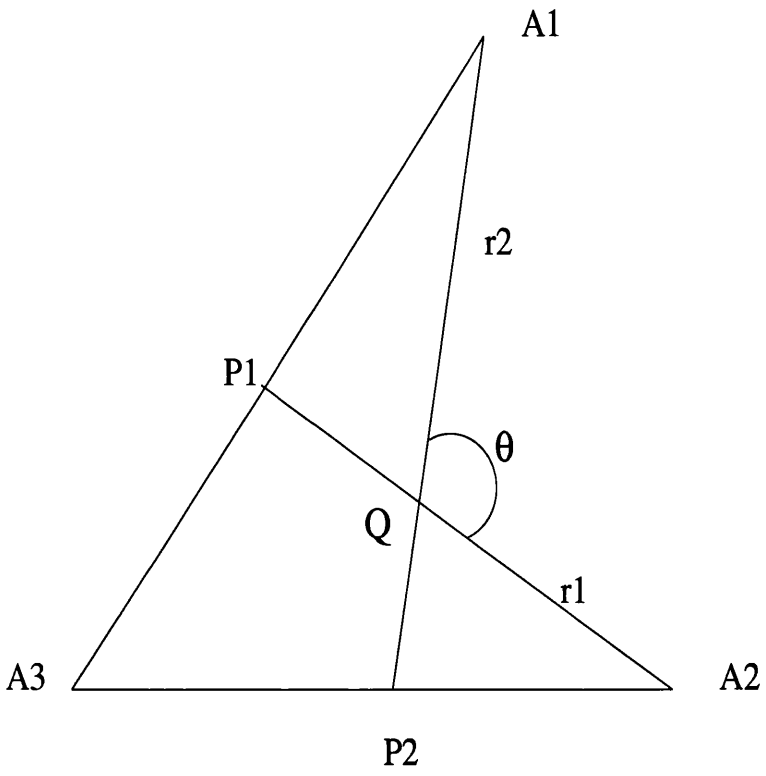

Figure 2.1: Generalised curvilinear internal co-ordinate system for internal degrees of freedom described by three co-ordinates (r_1, r_2, θ). The co-ordinates are given by $r_1 = A_2$ - P_1, $r_2 = A_1$ - P_2 and $\theta = A_1\hat{Q}A_2$

2.1 Sutcliffe and Tennyson Molecular Hamiltonian

This section introduces the Hamiltonians used for the nuclear motion calculations in this thesis. These Hamiltonians are chosen from those derived by Sutcliffe and Tennyson [136] for their curvilinear internal co-ordinates.

The generalised curvilinear internal co-ordinates describe the positions of the three atoms of a triatomic molecule (A_1, A_2 and A_3), two lengths (r_1, r_2) and angle θ. Figure 2.1 shows these relative positions.

The traditional curvilinear triatomic bond co-ordinates are the bond-length co-ordinates (r_1, r_2, θ), where the new r_1 and r_2 are the distances of A_1 and A_2 from A_3 and θ is the angle between r_1 and r_2 in figure 2.1. The major problem with this co-ordinate system is that there are cross-derivative terms in the kinetic energy operator. These terms are the result of the nonorthogonal nature of the bond-length coordinates. For molecules with

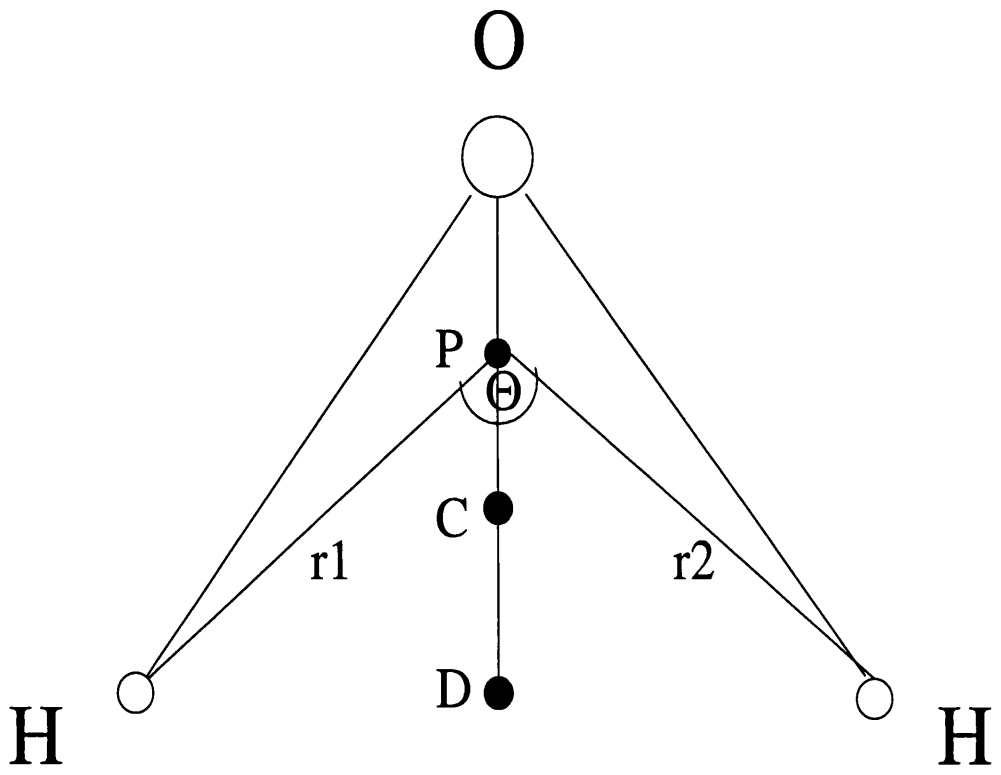

Figure 2.2: Radau co-ordinates for water. **D** is the centre-of-mass of the two hydrogen atoms, **C** is the centre-of-mass of the molecule, and **P** is the canonical point satisfying the condition $\overline{PD}^2 = \overline{OD}.\overline{CD}$

a central heavy mass, such as water, the preferred internal co-ordinates are the Radau co-ordinates, as these are orthogonal [24, 129, 145].

Radau co-ordinates were first introduced in 1868 by Radau [120] to study astronomical systems and more recently they have been used to study Light-Heavy-Light atomic systems like water [77, 30, 129]. Figure 2.2 shows the Radau co-ordinates for water. **O** is considered to be the centre-of-mass of oxygen, **C** is the centre-of-mass of the system, **D** is the centre-of-mass of the two light atoms and **P** is point satisfying the condition $\overline{PD}^2 = \overline{CD}.\overline{OD}$. $\mathbf{r}_1$ and $\mathbf{r}_2$ are now defined as the distances of the light atoms from **P** and the angle θ is the angle $\mathbf{H}\hat{P}\mathbf{H}$.

The Hamiltonian can be derived for a variety of internal curvilinear co-ordinates, inter-nuclear, Jacobi, Radau and bond co-ordinates. In this thesis we will focus on the the Hamiltonian found by Sutcliffe and Tennyson for bisector embedded (see below) Radau co-ordinates.

The contents of the Hamiltonian does not change with the change of the co-ordinate system. However, the form of the Hamiltonian does change. The form is therefore chosen to be computationally efficient and simple to implement.

For the generalised co-ordinate system, the body-fixed Hamiltonian can be written as in Tennyson *et al* [144]

$$\hat{H} = \hat{K} + V \tag{2.1}$$

where

$$\hat{K} = \hat{K}_V^{(1)} + \hat{K}_V^{(2)} + \hat{K}_{VR} \tag{2.2}$$

where

$$\hat{K}_V^{(1)} = -\frac{\hbar}{2}\left[\frac{1}{\mu_1}\frac{\partial^2}{\partial r_1^2} + \frac{1}{\mu_2}\frac{\partial^2}{\partial r_2^2} + \left(\frac{1}{\mu_1^2 r_1^2} + \frac{1}{\mu_2^2 r_2^2}\right)\left(\frac{1}{\sin\theta}\frac{\partial}{\partial\theta}\sin\theta\frac{\partial}{\partial\theta}\right)\right] \tag{2.3}$$

$$\hat{K}_V^{(2)} = \frac{\hbar}{\mu_{12}}[\cos\theta\frac{\partial^2}{\partial r_1 \partial r_2} + \left(\frac{1}{r_1}\frac{\partial}{\partial r_2} + \frac{1}{r_2}\frac{\partial}{\partial r_1} - \frac{1}{r_2 r_1}\right)\left(\sin\theta\frac{\partial}{\partial\theta} + \cos\theta\right) +$$

$$\frac{\cos\theta}{r_1 r_2}\left(\frac{1}{\sin\theta}\frac{\partial}{\partial\theta}\sin\theta\frac{\partial}{\partial\theta}\right)] \tag{2.4}$$

Thus $\hat{K}_{VR}$ contains the rotational motion and the Coriolis coupling terms. The operator $\hat{K}_{VR}$ is zero for J=0 (vibration only) and will be discussed further for the bisector embedded Radau co-ordinates.

The reduced masses given in the above equations are written as

$$\frac{1}{\mu_1} = \frac{g_2}{m_1} + \frac{1}{m_2} + \frac{(1-g_2)^2}{m_3} \tag{2.5}$$

$$\frac{1}{\mu_2} = \frac{1}{m_1} + \frac{g_1}{m_2} + \frac{(1-g_1)^2}{m_3} \tag{2.6}$$

$$\frac{1}{\mu_{12}} = \frac{(1-g_1)(1-g_2)}{m_3} - \frac{g_2}{m_1} - \frac{g_1}{m_2}. \tag{2.7}$$

$\mu_{12} = 0$ and hence $\hat{K}_V^{(2)} = 0$ for the orthogonal co-ordinate systems, such as jacobian and Radau. In this thesis we select Radau co-ordinates.

In order for the Hamiltonian to be body-fixed and unique for $J > 0$ we need to specify the orientation of the cartesian axis as well as the internal co-ordinates. The internal motion takes place in the body-fixed plane, which rotates in the space-fixed plane by means of the Euler angles (α, β, γ), as previously discussed. The final Hamiltonian is then a function of both the Euler angles and the internal co-ordinates.

The rotational matrices are given by $D^J_{k,M}(\alpha, \beta, \gamma)$ where k is the projection of J onto the fixed-body z-axis and M is the projection of J onto the space-fixed Z-axis. These rotational matrices form a complete set for a given J, as J is a constant of the motion. Using this fact and the Arthurs and Dalgarno [3] close coupling techniques, an effective radial Hamiltonian can be derived from the body-fixed co-ordinate embedding defined above. A full derivation of this effective radial Hamiltonian is given in Sutcliffe [137], and Tennyson and Sutcliffe [147]. This radial Hamiltonian defines the angular basis functions in the form

$$|j,k\rangle = \Theta_{j,k}(\theta) D^{J}_{k,M}(\alpha,\beta,\gamma) \tag{2.8}$$

where $\Theta_{j,k}(\theta)$ is the associated normalised Legendre Polynomial in the phase convention of Condon and Shortley [31]. The Hamiltonian is independent of M in the absence of a magnetic field.

In practice, the Sutcliffe-Tennyson Hamiltonian allows for many different orientations of the body-fixed axis system. However this section of the thesis will consider the case when the body-fixed x-axis is embedded along $\frac{\theta}{2}$ of the Radau co-ordinate system (bisector embedding). For water, the bisector embedding in Radau co-ordinates can be used to account for the permutation symmetry in H_2O. The effective Hamiltonian for bisector embedding in Radau co-ordinates is given by

$$\hat{H}(r_1,r_2) = \hat{K}^{(1)}_{V} + \hat{K}^{(1)}_{VR} + \hat{K}^{(2)}_{VR} + \hat{K}^{(3)}_{VR} + \delta_{k',k}\langle j',k|V(r_1,r_2,\theta)|j,k\rangle_{\theta} \tag{2.9}$$

where $V(r_1,r_2,\theta)$ is the potential energy function and

$$\hat{K}^{(1)}_{V} = \delta_{j'j}\delta_{k'k}\left[\frac{\hbar^2}{2\mu_1}\frac{\partial}{\partial r_1^2} - \frac{\hbar^2}{2\mu_2}\frac{\partial}{\partial r_2^2} + \frac{\hbar^2}{2}j(j+1)\left(\frac{1}{\mu_1 r_1^2} + \frac{1}{\mu_2 r_2^2}\right)\right] \tag{2.10}$$

$$\hat{K}^{(1)}_{VR} = \delta_{k'k}\frac{\hbar^2}{8}(J(J+1)-3k^2)\left(\frac{1}{\mu_1 r_1^2} + \frac{1}{\mu_2 r_2^2}\right) I^{(1)}_{j',k',j,k} + \delta_{k',k}\frac{\hbar^2}{16}(J(J+1)-k^2)\delta_{j'j}\left(\frac{1}{\mu_1 r_1^2} + \frac{1}{\mu_2 r_2^2}\right) \tag{2.11}$$

$$\hat{K}^{(2)}_{VR} = \delta_{k'k\pm1}\frac{\hbar^2}{4}C^{\pm}_{Jk}\left[\left(\frac{1}{\mu_1 r_1^2} - \frac{1}{\mu_2 r_2^2}\right)\left(\delta_{j'j}C^{\pm}_{jk} + (k\pm\frac{1}{2})I^{(2)}_{j',k',j,k}\right)\right] \tag{2.12}$$

$$\hat{K}^{(3)}_{VR} = \delta_{k'k\pm2}\frac{\hbar^2}{32}C^{\pm}_{Jk}C^{\pm}_{Jk}[(\frac{1}{\mu_1 r_1^2} + \frac{1}{\mu_2 r_2^2})(2I^{(1)}_{j',k',j,k} - I^{(3)}_{j',k',j,k})]. \tag{2.13}$$

The integrals $I^{(n)}$ are given by

$$I^{(1)}_{j',k',j,k} = \langle j'k'|\frac{1}{(1-\cos\theta)}|jk\rangle \tag{2.14}$$

$$I^{(2)}_{j',k',j,k} = \langle j'k'|\frac{1+\cos\theta}{\sin\theta}|jk\rangle \tag{2.15}$$

$$I^{(3)}_{j',k',j,k} = \langle j'k'|jk\rangle \tag{2.16}$$

and the angular factors are given by

$$C^{\pm}_{Jk} = [J(J+1) - k(k\pm 1)]^{\frac{1}{2}} \tag{2.17}$$

2.2 Perturbation Theory

Perturbation theory has been the bedrock of water calculations for 50 years. There have been many successes using this method and it continues to be useful to this day. Perturbation theory does not solve the Schrödinger equation directly, but assumes that each new system is a small perturbation from an already solved problem. This implies that the solution to the problem should be similar to the solution of the perturbed system. We define this mathematically by a two-part Hamiltonian, with the reference Hamiltonian as H_0 and a comparatively small perturbation of H'.

So we can write that

$$\hat{H} = \hat{H}_0 + \lambda H' \tag{2.18}$$

and

$$\hat{H}_0\Phi_i = E_i\Phi_i \ (i = 0, 1, 2....\infty). \tag{2.19}$$

$\hat{H}_0$ is Hermitian, so the solutions for the unperturbed Hamiltonian form a complete set, hence we choose them to be orthonormal. λ is a parameter determining the strength of the perturbation, which can take any value between 0 (small perturbation) and 1 (full

perturbation). A commonly used unperturbed Hamiltonian ($\hat{H}_0$) for vibrational motion is the un-coupled harmonic oscillator and for rotational motion the rigid rotor model can be used as the starting point.

Another way of using the perturbation theory is to find the rotational and vibrational energy as eigenvalues of matrices whose elements are functions of spectroscopic quantities (rotation-vibration constants) which parameterise the whole nuclear motion Hamiltonian for the system. The constants which determine these effective Hamiltonians are generally found by fitting to observed energy levels. The potential parameters and equilibrium structure can be obtained by interpreting these constants.

Perturbation theory can be used to invert data and obtain fits to perturbational Hamiltonian operators containing molecular constants. In principle this then leads to details of the potential energy surface.

The most commonly used ro-vibrational Hamiltonian operator is due to Eckart [39]. This Hamiltonian is written in terms of small displacements from the equilibrium in the normal co-ordinates of the system. The potential is then expressed as a Taylor series around the equilibrium and the Hamiltonian can be thought of as the zeroth order operator plus perturbations due to the quadratic, cubic, quartic, etc. The perturbation equations can be found using this Hamiltonian and similar expansions for the wavefunctions and energies [23]. The solutions are written in terms of truncated sums (Krohn *et al* [85]). In 1929 Van Vleck [161] developed a transformation of the Schrödinger equation which leads to the direct evaluation of definite operator integrals, instead of the evaluations of off-diagonal matrix elements. This makes perturbation techniques easier to carry out.

The main problem with perturbational methods is the assumption that the vibrational displacement from the equilibrium position is small. For large amplitude motion perturbation treatments do not converge. Another problem which arises from perturbational treatments is that the Hamiltonian is different for linear and non-linear molecules and thus problems arise when non-linear molecules reach linearity [170]. Unfortunately, for the water molecule both these problems are significant, as water undergoes large am-

plitude motion and reaches linearity. The frequently used quantum mechanical Watson Hamiltonian [170] was found to diverge widely for higher terms. In 1985 Polyansky formally discussed the convergence radius of the Watson effective Hamiltonian in perturbation expansions. He proved perturbation expansions to be increasingly divergent with the inclusion of higher order terms [105]. The rotational expansion particularly, diverges for J $>$ 7. However, perturbation theory is still useful for low energy states where the vibrational displacement is small. Bunker [19] used this idea in his "non-rigid bender" where perturbation theory is used for small-displacement modes, while employing more accurate treatments for high-displacement. This technique has been used for water [68, 69]. Further techniques are discussed below.

2.3 Variational Calculations

The presently preferred method of solving the Schrödinger Equation is from first principles using the Variational Principle, first presented by Rayleigh and Ritz [122, 123]. The rotational and vibrational levels and wavefunctions are found using basis set expansions along with the Variational Principle. This principle shows that the better the representation offered by the basis set, the lower the energy. Thus, variational calculations approach the values for the energy levels from above, a fact which is proved below. Therefore, by increasing the number of terms in the original basis set, the closer the calculated energy levels are to the exact values. The Sutcliffe-Tennyson Hamiltonian, discussed in section 2.1, can then be constructed and diagonalised. The first study of the water molecule using this technique was in 1974 by Bucknell *et al* [18]

If we calculate the energy expectation value for the ground state of the system.

$$\epsilon = \int \phi^* \hat{H} \phi dv. \tag{2.20}$$

where ϕ is a normalised arbitrary wavefunction, which is single valued, finite and continuous in accessible space, and $\hat{\mathrm{H}}$ is the full Hamiltonian operator of the system. For

ϕ equal to the true ground state of the system, ψ_0 is then

$$\int \psi_0^* \hat{H} \psi_0 d\upsilon = E_0. \tag{2.21}$$

ϕ can be written in terms of an expansion of the wavefunctions, ψ_n, i.e.

$$\phi = \sum_{n=0}^{\infty} a_n \psi_n \tag{2.22}$$

The wavefunctions form an orthonormal set and therefore

$$\sum_{n,m=0}^{\infty} a_n^* a_m = \delta_{mn} \tag{2.23}$$

And by substitution we have

$$\epsilon = \int \sum_{n=0}^{\infty} a_n^* \phi_n^* \hat{H} \sum_{m=0}^{\infty} a_m \phi_m d\upsilon \tag{2.24}$$

But using the orthonormal set condition and the fact that a_n^* and a_m are constants, we obtain

$$\epsilon = \sum_{n,m=0}^{\infty} a_n^* a_m \int \psi_n^* \hat{H} \psi_m d\upsilon \tag{2.25}$$

As ψ_n is the eigenfunction of $\hat{H}$ we can write that

$$\hat{H} \psi_n = E_n \psi_n \tag{2.26}$$

so it is easy to see that

$$\epsilon = \sum_n a_n^* a_n E_n \tag{2.27}$$

Now, subtracting $\sum_n a_n^* a_n E_0$ from each side and using the fact that

$$\sum_n a_n^* a_n E_0 = E_0 \sum_n a_n^* a_n = E_0 \tag{2.28}$$

then

$$\epsilon - E_0 = \sum_{n=0}^{\infty} a_n^* a_n (E_n - E_0). \tag{2.29}$$

The value of $a_n^* a_n$ is either zero or positive and so

$$\epsilon \geq E_0 \tag{2.30}$$

This proof shows that variational calculations approach the actual value of the energy levels from above. We can therefore minimise ϵ by increasing the basis set and find the best approximation of E_o for the original functions ϕ.

These calculations can be extended to the general case for the ith level. The variational principle for the excited states was proposed by Macdonald [90], amongst others, and states that for E_i, the exact value for the energy is given by

$$E_i \leq \epsilon_{n+1}^i \leq \epsilon_n^i \leq \epsilon_n^{i+1} \tag{2.31}$$

where ϵ_{n+1}^i uses one more basis set expansion function that ϵ_n^i. As with the ground state energy, by minimising the calculated energy with increased basis set functions, the best possible energy level values can be obtained.

Another important step forward in the variational treatment of rotationally excited systems is the two-step procedure, by Tennyson and Sutcliffe [151]. This procedure considerably extended the range of rotational quanta for which the variational treatment can give accurate results.

Variational calculations require eigenfunctions expanded in a basis set in which the matrix elements can be represented. The size of the matrix depends on the the choice of basis set functions representing the internal degrees of freedom. Also, as the size of the matrix determines whether or not it is solvable, the choice of basis functions is very important.

When choosing suitable basis functions for $\hat{H}$, several factors should be taken into account. The set of basis functions should be as complete as possible and the integrals of the

set should be relatively easy to evaluate. The basis set determines the rate of convergence nuclear motion calculations so a careful selection of the basis function representing the geometry and physics will increase this rate. Singularities arise from the choice of internal co-ordinates and embedding; it is therefore necessary to choose a basis set for which $\hat{H}$ is finite.

In 1985 Light *et al* [89] rediscovered that it is possible to express $\hat{H}$ in terms of either a set of basis functions or in terms of a basis consisting of N discrete points. The set of basis functions is referred to as the Finite Basis Set Representation (FBR) and the basis over discrete points known as Discrete Variable Representation (DVR), both of which are discussed below.

2.3.1 Comparison of Variational Calculations and Perturbation Theory

Variational calculations are more computationally costly than perturbation theory calculations. Variational techniques treat rotational and vibrational motion using the same potential. They also consider the nuclear motion from first principles, which means that these calculations can be more effectively extrapolated than perturbation theory calculations. Variational calculations automatically include resonant interaction between vibrational states, as they use the exact nuclear motion kinetic energy operators. Such interactions can only be treated in perturbation theory on a case by case basis. Also, perturbation theory, can not predict localised interactions not seen in the spectra.

2.4 Finite Basis Representation

The crucial factor in the finite basis set representation (FBR) is the choice of basis set. The form of the vibrational internal kinetic energy operator $\hat{K}_{vib}$ is used as a guide for the choice of basis set. The vibrational motion is represented as products of suitable one dimensional function $\phi(q)$. Using this description the ith vibrational state can be written as;

$$\Psi_i(q_1, q_2, q_3) = \sum_{j,k,l} c^i_{j,k,l} \phi_j(q_1)\phi_k(q_2)\phi_l(q_3). \tag{2.32}$$

The expansion coefficients, c^i, must be found for each wavefunction. This is done be diagonalising the real symmetric matrix given by

$$H_{s,s'} = \langle \phi_j \phi_k \phi_l | \hat{H} | \phi_j \phi_k \phi_l \rangle \tag{2.33}$$

where s is a compound index running over the basis functions used and H is the Hamiltonian operator. The integration runs over all the vibrational coordinates.

The best basis set representation of the angular vibrational motion is given by the Legendre and Jacobi basis sets [77]. The radial motion can be represented using many different basis sets, however it is usual to use Morse or Harmonic type functions [97], optimised for the potential energy surface involved.

After a particular basis set is chosen, variational calculations integrate over all co-ordinates to form the $\hat{H}$ matrix. If the basis functions are expressed as orthogonal polynomials then the integral can be numerically calculated using the appropriate Gaussian quadrature for each function found in Stroud and Secrest [135]. The Hamiltonian matrix is then diagonalised to find the eigenvalues and eigenfunctions.

Finite basis set representation (FBR) has successfully predicted spectra for a wide variety of triatomics. Unfortunately, many functions are needed to converge high energy states and to account for the large amplitude motion of the water molecule. This involves using very large basis sets, which in turn uses considerable computer memory and time. Some of these problems can be solved by using a discrete variable representation (DVR), which will be addressed in section 2.6.

2.5 Finite Basis Representation (FBR) Hamiltonian

The Sutcliffe and Tennyson [140] rotation-less hamiltonian ($\hat{H}$) matrix for the orthogonal co-ordinates (Jacobi and Radau) for the finite basis representation is given by

$$\langle m,n,j|\hat{H}|m',n',j'\rangle = \langle m|\hat{h}^{(1)}|m'\rangle\delta_{n,n'}\delta_{j',j} + \langle n|\hat{h}^{(2)}|n'\rangle\delta_{m,m'}\delta_{j,j'} +$$

$$\left(\langle m|\hat{g}^{(1)}|m'\rangle\delta_{n,n'} + \langle n|\hat{g}^{(2)}|n'\rangle\delta_{m,m'}\right) j(j+1)\delta_{jj'}$$

$$+\langle m,n,j|V(r_1,r_2,\theta)|m',n',j'\rangle \tag{2.34}$$

where $|m\rangle$ and $|n\rangle$ are the basis functions for the motion of r_1 and r_2 respectively. The angular basis functions $|j\rangle$ are Legendre polynomials representing the motion in θ. $\hat{h}^{(1)}$, $\hat{h}^{(2)}$ are the Kinetic Energy integrals for r_1 and r_2. $\hat{g}_{(1)}$, $\hat{g}_{(2)}$ are the kinetic energy integrals in θ:

$$\langle t|\hat{h}^{(i)}|t'\rangle = \langle t|\frac{-\hat{\hbar}^2}{2\mu_i}\frac{\partial^2}{\partial r_i^2}|t'\rangle \tag{2.35}$$

$$\langle t|\hat{g}^{(i)}|t'\rangle = \langle t|\frac{-\hat{\hbar}^2}{2\mu_i r_i^2}|t'\rangle. \tag{2.36}$$

Where $|t\rangle = |m\rangle$ for i=1 and $|t\rangle = |n\rangle$ for i=2 and μ_i are the reduced masses given in equations 2.5 and 2.6.

2.6 Discrete Variable Representation

In 1985 Light and co-workers [89] rediscovered the discrete variable representation (DVR) method to attenuate problems with the FBR. The first part of this theory multiplies the basis set expansion of the FBR by a transformation matrix to change from "function space" to "co-ordinate space" using the transformation rules described by Harris *et al* [58]. The method transforms the FBR, based on non-localised functions to DVR based on localised functions [89]. For the DVR we need to switch from associated Legendre polynomials to amplitudes represented by Gauss-associated Legendre quadrature points. Dickinson and Certain [36] showed that if the functions involved are a set of (j_{max}+1) classical orthogonal polynomials then there exists an orthogonal transformation to (j_{max}+1) weighted Gauss-polynomial quadrature points.

The second part of the DVR theory uses the idea of successive diagonalisation and truncation of the intermediate reduced dimension Hamiltonian ($\hat{H}$). This allows the user to create different basis sets of different types, and sizes, for different grid points over the potential energy function, according to the physical effects of the situation. This dramatically reduces the size of the final Hamiltonian matrix and hence the overall computational time and memory. The DVR method also allows the user to reject quadrature points that are energetically inaccessible and again reduces computational requirements.

2.7 Basis Functions

The choice of basis functions is very important for a high rate of convergence of variational calculations in the DVR method. The size of the overall problem is ultimately determined by the number of basis functions. It is therefore important to choose functions which give a good representation of the the motion in each given co-ordinate.

To set up the DVR for generalised body-fixed co-ordinates as in figure 2.1 we can discretise the angular dependence with Legendre polynomials and the FBR of the radial functions with either Morse Oscillator functions [147] or spherical operator functions [149]. Tennyson and Sutcliffe [148] defined a set of orthonormal functions based on the solutions to the Morse Oscillator Hamiltonian, written as

$$|t\rangle = H_t(r_i) = \beta^{\frac{1}{2}} N_{t\alpha} exp(-\frac{y}{2}) y^{\frac{\alpha+1}{2}} L_t^{\alpha}(y) \tag{2.37}$$

$$y = Aexp[-\beta(r_i - r_{ie})] \tag{2.38}$$

where

$$A = \frac{4D_e}{\beta},\ \beta = \omega_e(\frac{\mu}{2D_e}^{\frac{1}{2}}),\ \alpha = Integer(A). \tag{2.39}$$

The normalised associated Laguerre polynomials are given as

$$N_{t\alpha} L_t^{\alpha}(y). \tag{2.40}$$

For the maximum convergence rate for variational calculations the values of D_e (dissociation energy), ω_e (fundamental frequency), r_e (equilibrium bond-length of the effective Morse oscillator) must be optimised. In 1994 Fulton [45] tested values for r_e, D_e and ω_e (r_e=2.06a$_0$, D_e=0.14E$_h$,ω_e=0.014E$_h$) used by Henderson *et al* in 1993 [61] and found that certain high energy states had wavefunctions that attempted to access geometries not represented by the grid. The values used in this thesis were optimised by Viti [164] discussed in section 2.10.5.

2.8 The Hamiltonian for Discrete Variable Representation (DVR)

The full discrete variable representation (DVR) of the Hamiltonian can be obtained by a transformation given as:

$$H_{\alpha,\alpha',\beta,\beta',\gamma,\gamma'} = \sum_{m,n,j} \sum_{m',n',j'} T_{m,n,j}^{\alpha,\beta,\gamma} \langle m,n,j|H|m',n',j'\rangle T_{m',n',j'}^{\alpha',\beta',\gamma'}. \tag{2.41}$$

Where the full 3D transformation operator can be written as a produce of 1D transformation operators,

$$T_{m,,n,j}^{\alpha,\beta,\gamma} = T_m^{\alpha} T_n^{\beta} T_j^{\gamma}. \tag{2.42}$$

These 1D transformations are written in terms of points, η and weights, w_η for the Gauss Legendre or Gauss Laguerre quadrature of the FBR basis functions for the angular or radial co-ordinates.

$$T_t^{\eta} = (w_\eta)^{\frac{1}{2}} |t(\eta)\rangle \tag{2.43}$$

where $|t\rangle = |m\rangle$, $|n\rangle$, $|j\rangle$ for $\eta = \alpha, \beta, \gamma$ respectively.

The transformed H can then be written in terms of the DVR points α, β, γ as

$$H_{\alpha,\alpha',\beta,\beta',\gamma,\gamma'} = K^{(1)}_{\alpha,\alpha'}\delta_{\beta,\beta'}\delta_{\gamma,\gamma'} + K^{(2)}_{\beta,\beta'}\delta_{\alpha,\alpha'}\delta_{\gamma,\gamma'}$$

$$+L^{(1)}_{\alpha,\alpha',\gamma,\gamma'}\delta_{\beta,\beta'} + L^{(2)}_{\beta,\beta',\gamma,\gamma'}\delta_{\alpha,\alpha'}$$

$$+V(r_{1\alpha}, r_{2\alpha}, \theta_\gamma)\delta_{\alpha,\alpha'}\delta_{\beta,\beta'}\delta_{\gamma,\gamma'} \tag{2.44}$$

where $K^{(1)}$ and $K^{(2)}$ are the radial kinetic energy terms for r_1 and r_2 respectively. $L^{(1)}$ and $L^{(2)}$ are the angular kinetic energy terms with r_1 and r_2 coupling respectively. $V(r_1, r_2, \theta)$ is the potential diagonal contribution where $\alpha, \beta, \gamma, \alpha', \beta', \gamma'$ are the indices of the DVR grid points. Within the Gauss-associated Legendre quadrature approximation this potential energy operator is diagonal [36],

$$T^{\alpha,\beta,\gamma}_{m,n,j}\langle m, n, j|V(r_1, r_2, \theta)|m', n', j'\rangle T^{\alpha',\beta',\gamma'}_{m,n,j} \approx V(r_{1\alpha}, r_{2\beta}, \theta_\gamma)\delta_{\alpha,\alpha'}\delta_{\beta,\beta'}\delta_{\gamma,\gamma'}. \tag{2.45}$$

Where $r_{1\alpha}, r_{2\alpha}$ and θ_γ are the values of r_1,r_2 and θ at the the grid points (α, β, γ). This approximation means that the DVR is not strictly variational, owing to the number of functions being inextricably linked to the number of points. However, it does behave variationally if the number of grid points is large enough.

The kinetic energy terms in equation 2.44 can be given as

$$K^{(i)}_{\eta,\eta'} = T^\eta_t\langle t|\hat{h}^{(i)}|t'\rangle T^{\eta'}_{t'} \tag{2.46}$$

$$L^{(i)}_{\eta,\eta',\gamma,\gamma'} = J_{\gamma,\gamma'}\sum_{t,t'} T^\eta_t\langle t|\hat{g}^{(i)}|t'\rangle T^{\eta'}_{t'} \simeq \frac{J_{\gamma,\gamma'}\hat{h}^2}{2\mu_i r^2_{i\eta}}\delta_{\eta,\eta'} \tag{2.47}$$

where

$$J_{\gamma,\gamma'} = \sum_j T^\gamma_j j(j+1)T^{\gamma'}_j. \tag{2.48}$$

The kinetic energy integrals, $\hat{h}^i$, and the angular kinetic energy integrals $\hat{g}^i$ for r_1 and r_2 are defined by

$$\hat{h}^i = -\frac{-\hbar^2}{2\mu_i}\frac{\partial^2}{\partial r_1^i} \tag{2.49}$$

$$\hat{g}^i = -\frac{\hbar^2}{2\mu_i r_i^2}. \tag{2.50}$$

2.9 Discrete Variable Representation (DVR) for Water

In this thesis the DVR is used along with the two-step variational approach of Tennyson and Sutcliffe [151] for computational efficiency. This treats the non-Coriolis coupled problem in DVR for each k, the lowest of these solutions (for each k) is then transformed back into FBR and couples the k's to solve the full Coriolis coupled Hamiltonian, using the solutions of each k calculation expressed in an FBR as a basis to solve the final $\hat{H}$. This allows the user to only included the Coriolis coupled solutions that are required.

The DVR3D program suite, Henderson *et al* [61], uses the rotation-less Hamiltonian as given in equation, 2.44. To reduce the size of the overall calculations we then consider bisector embedding the symmetry around the S_2 axis. It is clear to see that $|m,n,j\rangle = |n,m,j\rangle$. Therefore this symmetrised representation can be given as

$$|m,n,j,q\rangle = \frac{1}{\sqrt{2}}\frac{1}{\sqrt{1+\delta_{m,n}}}(|m,n,j\rangle + (-1)^q|n,m,j\rangle) \tag{2.51}$$

for q=0 even and q=1 odd. and $0 < m \leq (n-q)$

Which written in the DVR is given as

$$|\alpha,\beta,\gamma,q\rangle = \frac{1}{\sqrt{2}}\frac{1}{\sqrt{1+\delta_{\alpha,\beta}}}(|\alpha,\beta,\gamma\rangle + (-1)^q|\beta,\alpha,\gamma\rangle) \tag{2.52}$$

again q = 0,1 and $1 \leq \alpha \leq \beta - q$. If we apply the symmetry to the DVR we get

$$H_{\alpha,\alpha',\beta,\beta',\gamma,\gamma',q,q'} = \langle\alpha,\beta,\gamma,q|H|\alpha',\beta',\gamma',q'\rangle$$

$$= \frac{1}{2\sqrt{1+\delta_{\alpha,\beta}}\sqrt{1+\delta_{\alpha',\beta'}}} \times [\langle\alpha,\beta,\gamma|H|\alpha',\beta'\gamma'\rangle + (-1)^q\langle\alpha,\beta,\gamma|H|\beta',\alpha',\gamma'\rangle$$

$$+(-1)^q\langle\beta,\alpha,\gamma|H|\alpha',\beta',\gamma'\rangle + \langle\beta,\alpha,\gamma|H|\beta',\alpha',\gamma'\rangle] \tag{2.53}$$

and the terms in the hamiltonian become

$$\hat{H}_{\alpha,\alpha',\beta,\beta',\gamma,\gamma',q,q'} = \frac{1}{2\sqrt{1+\delta_{\alpha,\beta}}\sqrt{1+\delta_{\alpha',\beta'}}}$$

$$\times(K^{(1)}_{\alpha,\alpha'}\delta_{\beta,\beta'}\delta_{\gamma,\gamma'} + (-1)^q K^{(1)}_{\alpha,\beta'}\delta_{\beta,\alpha'}\delta_{\gamma,\gamma'} + (-1)^q K^{(1)}_{\beta,\alpha'}\delta_{\alpha,\beta'}\delta_{\gamma,\gamma'} +$$

$$K^{(2)}_{\beta,\beta'}\delta_{\alpha,\alpha'}\delta_{\gamma,\gamma'} + (-1)^q K^{(2)}_{\beta,\alpha'}\delta_{\alpha,\beta'}\delta_{\gamma,\gamma'} + (-1)^q K^{(2)}_{\alpha,\beta'}\delta_{\beta,\alpha'}\delta_{\gamma,\gamma'} + K^{(2)}_{\alpha,\alpha'}\delta_{\beta,\beta'}\delta_{\gamma,\gamma'}$$

$$+L^{(1)}_{\alpha,\alpha',\gamma,\gamma'}\delta_{\beta,\beta'} + (-1)^q L^{(1)}_{\alpha,\beta',\gamma,\gamma'}\delta_{\beta,\alpha'} + (-1)^q L^{(1)}_{\beta,\alpha',\gamma,\gamma'}\delta_{\alpha,\beta'} + L^{(1)}_{\beta,\beta',\gamma,\gamma'}\delta_{\alpha,\alpha'}$$

$$+L^{(2)}_{\beta,\beta',\gamma,\gamma'}\delta_{\alpha,\alpha'} + (-1)^q L^{(2)}_{\beta,\alpha',\gamma,\gamma'}\delta_{\alpha,\beta'} + (-1)^q L^{(2)}_{\alpha,\beta',\gamma,\gamma'}\delta_{\beta,\alpha'} + L^{(2)}_{\alpha,\alpha',\gamma,\gamma'}\delta_{\beta,\beta'} +$$

$$V(r_{1\alpha}, r_{2\beta}, \theta_\gamma)\delta_{\alpha,\alpha'}\delta_{\beta,\beta'}\delta_{\gamma,\gamma'} + (-1)^q V(r_{1\alpha}, r_{2\beta}, \theta_\gamma)\delta_{\alpha,\beta'}\delta_{\beta,\alpha'}\delta_{\gamma,\gamma'} +$$

$$(-1)^q V(r_{1\alpha}, r_{2\beta}, \theta_\gamma)\delta_{\beta,\alpha,'}\delta_{\alpha,\beta'}\delta_{\gamma,\gamma'} + V(r_{1\alpha}, r_{2\beta}, \theta_\gamma)\delta_{\beta,\beta'}\delta_{\alpha,\alpha'}\delta_{\gamma,\gamma'}) \qquad (2.54)$$

Since $K^{(1)} = K^{(2)} = K$ and $L^{(1)} = L^{(2)} = L$ due to the symmetry of the two Hydrogen atoms the equation becomes

$$\hat{H}_{\alpha,\alpha',\beta,\beta',\gamma,\gamma'} = \frac{1}{\sqrt{1+\delta_{\alpha,\beta}}\sqrt{1+\delta_{\alpha',\beta'}}}$$

$$\times[(K_{\alpha,\alpha'}\delta_{\beta,\beta'} + (-1)^q K_{\alpha,\beta'}\delta_{\beta,\alpha'} + (-1)^q K_{\beta,\alpha'}\delta_{\alpha,\beta'} + K_{\beta,\beta'}\delta_{\alpha,\alpha'} +$$

$$V(r_{1\alpha}, r_{2\beta}, \theta_\gamma)\delta_{\alpha,\alpha'}\delta_{\beta,\beta'} + (-1)^q V(r_{1\alpha}, r_{2\beta}, \theta_\gamma)\delta_{\alpha,\beta'}\delta_{\beta,\alpha'})\delta_{\gamma,\gamma'} +$$

$$L_{\alpha,\alpha',\gamma,\gamma'}\delta_{\beta,\beta'} + (-1)^q L_{\alpha,\beta,\gamma,\gamma'}\delta_{\beta,\alpha'} + (-1)^q L_{\beta,\alpha',\gamma,\gamma'}\delta_{\alpha,\beta'} + L_{\beta,\beta',\gamma,\gamma'}\delta_{\alpha,\alpha'}] \qquad (2.55)$$

Since there is an implicit symmetry between the two hydrogen atoms the solution of variational calculations can be reduced to a two-step approach of intermediate diagonalisations and truncations.

The simplest way to implement the two-step approach is by first diagonalising the n_θ 2D Hamiltonians each with r_1 and r_2 motion for each fixed θ. This is a very rapid calculation as all the 1D multiplication is removed.

$$(H^{2D})^{\theta,\gamma,q}_{r_1,r_2,\alpha,\alpha',\beta,\beta'} = \frac{1}{\sqrt{1+\delta_{\alpha,\beta}}\sqrt{1+\delta_{\alpha',\beta'}}}$$

$$\times[K_{\alpha,\alpha'}\delta_{\beta,\beta'} + (-1)^q K_{\alpha,\beta'}\delta_{\beta,\alpha'} + (-1)^q K_{\beta,\alpha'}\delta_{\alpha,\beta'} + K_{\beta,beta'}\delta_{\alpha,\alpha'} +$$

$$V(r_{1\alpha}, r_{2\beta}, \theta_\gamma)\delta_{\alpha,\alpha'}\delta_{\beta,beta'} + (-1)^q V(r_{1\alpha}, r_{2\beta}\theta_\gamma\delta_{\alpha,\beta'}\delta_{\beta,\alpha'}] \qquad (2.56)$$

These diagonalisations yield eigenvectors $(C^{2D})^{\gamma q}$ and eigenenergies $(E^{2D})^{\gamma q}$ although only one symmetry block is considered at a time so q=0(even) is calculated separately to q=1(odd).

The truncations are performed by selecting $(n^{2D})^{\gamma q}$ eigenvectors below a specified energy cut-off. This cut-off is explicitly defined such that

$$\sum_{\gamma}(n^{2D})^{\gamma q} = N^{3D} \tag{2.57}$$

where N^{3D} is the size of final Hamiltonian to be diagonalised. $(n^{2D})^{\gamma q}$ is found by selecting the lowest eigenenergies from all the γ 2D diagonalisations for each q. To obtain comparative convergence in both the symmetry cases, even symmetry calculations are performed for fixed N^{3D}, then the odd symmetry calculation is done with a cut-off corresponding to the cut-off that gave N^{3D} eigenenergies in even calculations.

The selected eigenvectors are then used for the basis of the 3D calculation which also includes the angular kinetic energy. The 3D Hamiltonian, where j index runs from 1 to $(n^{2D})^{\gamma q}$, can be written as

$$\begin{aligned}(H^{3D})^{q}_{\gamma,\gamma',j,j'} &= (E^{2D})^{\gamma q}_{j}\delta_{\gamma,\gamma'}\delta_{jj'}+ \\ \sum_{\beta}\sum_{\alpha=1}^{\beta-q} &\frac{1}{\sqrt{1+\delta_{\alpha,\beta}}\sqrt{1+\delta_{\alpha',\beta'}}}(C^{2D})^{\gamma q}_{\alpha,\beta,j}(C^{2D})^{\gamma' q}_{\alpha,\beta,j'} \\ &\times(L_{\alpha,\alpha',\gamma,\gamma'}\delta_{\beta,beta'} + (-1)^{q}L_{\alpha,\beta',\gamma,\gamma'}\delta_{\beta,\alpha'}+ \\ &(-1)^{q}L_{\beta,\alpha',\gamma,\gamma'}\delta_{\alpha,\beta'} + L_{\beta,\beta',\gamma,\gamma'}\delta_{\alpha,\alpha'})\end{aligned} \tag{2.58}$$

This is then diagonalised to give eigenvalues and eigenvectors which can then be transformed into the DVR wavefunctions.

2.10 Computational Methods: the DVR3D Program Suite

Tennyson *et al* [141, 143, 145] have produced and upgraded over the years the TRIATOM suite of programs which calculates the bound vibrational or the ro-vibrational spectra for triatomics using the FBR. In 1995 this program suite was updated to include the DVR

methodology set out by Henderson *et al* [62] and is called the DVR3D program suite [142]. The main improvement from the 1993 version is the move from FBR to DVR, as discussed in section 2.3.1. TRIATOM uses associated Legendre polynomials for the angular co-ordinate and the Morse oscillator or spherical oscillator function for the radial co-ordinates. DVR3D uses grids based on these functions. These programs are used as they are efficient for dealing with large quantities of data. Tennyson *et al* [141, 143, 145] programs produce energy levels, wavefunctions and dipole transition moments for triatomics.

To produce spectra, the DVR3D program suite requires two subroutines from the user. Firstly, a potential energy surface, which is the main consideration of this thesis, and secondly a dipole surface.

The DVR3D program uses the Born-Oppenheimer approximation for the kinetic energy operator and has an intermediate step of diagonalisation and truncations of the hamiltonian operator to produce the final secular problem.

It uses either body-fixed Jacobi or Radau internal co-ordinates. The DVR is based on Gauss-Legendre and Gauss-Laguerre quadrature for all three internal co-ordinates.

The four different programs involved are DVR3DJ, ROTLEV3, ROTLEV3B and DIPOLE3. DVR3DJ calculates the vibrational wavefunctions. ROTLEV3 and ROTLEV3B calculate the rotational excitation. DIPOLE3 calculates the ro-vibrational transition strengths. There is also an additional program called SPECTRA which reproduces the calculated spectra in a visual format. As part of this work a program called XPECT3 has been modified to calculate expectation values from the wavefunctions from either DVR3D for vibrations and ROTLEV3/ROTLEV3B for rotations, see appendix A.

The restrictions on the DVR3D program and ROTLEV3/3B programs are mainly the overall size of the Hamiltonian matrix that can actually be diagonalised and the order of integration of the radial co-ordinates with the machine exponent range. It is for this reason that Serena Viti in her PhD thesis explored the most efficient basis sets for convergence, further explanation of this follows in section 2.10.5.

2.10.1 DIPOLE Surface

If the frequencies of a set of transitions is known then we can recognise the spectrum, however it is very useful to also know the probability of a particular transition. For example this can be used to determine the temperature and the amount of a particular molecule present in the spectra studied. Transition probability information is vital for analysing highly complex spectra of hot species. For this information we need the dipole moments. Strengths of pure rotational transitions is determined by the size of the permanent dipole moment of the molecule. However, vibrational transition strengths depend on changes in this dipole moment. For water there is a permanent dipole along the B axis, see figure 1.1.

Vibrational excitation results in a change of the dipole. It so happens that the stretches make a larger change in the dipole than the bending modes and therefore these transitions are stronger. To calculate the probability of a ro-vibrational transition the dipole moment at each geometry is needed, which most electronic structure calculations produce. The dipole moments are calculated using the DIPOLE routine in the DVR3D program suite. This suite requires that the user supplies a dipole surface. For water the most accurate, calculated dipoles are due to Partridge and Schwenke [102].

Partridge and Schwenke represented their dipole moment data by writing [130]

$$\mu(r_1, r_2, \theta) = q(r_1, r_2, \theta)(\mathbf{x}_{H_1} - \mathbf{x}_O) + q(r_2, r_1, \theta)(\mathbf{x}_{H_2} - \mathbf{x}_O) \tag{2.59}$$

where q is the point charge and $\mathbf{x}_{H_i}, \mathbf{x}_O$ are position vectors of the atoms in the chosen co-ordinate system, Radau. In this equation q is a scalar and is therefore independent of the definition of the body-fixed co-ordinate axes. It should be noted that q is not symmetric with the interchange of r_1 and r_2. Partridge and Schwenke used the dipole moment computed as an expectation value from the ICMRCI wave function using the cc-pV5Z basis set. q can be represented as

$$q(r_1, r_2, \theta) = q^0(r_1, r_2, \theta) + q^c(r_1, r_2, \theta), \tag{2.60}$$

where q^0 is the zeroth order term and q^c the correction term. They define

$$q^0(r_1, r_2, \theta) = A(r_1^{-b} + r_2^{-b}) \times [c_0 + c_1 P_1(\cos\theta) + c_2 P_2(\cos\theta)]. \tag{2.61}$$

P_l are the Legendre polynomial and q_c are given as

$$q^c = c_{ooo} + exp{-\beta}[(r_1 - r_e)^2 + (r_2 - r_e)^2]$$

$$\times \sum_{ijk} c_{ijk}[(r_1 - r_e)/r_e]^i[(r_2 - r_e)/r_e]^j$$

$$\times[\cos\theta - \cos\theta_e]^k$$

where c_{ooo}, and c_{ijk} were determined by a weighted least squares fit. β was fixed to $2a_o^{-2}$ and r_e and θ_e remained fixed.

The parameters in q^0 were determined by approximately fitting the point charges determined by inverting equation 2.59 for symmetric geometries. q^c was determined by a least squares fit using the functions with i+j+k$\leq$ 6.

After this publication by Partridge and Schwenke [102] of their dipole moment surface it was realised that the main error in their overall calculations of both PES and DMS, was the DMS. In 2000 Schwenke and Partridge [132] reproduced the same data with a new functional form, as the previous was found not to yield a zero dipole moment when water dissociated into atomic fragments. μ is the same as defined above but q becomes

$$q(r_1, r_2, \theta) = exp(-\beta[r_1 - r_e]^2)(\sum_{i=0}^{n_r} c_i[(r_1 - r_e)/r_e]^i$$

$$+exp(-\beta[r_2 - r_e]^2) \sum_{ijk} c_{ijk}[(r_1 - r_e)/r_e]^i$$

$$\times[(r_2 - r_e)/r_e]^j[\cos(\theta) - \cos(\theta_e)]^k) \tag{2.62}$$

This new function and a lot more detailed consideration of the included parameters led the accuracy of the fit to be increased by an order of magnitude.

2.10.2 SPECTRA

SPECTRA is another program from the TRIATOM suite [141, 143, 145] which works in conjunction with the DVR3D program suite from the output streams of the DIPOLE routine. To calculate the partition function this routine also requires energy levels from DVR3D/ROTLEV/ROTLEV3B. The SPECTRA routine can also calculate the integrated absorption coefficients. This original program has been modified by a number of people including Serena Viti [164].

2.10.3 XPECT3

XPECT3 is an unpublished part of the DVR3D program suite. It computes expectation values for a set of arbitrary (scalar) properties. In the program the user has to supply the subroutine "prop" which includes the scalar properties. These expectation values can be diagonal or off-diagonal (transitional)

The program was modified to read bra and ket files from the DVR3D program for vibrational levels and from either ROTLEV or ROTLEV3B for ro-vibrational levels as part of this work. The program is used in conjunction with the Hellmann-Feynman theorem [60], discussed below, to compute analytical derivatives which can be passed to the fitting routines. User instructions for XPECT3 are found in appendix A.

2.10.4 Hellmann-Feynman Theorem

The Hellmann-Feynman theorem[1] states that for the exact wavefunction of the energy level Ψ_n:

$$\frac{\partial E_n}{\partial p} = \langle \Psi_n | \frac{\partial H}{\partial p} | \Psi_n \rangle \tag{2.63}$$

Where p are the parameters and $\frac{\partial H}{\partial p}$ is the derivative of the Hamiltonian with respect to the parameters.

[1] Details taken from Epstein [40]

The Hamiltonian is just the Kinetic Energy operator(K) plus the potential energy operator(V) i.e. H = K + V. However, for fits of the potential, K does not depend on the parameters and so has a zero derivative and equation 2.63 becomes

$$\frac{\partial E_n}{\partial p} = \langle \Psi_n | \frac{\partial V}{\partial p} | \Psi_n \rangle \tag{2.64}$$

Where for linear fits, which are the only fits considered in this thesis, V can be written as

$$V = \sum_{ijk} p_{ijk} G_{ijk}(q_1, q_2, q_3), \tag{2.65}$$

and p_{ijk} are the potential parameters. Equation 2.64 is then

$$\frac{\partial E_n}{\partial p_{i,j,k}} = \langle \Psi_n | G_{ijk} | \Psi_n \rangle. \tag{2.66}$$

In the Discrete Variable Representation (DVR) the wavefunction can be represented as an amplitude at each grid point (α, β, γ) i.e. $\Psi_n(\alpha, \beta, \gamma) = d^m_{\alpha,\beta,\gamma}$ and therefore,

$$\frac{\partial E_n}{\partial p} = \sum_{\alpha,\beta,\gamma} (d^m_{\alpha,\beta,\gamma})^2 G_{i,j,k}(\alpha, \beta, \gamma). \tag{2.67}$$

XPECT3 calculates this expression at the DVR points and is therefore a very rapid way of calculating the derivatives with respect to the potential parameters.

2.10.5 Optimised Basis Sets for the DVR3d program suite

For the angular motion of the water molecule associated Legendre polynomials give a good representation. The radial motion, however can be represented with a number of different basis sets. For the Sutcliffe-Tennyson Hamiltonian, however, Morse like functions are have been found to represent well the radial motion, as discussed in section 2.7. These parameters used in equations 2.37,2.38,2.39,2.40 of this section can be varied to find the optimal value for water calculations. These and other optimised basis sets are summarised in table 2.10.5.

Optimised basis sets greatly reduce computational time and memory. In the main the basis sets used in the DVR3D program suite are taken from Serena Viti thesis, where she discusses, in full, the convergence of the different factors [164].

Parameters used	**DVR3D**	This work
NEVAL	Number of eigenvalues and and eigenvectors required	Range dependent on energy range.
NPNT2	Number of DVR points in r_2 from Gauss-associated Laguerre quadrature	21-28 (18000-25000cm^{-1})
NALF	Number of DVR points in θ from Gauss-associated Laguerre quadrature	30-40 (18000-25000cm^{-1})
MAX3D	Maximum dimension of the final Hamiltonian	1000-1500 (18000-25000cm^{-1})
RE1 (r_e)	Morse like function parameters equilibrium radius	2.55 a_h
DISS1 (D_e)	Morse like function parameters dissociation energy	0.25 E_h
WE2 (ω_e)	Morse like function parameters fundamental frequency	0.007 E_h

Parameters used	**ROTLEV3B**	This work
NVIB	Number of vibrational levels from DVR3D to be read for each k block	$\approx \frac{NEVAL}{2}$
NEVAL	Number of eigenvalues requested for the first (e parity) set	Range dependent on energy range. Must be less than NEVAL from DVR3D
KMIN	Parity - 0 for f parity 1 for e parity and 2 for both	usually 2
IBASS	Size of the final hamiltonian	3×(J+1)
NEVAL2	Number of eigenvalues requested for the second (f parity) set	Range dependent on energy range. Must be less than NEVAL from DVR3D

Table 2.1: A table to show the parameters used for calculations in this thesis, using the DVR3D program suite

Chapter 3

Spectroscopy

In 1814 high resolution spectroscopy was born when Fraunhofer projected light through a shutter, a prism and onto a white wall. He observed not only the seven colours of the visible spectrum, already observed since Newton, but also both strong and weak vertical lines [59] which differ depending on the material used to diffract the light. This was the first experiment to suggest that light holds hidden information about atomic and molecular physics.

It was not until half a century later that the features that Fraunhofer saw were attributed to the chemical composition of the sun. Bunsen and Kirchoff compared absorption features in the spectrum to emission lines found from hot atoms in the laboratory. It took, however, the development of quantum mechanics and several more decades before any real information about the molecules involved was found. It was found that this spectra has many features from the absorption of CH in the Sun's photosphere and other features such as oxygen and water from the earth's atmosphere. It then became apparent that spectral analysis could provide information about both the distant parts of the Universe and the internal structure of molecules.

3.1 Assignment of the Sunspot Spectra

Sunspots were first identified by the Chinese some 2000 years ago. However, it was Galileo who made the first western observations of these dark patches on the sun. A sunspot is an area on the sun where there is intense solar magnetic activity which are know to occur in a twenty two year cycle. These dark patches on the sun are very much cooler than the rest of the sun as they are only around 3300 K relative to 5785 K on the rest of the sun. This enormous change in temperature completely changes the chemistry of these two environments [146].

At 5785 K in the photosphere there are few molecules and definitely no triatomics, there is a large abundance of OH. At temperatures of 4000 K around half of OH reacts to form H_2O. On the sunspots, therefore, there is an abundance of H_2O.

Large portions of the sunspot spectra were originally considered un-assignable. In 1970, however, Hall [53] first suspected that there were water lines in the immensely complicated sunspot spectra. After this Benedict reportedly managed to assign more of this spectra to water which unfortunately still remains unpublished. The next successful attempt to analyse the spectra was by Wallace and Livingston [169] where they firstly published an atlas of the the dark sunspot umbra in the 1970-8640 cm^{-1} region and again found water absorption bands. Wallace *et al* published several atlases of the solar spectrum [167, 168], recorded using a high resolution Fourier transform spectrometer at Kitt Peak Solar Observatory.

In 1995 a high-temperature laboratory spectrum was recorded at the University of Waterloo by Bernath's group where they heated steam to 1500 K and recorded the resulting emissions [10]. The spectrum from the sun is absorption of light as a function of frequency and as the continuous radiation is from the centre of the sun the spectra appears as a complicated absorption spectra. In green in figure 3.1 shows Bernath's laboratory emission spectra. This laboratory data was limited in temperature as above 1800 K the equipment may melt. At this lower temperature there are a lot fewer occupied water levels. However, there is a clear match between the emission and absorption spectra and water is definitely

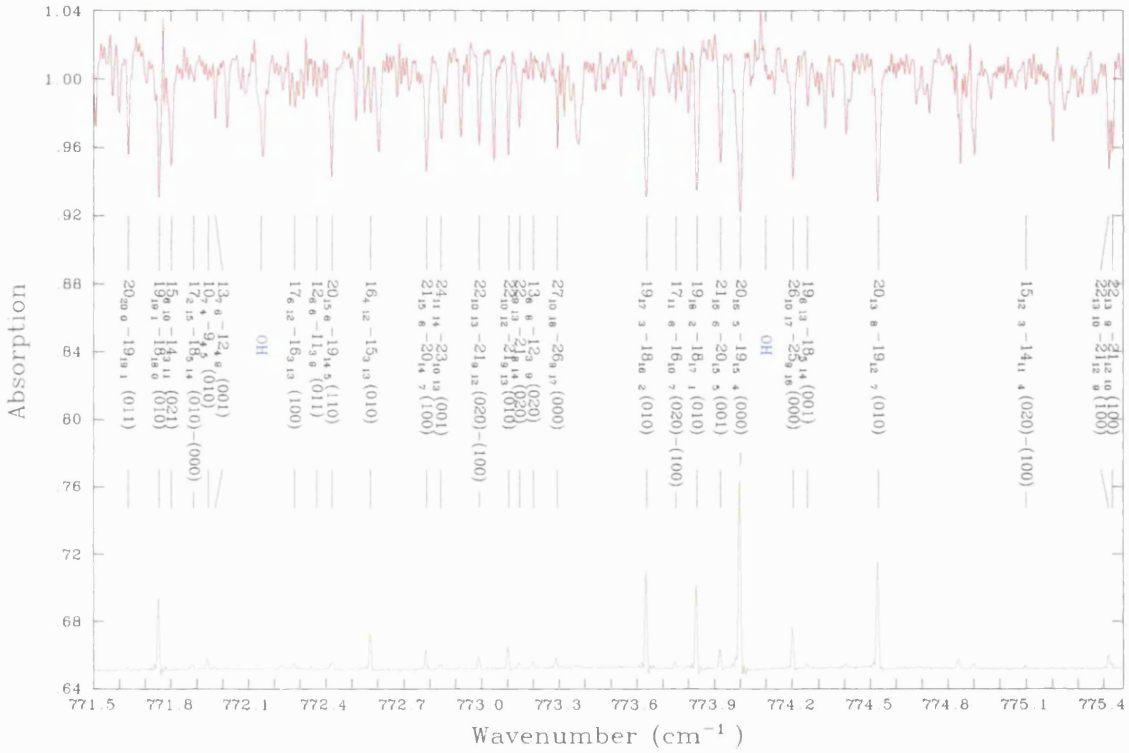

Figure 3.1: A sample portion of the sunspot absorption spectrum (upper trace) and laboratory emission spectrum (lower trace). The vertical scale belongs to the sunspot absorption spectrum. Unity corresponds to no absorption of sunlight, 0.96 to absorption of 4% of the light. The strength of the laboratory emission was not recorded on an absolute scale. Quantum number assignments, given as J_{K_a,K_c}(Upper) - J_{K_a,K_c}(Lower) for various vibrational states, are marked. The spectra illustrate the congested nature of the whole sunspot spectrum in the 10-20 μ m region (figure courtesy of Serena Viti [164])

present.

The sunspot spectrum is dense and in places "grass-like". However all the features, even those that appear to be noise, are reproducible. The struture occurs dues to the processes in the sunspot. However the density of this spectra is around 50 lines per cm^{-1}. For assignment of such a spectra using simple frequency matches we would need an accuracy of 0.01 cm^{-1} or better. As yet the best *ab initio* surface available to us by Partridge and Schwenke [102] only predicts the fundamentals to within 2 or 3 cm^{-1} . In fact the Born-Oppenheimer surface is only valid at the 1 cm^{-1} level for molecules which have light H atoms [176].

It is not entirely necessary, however, to achieve this level of accuracy as not all transitions are equally probable and some are stronger than others. As strong features are less common the density of these features is reduced. Also, with careful treatment errors are systematic for high quality *ab initio* electronic structure calculations which makes energy level predictions easier. It was therefore possible for Polyansky *et al* to assign all the strong lines in this spectra and some of the weak lines [115]. These assignments were done by following a branch. For example 20_{200} - 19_{191}, 21_{210} - 20_{201}, 22_{220} - 21_{211} can be described as a single branch defined by,

$$K_a = J - n \tag{3.1}$$

where n is constant for each set of levels. For each branch the error in the predicted frequency varies very little along each branch. The error can, as a starting point, be accurately determined from low J values where there is a wealth of experimental data. It is then simply the technique of following the branch through the spectrum to high rotational levels. Figure 3.1 is a part of the N window (10 μm) which was the first band to be assigned by Polyansky *et al* [115]. They then went on to assign transitions in the K(2μm) [118] and L(3-4μm) Bands [177]. This proved to be more difficult for two reasons. For the K window many of the trivial transitions did not lie in the window. In this context "trivial" refers to assignments based on selection rules governing which levels are linked

to previously experimentally known transitions in order to predict new transitions. The word "trivial" is used as they do not required large scale quantum calculations. These "trivial" assignments do not, however, give new energy levels for further assignments but can confirm previously assigned transitions.

For the K window, however, many of transitions involve high vibrational levels for which there is a serious deficit of laboratory data. Secondly, telluric absorption (when observing from the earth) in these windows means that there are gaps in the frequency, making it difficult to follow the branches, however this assignment is made easier as the spectra is significantly less dense. Many assignments were made by the group [112, 116] with additional experimental results from the University of Waterloo, however there still remains a lot more lines to be assigned. The only way that more assignments can be made will be to improve the accuracy of our theoretical methods, which will be discussed further.

3.2 Previous Experimental Work

The main bulk of the experimental data on the water spectra available to date is found in the HITRAN databases [125, 126]. HITRAN is an acronym for high resolution transmission molecular absorption database. This database is a compilation of spectroscopic parameters used for codes to predict transmission and emission of light in the atmosphere. As discussed in section 1.1.1 water absorbs around 70% of sunlight in the earth's atmosphere so this database includes a lot of water lines. Of the 1,000,000 lines in the 1996 database [125] around 50,000 of the lines are attributed to water and its isotopomers. The lines above 8,000 cm^{-1} have been updated since the 1998 HITRAN database [126]. This database contains, in the main, the observational results that we use to compare with our theoretical calculations. Some of the additional water lines in this recent addition are attributed to Esplin *et al* for the 720 -1400 cm^{-1} region [41].

A new addition to the database is HITEMP [125] (high temperature spectroscopic absorption parameters) which includes water lines for higher temperatures but the majority

of this database is theoretical and is actually less accurate than present theory. It is therefore a lot less useful. Since the last edition of the HITRAN database new experimental data has become available, this is shown in table 3.1.

3.2.1 Calculated Line-lists

Many of the above theoretical assignments use line-lists, which are essentially large databases of energy levels and quantum numbers for ro-vibrational energy levels and transitions for water. All of these linelists are presented in table 3.2.

While Partridge and Schwenke's empirical line-list has the least absolute error for all the vibrational and rotational spectra up to 23000 cm^{-1} Polyansky *et al* ś *ab initio* line-list (ZVPT) has more consistent errors. The other *ab initio* line-list by Zobov *et al* [175] referred to in this table 3.2 is based on the work presented here in chapters 4 and 5. The energy levels calculated in this line-list are more accurate than those calculated using the Partridge and Schwenke *ab initio* potential. Usually for quantum assignments both *ab initio* line-lists are used along with the best empirical line-list due to Partridge and Schwenke [102]. Although this line-list is the best it can be seen from the table that even this does not go high enough in energy or to great enough accuracy for spectroscopic needs. The aim of this thesis is to create a potential energy surface on which a more accurate line-list can be based and many more spectroscopic assignments can be made.

Table 3.1: Experimental data for $H_2^{16}O$ since 1996

Reference	Year	Experimental Set up	Temperature/Region	New levels
Flaud *et al* [42]	1997	FTS Resolution 0.012 cm^{-1} Path length 434 m	11600-12750 cm^{-1}	506 accurate levels in agreement with Toth's [157] for $3\nu + \delta$ polyad for strong bands.
Flaud *et al* [43]	1997	From above experimental work		Line-strengths in the $3\nu + \delta$ of interacting vibrational states. Accurate dipole moment transition parameters found.
Polyansky *et al* [114]	1997	Emission spectra of hot water.	1000^oC /1550^oC 900-2000 cm^{-1}	4381 lines, 1750 assigned mostly ν_2, $2\nu_2$ - ν_2, $3\nu_2$ - $2\nu_2$, $4\nu_2$ - $3\nu_2$,$5\nu_2$ - $4\nu_2$ 050 found at 7542.39 $\pm$ 0.05 cm^{-1}
Polyansky *et al* [118]	1997	Sunspot spectra by Wallace *et al* [167, 168]	4600 - 5100 cm^{-1}	485 new lines assigned in K Band (061)-(050) and (071)-(060) Vibrational transitions Assignments up to 17000 K

Table 3.1: continued.

Reference	Year	Experimental Set up	Temperature/Region	New levels
Polyansky *et al* [117]	1997	Sunspot spectra by Wallace *et al* [167, 168]	Sunspot T 3000^{o}C,750 $\leq \tilde{\nu} \leq$ 1010 cm^{-1} Laboratory T 1550^{o}C,370 $\leq \tilde{\nu} \leq$ 930 cm^{-1}	Assigned 3000 of 4700 of lab spectra using PS. Assigned 1687 of sunspot spectra (all the strong) lines. High J for 000,010,020,100, 001, and transitions within 030,040 110,011,021,111,120,101
Toth [154]	1998	Emission spectra of hot water.	590-2583 cm^{-1}	Line positions of 1700 lines of H_2O Vibrational energy levels for (000) and (010) for $H_2^{16}O$, $H_2^{17}O$, $H_2^{18}O$
Toth [155]	1999	FTS High resolution up to the far infrared	1100-2300cm^{-1}	810 line positions and strength of $H_2^{16}O$ of the (020)-(110), (100)-(010),(001)-(000) transitions

Table 3.1: continued.

Reference	Year	Experimental Set up	Temperature/Region	New levels
Carleer *et al* [22]	1999	FTS measured, near infrared, visible and near ultraviolet water lines for all polyads from 3ν to 8ν.	13098-21400 cm^{-1} room temp.	Assigned 2286 transitions 15 new overtones and combination bands [1]
Lanquetin *et al* [87]	1999	Methane-oxygen flames. Resolution 0.02 cm^{-1}	1850K 780-1370 cm^{-1} 1800-5000 cm^{-1}	Experimental energies for two states fitted with bending rotation $\hat{H}$ [32] Comparison with these calc values and previously obs.
Zobov *et al* [177]	2000	Infrared spectrum	Lab T=1500°C 2500-6000cm^{-1}(emission) Sunspot 2497-3195cm^{-1}(L-band) 4251-4962cm^{-1}(K-band)	1207 in L and 508 in K band Vib band origins of 11242.8 ± 0.1cm^{-1} and 12586 ± 1cm^{-1} for 051 and 061 states

[1] In this paper they suggest that local mode rather than normal mode vibrational assignments are more appropriate fro the vibrational states of water for polyads 4ν and above. This is dues to the fact that normal mode assignment becomes increasingly more difficult to support as there is a near-degeneracy of $(n,0)^{+}0$ and $(n,0)^{-}0$ for n=4,5,6.

Table 3.1: continued.

Reference	Year	Experimental Set up	Temperature/Region	New levels
Polyansky *et al* [106]	1996	High resolution hot emission FTS Resolution 0.01 cm^{-1}	350-1000cm^{-1} 1550^{o}C	4000 pure J lines 600 of the strongest lines for (000) and (010) assigned
Polyansky *et al* [112]	1997	Above data further assigned		Assignment of (330) J lines for (100), (001), (020) vib states. Vib (020) up to K_a=18 Assignment of 020-100 100-020 & pure 020-100
Polyansky *et al* [115]	1998	Theoretical reanalysis of spectrum of Mandin *et al* [91]	13200 - 16500 cm^{-1}	Assigned 663 of the unassigned 795,reassigned 38 Extension of measurement of the 4ν and $4\nu + \delta$ polyad 1st info. on (240),(033),(160),(170),(071)

Table 3.1: continued.

Reference	Year	Experimental Set up	Temperature/Region	New levels
Schwenke [131]	1998	Analysis of unassigned and mis-assigned HITRAN lines		Reassigned 133 lines 831 assignment of the 1725 unassigned lines. Most new lines for 320-000 band (64%) and 121-010 (most) 340-000 (96%)
Zobov *et al* [178]	1999	Emission spectra for hot water	1550°C 800-1900 cm^{-1} 1800-2500 cm^{-1}	Assignment using PS and ZVPT Analysis of 030-110,040-110,120-030 012-030,011-100,110-001,101-110. Assigned 4556 of 8959 lines recorded (060) found at 8870.54 $\pm$ 0.05 cm^{-1} (050) confirmed at 7542.40 $\pm$ 0.03 cm^{-1}

Table 3.2: Empirical and *ab initio* line-lists

Reference	Year	Potential Used	Dipole Surface Used	Details
Jørgensen and Jensen [78] Empirical	1993	Jensen [75]	Calculated in paper	Only for J=0 up to 30000 cm^{-1} J = 0, σ_{vib} = 0.7 cm^{-1}
Miller *et al* [96] Empirical	1994	Jensen [75]	Wattson and Rothman [171]	6.4 million lines, J $\leq$ 30. Energy levels up to 11,000 cm^{-1}. Good convergence up to J = 20 but $\sigma \approx 10$ cm^{-1} up to J= 30
Partridge and Schwenke (PS) *ab initio* [102] Empirical	1997	Calculated in paper	Calculated in paper	300 Million lines. J up to 55. J=0, σ_{vib} max 0.49, J=20, σ_{rot} = 0.07 Only up to 28000 cm^{-1} Only 70% transitions to J=10 Only 50% transitions to J=20 Only 60% transitions to J=28 Low residual errors becoming large and erratic

Table 3.2: continued.

Reference	Year	Potential Used	Dipole Surface Used	Details
Viti *et al* [166] (VTP1) Empirical	1997	Polyansky *et al* [107] (PJT1)	Wattson and Rothman [171]	Very accurate for low vibrational states i.e. 000 all J, 0.03 cm^{-1} . Up to J=38
Polyansky *et al* [116] (ZVPT) *ab initio*	1998	PS *ab initio* [102] + BODC Zobov *et al* [176] Middle masses	Gabriel *et al* [46]	18000 $cm^{-1}$for $J \leq 25$ and 23000 cm^{-1} for $25 \leq J \leq 33$ Less accurate than PS or VTP1 but errors are more consistent
Zobov *et al* [175] *ab initio*	2000	PS *ab initio* [102] + BODC Zobov *et al* [176] Middle masses [176] Relativistic correction,section 4 Barrier correction,section 5	PS Dipole surface [102]	Up to 26000 cm^{-1} Intensities for transitions starting from less than 9000 cm^{-1} Assigned 299 of 868 transitions by Carleer *et al* [22]

Chapter 4

The Relativistic Correction

4.1 Electronic Structure Calculations

As part of this work Császár [W.1] computed the electronic relativistic effects using first-order perturbation theory applied to one-electron Darwin terms [6, 33], as implemented with the ACES II program system [104, 134]. Up to this point no one had performed a systematic comparison of the geometry dependence of the relativistic effects computed with the Full Dirac Hamiltonian, but the above method was considered reliable for light atoms [80, 104, 163]. Quiney *et al* [119] also computed a second order calculation, which will be discussed in this chapter. Our calculations of the relativistic correction in water employed correlated coupled cluster wavefunctions at the CCSD(T) level of theory and extended the cc-pVQZ basis set [38]. 324 structures in the range of bond-lengths $1.47 \leq r \leq 2.79 a_o$ and angles $41^o \leq \theta \leq 180^o$ were considered.

It was necessary to fit this relativistic correction data to a functional form in order to do nuclear motion calculations. Two sets of variables (S_1,S_2, S_3) were fitted to a simple power series, 4.1, in the displacement coordinates. The two sets of variables were; the linear set (equations 4.2, 4.3, 4.4) and the Jensen [75] set (equations 4.5, 4.6, 4.7) . The equilibrium values included in these sets of variables are (r_e=1.80965 a_o,θ_e=1.824045 rad).

The linear set of variables, given in equations 4.2, 4.3, 4.4, was tested as it often needs fewer parameters for the fit, however this set of variables does not have a zero differential

at π and therefore may not describe the behaviour at linearity appropriately.

$$\Delta V_{rel}(S_1, S_2, S_3) = \sum_{i,j,k} c_{i,j,k} S_1^i S_2^j S_3^k \tag{4.1}$$

$$S_1 = \frac{r_1 + r_2}{2} - r_e \tag{4.2}$$

$$S_2 = \theta - \theta_e \tag{4.3}$$

$$S_3 = \frac{r_1 - r_2}{2} \tag{4.4}$$

This linear set of variables can only be used if compared with a set of variables that does have a zero differential at π i.e. the Jensen set

$$S_1 = \frac{r_1 + r_2}{2} - r_e \tag{4.5}$$

$$S_2 = \cos\theta - \cos\theta_e \tag{4.6}$$

$$S_3 = \frac{r_1 - r_2}{2}. \tag{4.7}$$

4.2 Least-Squares Fitting

The fitting procedure involves adding/subtracting parameters to make the solution increasingly more accurate. There is usually a point at which adding more parameters would make little or no difference to the overall standard deviation. The least squares fitting program used involved manually removing the badly correlated parameters. A few different numbers of coefficients were tested. We originally obtained, for the linear set, an overall standard deviation of 0.2 cm^{-1} for 32 parameters for $i + j + k \leq 5$, however this standard deviation is not within spectroscopic accuracy. Fourteen more parameters were added and the overall standard deviation became 0.07 cm^{-1} . Eventually, for the linear set of variables, all the well determined parameters were retained up to $i + j + k \leq 7$. The (ijk) = (080) term was also kept in the expansion as it is significant to the overall

potential; as explained later, the relativistic correction is sensitive to the bending overtones. The number of coefficients obtained from the linear set was 55. This fit gives an accurate representation of the data and has a standard deviation of 0.02 cm^{-1} . The final parameters were tested for convergence by further iterations of the fitting process to check that the final parameters do not change.

We then repeated the fitting process with the Jensen definition of the angular displacement co-ordinate $\cos\theta - \cos\theta_e$. For the Jensen potential for 55 contributing parameters the resulting standard deviation is 0.07 cm^{-1} . To obtain a similar level of accuracy as the linear set, the Jensen definition of the displacement co-ordinate uses 109 parameters to get a standard deviation of 0.01 cm^{-1} .

The coefficients for the linear set of variables and the Jensen set are presented in tables 4.1 and 4.2 .

The electronic relativistic correction arises largely from the oxygen 1s electrons and is geometry independent. Its value is approximately $-0.05\ E_h$, which corresponds to the leading term in the fit. However, as spectra contain transition energies only, this term has no influence on the ro-vibrational spectra. The changes in relativistic energy correction with geometry are two orders of magnitude smaller and have different signs upon bending and stretching of the water molecule.

Figures 4.1 and 4.2 show the variation in the relativistic correction as a function of bond angle and symmetric stretch co-ordinate for the linear and Jensen sets of variables. It is notable that the choice of set of variables does not appear to effect the overall potential and that both figures have a strong linear dependence for bond-angles close to equilibrium (1.82 rad). A figure can be plotted which shows the linear potential minus the Jensen potential, but the difference is so minimal that to a reasonable scale it is flat and zero. As this difference is insignificantly small the set of variables was chosen as it uses less parameters. These calculations also showed that the Jensen form may constrain the bending potential un-physically, this will be discussed later.

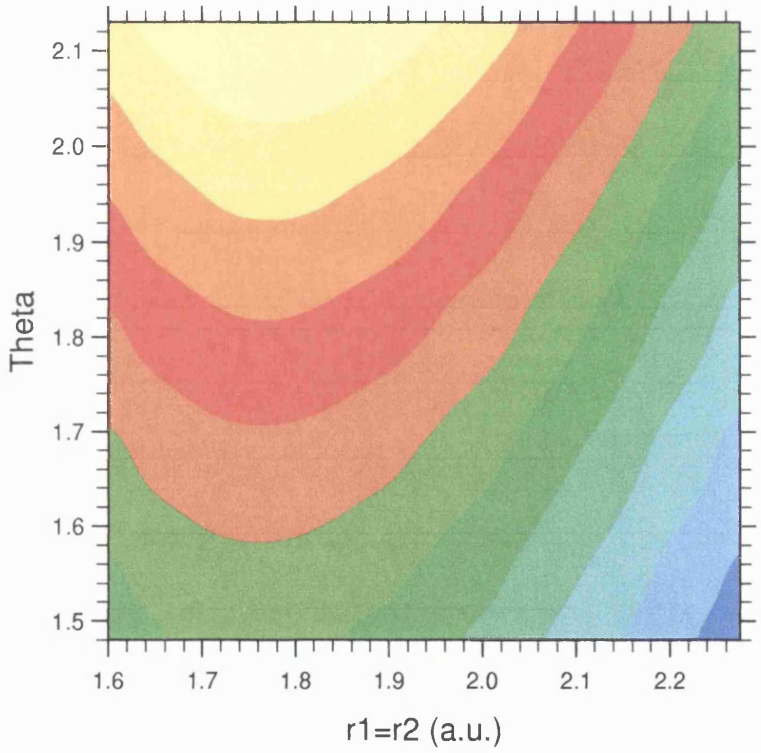

Figure 4.1: Variation of the Relativistic Correction for the linear set of variables as a function of bond angle, θ, and bond-lengths r_1=r_2. The plot is for symmetric stretches only. Contours are spaced by 20 cm^{-1} from -0.051992 E_h.

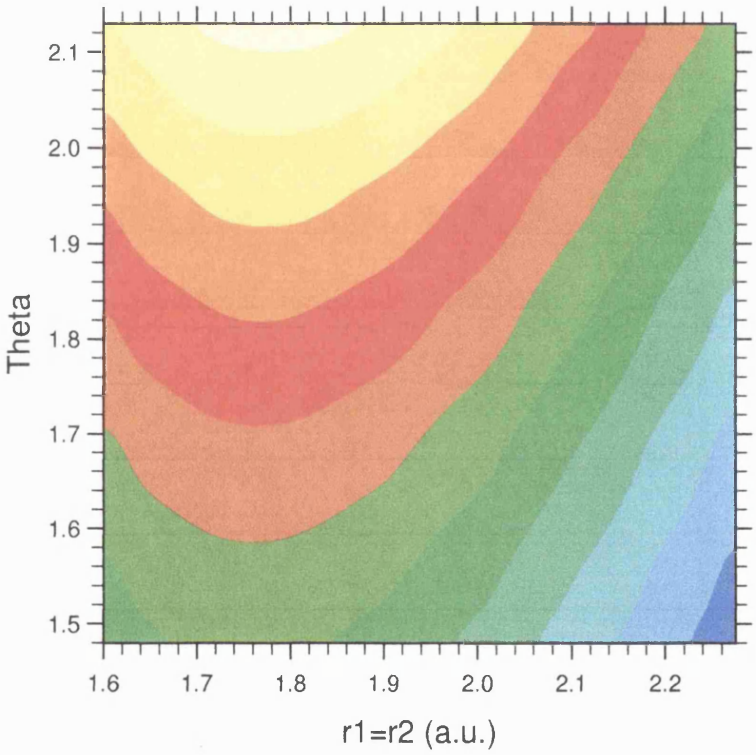

Figure 4.2: Variation of the Relativistic Correction for the Jensen set of variables as a function of bond angle, θ, and bond-lengths r_1=r_2. The plot is for symmetric stretches only. Contours are spaced by 20 cm^{-1} from -0.051992 E_h.

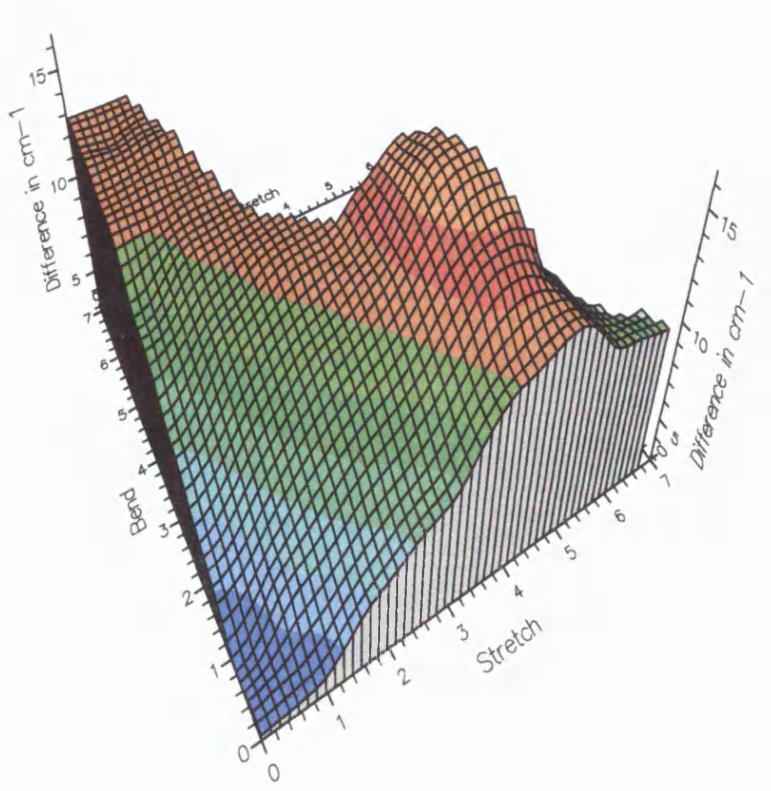

Figure 4.3: Vibrational calculations on Partridge and Schwenke's *ab initio* PES. A 3D representation of how Calcs - Obs varies, with quanta of stretch and quanta of bend for J=0.

4.3 Nuclear Motion Calculations

Nuclear motion calculations were performed using the DVR3D program suite, section 2.10, and previously optimised basis sets, section 2.10.5 . Ro-vibrational calculations were performed for the $H_2^{16}O$ isotopomer and vibrational calculations only for the HDO, HTO, D_2O, T_2O isotopomers. Combinations of *ab initio* Born-Oppenheimer by Partridge and Schwenke [102], the adiabatically corrected potential (BODC), calculated by Zobov *et al* [176] and the relativistic correction were used to perform calculations. Different hydrogenic masses were also tested. The masses presented here are mainly for a hydrogenic mass chosen mid-way between the atomic mass and the nuclear mass of hydrogen, as suggested by Zobov *et al* [176].

Tables 4.3 and 4.4 give a summary of the rotational and vibrational energy levels in water for $H_2^{16}O$.

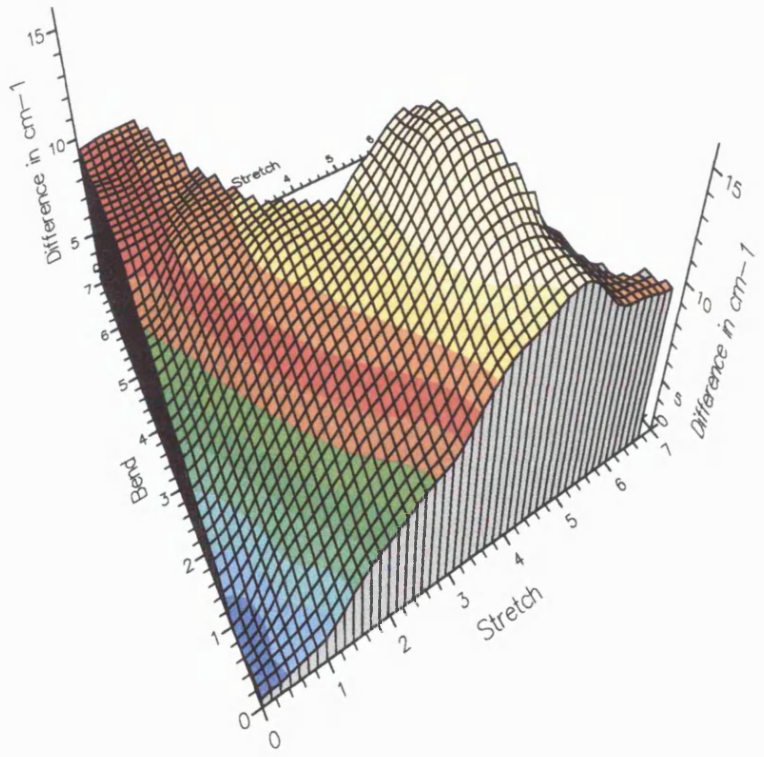

Figure 4.4: Vibrational calculations on Partridge and Schwenke's *ab initio* PES augmented by the Adiabatic Correction. A 3D representation of how Calcs - Obs varies, with quanta of stretch and quanta of bend for J=0.

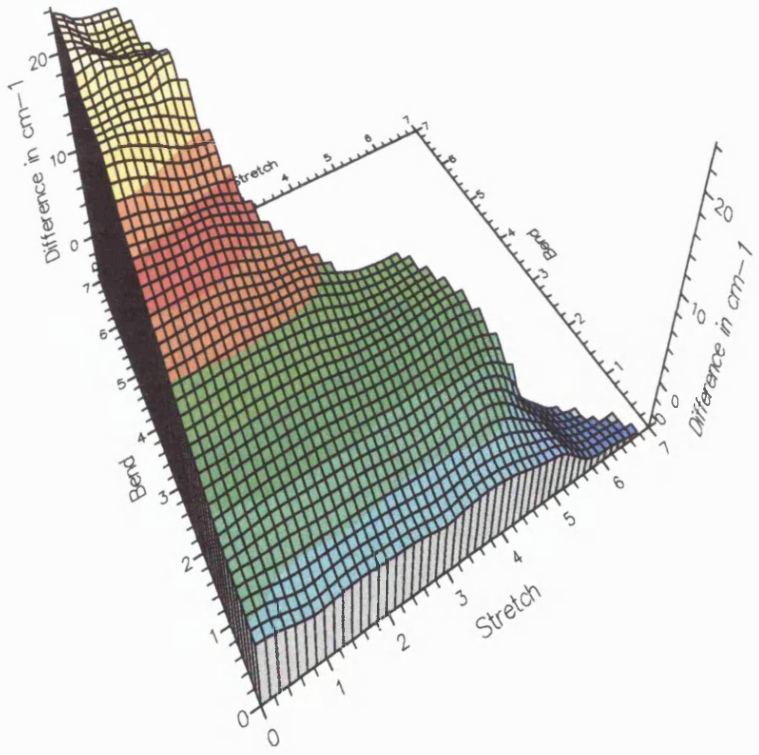

Figure 4.5: Vibrational calculations on Partridge and Schwenke's *ab initio* PES augmented by the Adiabatic Correction and the Relativistic Correction. A 3D representation of how Calcs - Obs varies, with quanta of stretch and quanta of bend for J=0.

Table 4.3 shows the vibrational energy levels for $H_2^{16}O$ and shows the sensitivity of the results to the relativistic correction and compares them to the sensitivity of the results to the inclusion of the BODC. Perhaps a better representation of this sensitivity is shown in figures 4.3, 4.4 and 4.5 . The addition of the BODC is shown by the comparison of figures 4.3 and 4.4 , notably these figures are not significantly different. However if figure 4.5 is compared to figure 4.3 the results are dramatically different. The general effect of the inclusion of the relativistic correction is that it lowers the band origins of the stretching states (v_2=0) and raises the band origins of the bending modes. The effect on the bending modes is generally larger .

The BO and the BODC calculations both systematically over-estimate the band origins so therefore the overall effect of the inclusion of the relativistic correction brings the stretching states significantly closer to the experimental values while pushing the bending modes further away.

Table 4.5 shows the fundamental vibrational energy levels for HDO, HTO, T_2O and D_2O. We can see that for these other isotopomers of water the relativistic effect again improves the stretches while making the bending modes far worse.

The rotational term values for J=20 are shown in table 4.4 for a series of similar calculations to those presented for vibrations. The results for the ground state and the first bending fundamental only are presented here, as this is the extent to which complete experimental data for J=20 is available.

Figure 4.6 as well as table 4.4 show how the inclusion of the BODC and the relativistic correction effect the overall results. It is apparent that the relativistic correction has little or no effect for low K_a and a small effect for mid K_a of around 1 cm^{-1}, probably due to a cancellation of errors. For high K_a the relativistic correction significantly lowers the predicted energy levels and thus the difference between the observations and the calculated energies is quite large.

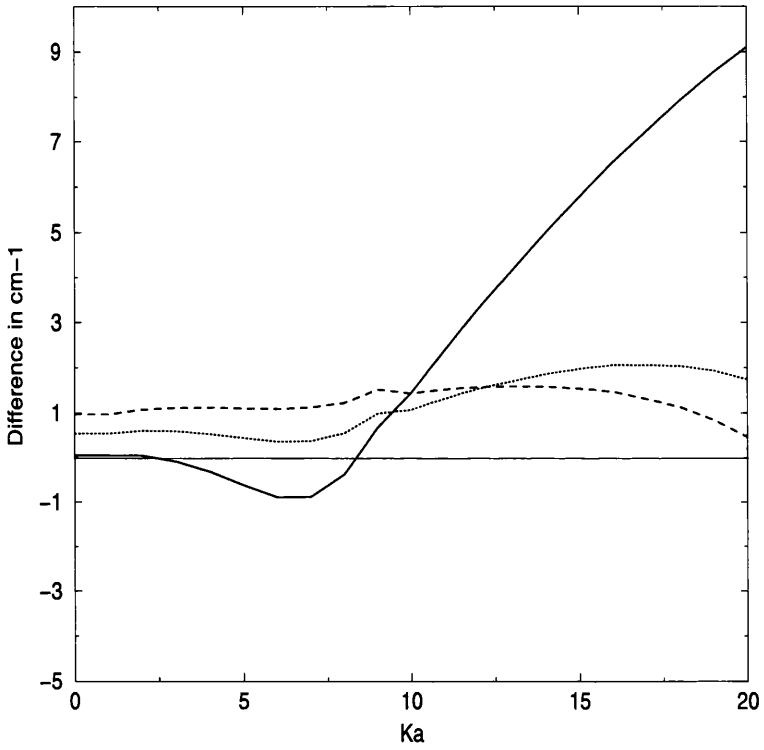

Figure 4.6: A graph to show Obs-Calcs for J=20 with increasing K_a. Dotted line, PS *ab initio* ; dashed line, PS *ab initio* + adiabatic; solid line, PS *ab initio* + adiabatic + relativistic.

4.4 Comparison with the Relativistic Surface by Quiney *et al*

At the same time as our work, Quiney *et al* [119] performed *ab initio* calculations on the electronic structure of water using a full Dirac Hamiltonian compared to our first order perturbation theory calculations applied to one-electron Darwin terms. They also used correlation consistent basis sets and calculated electron correlations using second order perturbation theory at the MP2 level. They included NMR shielding constants in the four-component relativistic interaction Hamiltonian formulation of QED. Their calculation is the first of its sort to include the Breit interaction. As their calculations of the relativistic effects in water are so very different to the above calculations it is important to compare the results.

Quiney *et al* give a representation of their potential in a similar form to figures 4.1 and 4.2 . Their relativistic correction has a leading term which arises substantially from the oxygen 1s electrons of -0.054880 E_h compared with our leading term of -0.051992 E_h . This term has no influence on the vibration-rotation spectrum. If we re-plot our relativistic correction on a smaller grid and compare this with the correction of Quiney *et al* in figure, 4.7 we can see that they are in extremely good agreement. In fact to the accuracy of their published data the comparative differences between the contour plots are almost unobservable. This agreement confirms our calculations and leads us to believe that first order perturbation theory gives reliable results for the electronic relativistic correction surface for light atoms.

4.5 Discussion and Conclusion

These results show that the relativistic correction has a significant effect on the results of ro-vibrational calculations for the water molecule. The relativistic correction increases the barrier to linearity for water, i.e. $V(R_\pi,R_\pi,\pi)$ - $V(R_e,R_e,\theta_e)$. The effect of this is to raise the band origins of the bending states while bringing the stretching states closer to the

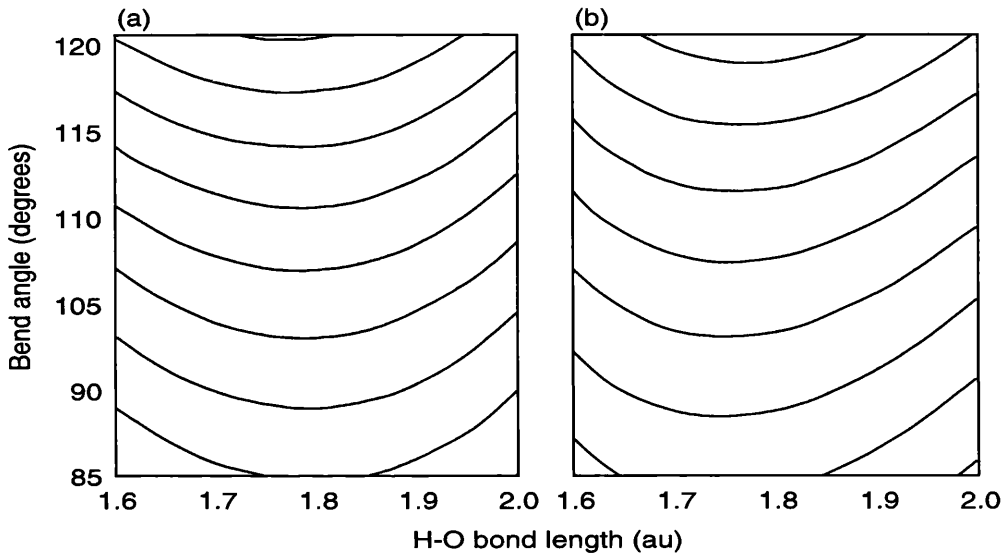

Figure 4.7: Variation of the Relativistic Correction a) Quiney *et al* b) the linear set of variables as a function of bond angle, θ, and bond-lengths r_1 and r_2. The plots are for symmetric stretches only. Contours are spaced by 20 cm^{-1} .

observed values. Conversely however, the relativistic correction lowers the energy of high K_a states. These two effects of the relativistic correction appear to be counter-intuitive as high K_a states are also sensitive to the bending potential. If, however, calculations are performed with just a Born-Oppenheimer potential and a simple augmentation proportional to S_2 this has a similar effect of raising the band-origins of the bending states while lowering the high K_a energy levels, see the following chapter. This effect is due to the linear dependence of the relativistic correction on the angular co-ordinate.

Previous to this work there have been notable difficulties in representing the bending excitations in water and H_2S for spectroscopic data [108, 109]. Our fitting results suggest that the Jensen form of representing the bending potential, used in these works, may constrain the potential for the bending co-ordinates.

The difference in the standard deviation between the *ab initio* potential and the potential with the included relativistic correction is not significantly changed. However the shift in the error is such that the potential greatly improves the predictions of the stretching states but shifts the bending modes away from the observed values. The error in the bending modes will be further discussed in the next chapter of this thesis.

Since publication of these results Polyansky *et al* in 1999 [113] used this relativistic correction in conjunction with the adiabatic and non-adiabatic corrections to analyse many observed water spectra. This led to a major increase in full quantum number assignment for many levels. They doubled the number and energy range of measured energy levels for water. They presented new energy levels for 010, 100, 020, 001, 110, 030, 011, 040 and 050, 060. These levels showed unanticipated features including rotational difference bands and absence of clustering.

Table 4.1: Coefficients in Eq. (2) for the relativistic correction surface of $H_2^{16}O$ for the linear set of variables.

i	j	k	$c_{i,j,k}$	i	j	k	$c_{i,j,k}$
0	0	0	−51992.84954	2	3	0	−64.72097
1	0	0	−53.95314	0	3	2	6.90706
0	1	0	181.69823	1	2	2	75.01079
2	0	0	−623.11790	6	0	0	−480.58626
0	2	0	52.56205	0	6	0	−14.29775
0	0	2	−480.21449	0	0	6	−106.73778
1	1	0	26.32762	1	5	0	−32.71663
3	0	0	638.79701	4	2	0	−150.43974
0	3	0	21.32618	4	0	2	−6951.40466
2	1	0	−281.81284	2	4	0	94.30314
1	2	0	34.28257	0	4	2	83.82776
1	0	2	1873.16555	2	0	4	−3495.23102
0	1	2	−118.38395	0	2	4	173.88804
4	0	0	−347.16232	3	3	0	−233.91349
0	4	0	−8.42200	1	1	2	−35.63530
0	0	4	−553.09740	0	7	0	−3.93461
3	1	0	120.23015	6	1	0	−441.23567
1	3	0	141.02871	1	6	0	−28.51688
2	2	0	−72.44424	5	0	2	5254.70283
2	0	2	−2831.20672	2	5	0	82.57348
0	2	2	−61.31686	4	3	0	357.18441
1	1	2	−9.86563	3	4	0	79.20561
5	0	0	450.82710	3	0	4	3012.69084
0	5	0	−5.02180	4	1	2	161.31404

Table 4.1: continued.

i	j	k	$c_{i,j,k}$	i	j	k	$c_{i,j,k}$
1	4	0	38.88296	2	1	4	−596.36895
1	0	4	1950.21929	1	2	4	−1009.70103
3	2	0	−83.44686	0	8	0	1.68231
3	0	2	4215.27185				

[a] Units are consistent with bond lengths in a_0 and bond angle in rads for energies in μE_h.

Table 4.2: Coefficients in Eq. (2) for the relativistic correction surface of $H_2^{16}O$ for the Jensen set of variables.

i	j	k	$c_{i,j,k}$	i	j	k	$c_{i,j,k}$
0	0	0	−51992.82027	0	1	6	2183.38645
1	0	0	−53.63382	5	2	0	222.30397
0	1	0	−187.80958	5	0	2	3316.60921
2	0	0	−623.83359	2	5	0	620.09708
0	2	0	78.83349	0	5	2	283.58638
0	0	2	−480.68557	4	3	0	399.29719
1	1	0	−26.04338	3	4	0	57.39077
3	0	0	649.49680	3	0	4	−1394.66871
0	3	0	−75.06954	0	3	4	−194.84573
2	1	0	293.20692	4	1	2	−3319.67802
1	2	0	28.13020	1	4	2	−1478.71431
1	0	2	1857.50305	2	1	4	1062.72320
0	1	2	134.74767	1	2	4	−2029.33982
4	0	0	−359.07515	2	3	2	2251.33757
0	4	0	66.73906	3	2	2	−11.17484
0	0	4	−526.86983	8	0	0	380.00884
3	1	0	−130.64582	0	8	0	72.53895
1	3	0	−203.88766	0	0	8	2521.70024
2	2	0	−26.61028	0	2	6	−2566.70935
2	0	2	−2846.46428	4	4	0	384.32905
0	2	2	−87.83111	6	2	0	31.79701
1	1	2	−45.06373	1	1	6	2013.20363
5	0	0	327.48221	1	3	4	592.24438
0	5	0	−76.24252	1	5	2	199.47693

Table 4.2: continued.

i	j	k	$c_{i,j,k}$	i	j	k	$c_{i,j,k}$
4	1	0	46.11794	1	7	0	−528.29951
1	4	0	227.01642	2	0	6	6484.87893
1	0	4	2147.94726	2	2	4	390.14988
0	1	4	−127.65836	2	4	2	1694.46320
3	2	0	−108.03838	2	6	0	1323.88579
3	0	2	3601.47692	3	1	4	−3028.66978
2	3	0	32.13504	3	3	2	26.48411
0	3	2	−67.53152	3	5	0	240.16525
2	1	2	178.42518	4	0	4	2262.60364
1	2	2	456.56520	4	2	2	1836.94086
6	0	0	−402.54046	4	4	0	−483.16699
0	6	0	−26.17174	5	1	2	1324.06660
0	0	6	−544.63778	5	3	0	−669.55108
5	1	0	434.91000	6	0	2	−2434.68170
1	5	0	133.87443	6	2	0	150.83108
4	2	0	−130.27505	7	1	0	1233.80442
4	0	2	−3614.03003	1	8	0	−9495.96490
2	4	0	−640.64613	0	3	6	1506.91447
0	4	2	92.25434	0	5	4	−221.72802
2	0	4	−3152.37862	7	2	0	−357.07978
0	2	4	411.96537	0	9	0	−77.83246
3	3	0	88.50843	1	8	0	−7426.34406
1	1	4	−334.17188	1	2	6	16843.22388
3	1	2	678.79703	1	4	4	−6739.74679
1	3	2	−30.78848	1	6	2	2643.22711

Table 4.2: continued.

i	j	k	$c_{i,j,k}$	i	j	k	$c_{i,j,k}$
2	2	2	−1103.51278	1	8	0	575.85709
7	0	0	3.32992	2	1	6	−19518.01743
0	7	0	39.37177	2	3	4	11922.78448
6	1	0	−1320.00553	2	7	0	−6117.29122
1	6	0	−282.94703	3	0	6	−1412.52945
1	0	6	−809.80386				

[a] Units are consistent with bond lengths in a_0 and bond angle in rads for energies in μE_h.

Table 4.3: Band origins, in cm^{-1}, for $H_2^{16}O$. Results calculated using Born-Oppenheimer (BO), Born-Oppenheimer Diagonal Correction (ΔV^{ad}) and with the relativistic correction (ΔV_{rel}), are given as observed − calculated.

ν_3 even	Obs[a]	b	c	d
(010)	1594.75	−2.65	−2.15	−3.75
(020)	3151.63	−5.12	−4.13	−7.47
(100)	3657.05	−3.49	−3.42	−0.72
(030)	4666.80	−7.53	−6.05	−11.36
(110)	5235.00	−6.20	−5.70	−4.51
(040)	6134.03	−9.90	−7.88	−15.51
(120)	6775.10	−8.64	−7.70	−8.15
(200)	7201.54	−6.38	−6.30	−0.92
(002)	7445.07	−4.89	−5.08	0.38
(050)	7542.39	−12.39	−9.74	−20.33
(130)	8273.98	−11.06	−9.69	−12.00
(210)	8761.59	−9.07	−8.59	−4.65
(060)	8870.5	−14.9	−11.3	−26.2
(012)	9000.14	−7.50	−7.30	−3.15
(220)	10284.37	−11.39	−10.57	−8.10
(022)	10524.3	−7.5	−7.0	−4.2
(300)	10599.69	−8.20	−8.19	−0.17
(102)	10868.88	−8.81	−8.82	−0.71
(310)	12139.2	−10.9	−10.6	−3.8
(112)	12407.64	−11.53	−11.18	−0.86
(240)	13205.1	−16.0	−14.3	−15.7
(042)	13453.7	−14.8	−13.5	−14.3

Table 4.3: continued.

	Obs[a]	b	c	d
(320)	13640.8	−13.0	−12.3	−7.2
(170)	13661.3	−19.7	−16.0	−30.0
(202)	13828.28	−9.43	−9.48	1.09
(122)	13910.90	−13.82	−13.20	−7.77
(400)	14221.16	−12.00	−11.89	−1.15
(004)	14537.5	−9.2	−9.6	1.5
(330)	15108.1	−15.3	−14.4	−10.3
(212)	15344.50	−12.02	−11.80	−2.56
(410)	15742.80	−14.60	−14.23	−4.73
(222)	16825.23	−12.25	−11.78	−4.23
(302)	16898.4	−10.6	−10.7	1.7
(420)	17227.70	−16.36	−15.78	−7.63
(104)	17458.30	−13.38	−13.32	0.03
(500)	17748.07	−13.06	−13.19	0.36
(312)	18392.98	−12.28	−12.25	−0.86
ν_3 odd	Obs[a]	b	c	d
(001)	3755.93	−2.25	−2.34	0.28
(011)	5331.27	−4.83	−4.47	−3.31
(021)	6871.51	−7.39	−6.62	−7.00
(101)	7249.81	−5.32	−5.36	−0.04
(031)	8373.8	−9.9	−8.8	−10.9
(111)	8807.00	−7.95	−7.60	−3.65
(041)	9833.58	−12.24	−10.64	−14.79
(121)	10328.73	−10.29	−9.60	−7.07
(201)	10613.36	−7.72	−7.74	0.22

Table 4.3: continued.

	Obs[a]	b	c	d
(003)	11032.41	−7.01	−7.29	0.93
(131)	11813.19	−12.73	−11.69	−10.74
(211)	12151.26	−10.30	−10.00	−3.31
(013)	12565.00	−9.63	−9.56	−2.50
(141)	13256.2	−15.0	−13.6	−14.6
(221)	13652.66	−12.33	−11.75	−6.27
(301)	13830.94	−9.36	−9.40	1.10
(071)	13835.37	−20.23	−16.61	−31.66
(023)	14066.19	−12.12	−11.79	−5.91
(103)	14318.81	−10.09	−10.23	0.58
(231)	15119.03	−14.77	−13.93	−9.87
(311)	15347.96	−11.77	−11.58	−2.24
(033)	15534.71	−14.60	−14.02	−9.47
(113)	15832.77	−12.66	−12.55	−2.86
(321)	16821.64	−12.94	−12.59	−3.50
(203)	16898.84	−10.53	−10.60	1.72
(123)	17312.54	−14.76	−14.44	−5.84
(401)	17495.53	−12.30	−12.38	0.94
(331)	18265.82	−15.60	−14.99	−7.34
(213)	18393.31	−12.49	−12.44	−1.19
(411)	18989.96	−14.72	−14.65	−2.38
(303)	19781.11	−10.60	−10.66	4.36
(501)	20543.14	−13.65	−13.73	−1.61
(511)	21221.8	−14.0	−13.9	−0.5
(403)	22529.4	−9.4	−9.6	8.2

Table 4.3: continued.

	Obs[a]	*b*	*c*	*d*

[a] Observed fundamentals from refs [114, 115, 125].

[b] Born-Oppenheimer (BO) potential only

[c] BO $+\Delta V^{ad}$ (BODC)

[d] BO $+\Delta V^{ad} + \Delta V_{\text{rel}}$

Table 4.4: Rotational term values, in cm^{-1}, for the vibrational ground state and (010) state of $H_2^{16}O$. Results calculated using Born-Oppenheimer (BO), Born-Oppenheimer Diagonal Correction (ΔV^{ad}) and with the relativistic correction (ΔV_{rel}), are given as observed − calculated.

	Ground state				(010) state			
	Obs[a]	b	c	d	Obs[a]	b	c	d
20_{020}	4048.252	0.542	0.972	0.045	4016.581	0.845	1.216	0.386
20_{120}	4048.252	0.542	0.972	0.045	4016.581	0.844	1.216	0.386
20_{119}	4412.317	0.604	1.077	0.050	4428.049	1.016	1.414	0.554
20_{219}	4412.317	0.603	1.077	0.049	4428.051	1.014	1.406	0.556
20_{218}	4738.624	0.590	1.114	−0.082	4784.599	1.010	1.464	0.404
20_{318}	4738.636	0.590	1.116	−0.081	4784.645	1.010	1.460	0.450
20_{317}	5031.796	0.529	1.116	−0.316	5100.008	0.959	1.493	0.113
20_{417}	5031.977	0.530	1.117	−0.308	5100.554	0.959	1.489	0.159
20_{416}	5292.096	0.402	1.086	−0.719	5374.660	0.802	1.465	−0.435
20_{516}	5294.035	0.441	1.105	−0.610	5379.620	0.880	1.495	−0.175
20_{515}	5513.266	0.192	1.036	−1.479	5598.487	0.488	1.382	−1.608
20_{615}	5527.046	0.364	1.096	−0.886	5627.511	0.832	1.496	−0.384
20_{614}	5680.787	−0.200	0.877	−2.683	5762.306	0.201	1.311	−2.589
20_{714}	5739.232	0.374	1.122	−0.881	5857.784	0.908	1.549	−0.111
20_{713}	5812.074	−0.190	0.894	−2.703	5909.823	0.429	1.398	−1.886
20_{813}	5947.327	0.549	1.227	−0.369	6090.365	1.126	1.630	0.570
20_{812}	5966.827	0.285	1.107	−1.202	6101.535	0.915	1.530	0.040
20_{912}	6167.909	0.985	1.519	0.672	6339.423	1.413	1.728	1.628
20_{911}	6170.964	0.871	1.434	0.438	6341.018	1.385	1.723	1.523
20_{1011}	6407.084	1.071	1.434	1.453	6608.002	1.682	1.797	2.707

Table 4.4: continued

	Ground state				(010) state			
	Obs[a]	b	c	d	Obs[a]	b	c	d
20_{1010}	6407.446	1.063	1.426	1.429	6608.180	1.681	1.805	2.685
20_{1110}	6664.138	1.315	1.518	2.395	6893.156	1.925	1.851	3.761
20_{119}	6664.172	1.317	1.512	2.395	6893.153	1.903	1.828	3.758
20_{129}	6935.425	1.536	1.575	3.304	7191.043	2.126	1.858	4.648
20_{128}	6935.428	1.537	1.578	3.305	7191.041	2.121	1.856	4.646
20_{138}	7217.560	1.711	1.590	4.160	7498.245	2.290	1.840	5.550
20_{137}	7217.560	1.710	1.590	4.159	7498.245	2.286	1.840	5.550
20_{147}	7507.575	1.863	1.585	4.989	7811.766	2.805	2.371	6.471
20_{146}	7507.575	1.863	1.585	4.989	7811.736	2.410	1.771	6.441
20_{156}	7802.700	1.974	1.540	5.778	8128.763	2.495	1.668	7.268
20_{155}	7802.700	1.974	1.540	5.778	8128.763	2.495	1.668	7.268
20_{165}	8100.292	2.054	1.472	6.541	8446.615	2.532	1.520	8.020
20_{164}	8100.292	2.054	1.472	6.541	8446.615	2.532	1.520	8.020
20_{174}	8397.625	2.056	1.305	7.231	8762.590	2.526	1.315	8.695
20_{173}	8397.625	2.056	1.305	7.231	8762.590	2.526	1.315	8.695
20_{183}	8691.916	2.043	1.126	7.919	9073.744	2.441	1.029	9.349
20_{182}	8691.916	2.043	1.126	7.919	9073.744	2.441	1.029	9.349
20_{192}	8979.854	1.939	0.844	8.536	9376.758	2.307	0.673	10.063
20_{191}	8979.854	1.939	0.844	8.536	9376.758	2.307	0.673	10.063
20_{201}	9257.408	1.745	0.458	9.099	9667.337	2.080	0.192	10.542
20_{200}	9257.408	1.745	0.458	9.099	9667.337	2.080	0.192	10.542

[a] Observed rotational term values from refs. [44, 106, 114].

[b] Born-Oppenheimer (BO) potential only

[c] BO $+\Delta V^{ad}$

[d] BO $+\Delta V^{ad} + \Delta V_{\mathrm{rel}}$

Table 4.5: Band origins, in cm^{-1}, for 4 isotopomers of water calculated using (a)Born-Oppenheimer of Partridge and Schwenke, (b) with adiabatic c) with both the adiabatic correction and the relativistic correction

		Obs	a	b	c
D_2O	(010)	1178.38	−1.82	−1.63	−2.54
	(020)	2336.84	−3.49	−3.06	−5.10
	(100)	2671.65	−2.44	−2.45	−0.50
	(001)	2787.72	−2.12	−1.69	−0.50
	(030)	3474.32	−5.09	−4.54	−7.47
	(011)	3956.03	−3.33	−3.26	−1.91
	(031)	6235.08	−6.79	−6.39	−6.90
	(210)	6452.98	−6.62	−6.54	−3.51
	(111)	6533.24	−5.72	−5.66	−2.36
	(121)	7672.92	−7.46	−7.26	−4.82
HDO	(010)	1403.48	−2.30	−2.13	−3.24
	(100)	2723.68	−2.23	−2.29	−0.43
	(020)	2782.01	−4.31	−4.00	−6.13
	(001)	3707.46	−2.94	−2.97	−0.12
	(111)	4099.95	−5.47	−6.13	−6.26
	(030)	4145.48	−6.48	−5.33	−6.95
	(011)	5089.54	−5.19	−5.07	−3.25
	(200)	5363.82	−4.31	−4.46	−0.44
	(101)	6415.46	−5.77	−5.81	−1.60
	(021)	6451.90	−7.07	−6.89	−5.52
	(210)	6746.91	−7.97	−7.93	−5.54
	(002)	7250.52	−5.56	−6.08	0.06

Table 4.5: continued.

		Obs	a	b	c
HTO	(010)	1332.5	−2.13	−1.97	−3.02
	(100)	2299.8	−1.81	−1.83	−0.15
	(001)	3716.6	−3.13	−3.14	−0.49
T_2O	(010)	995.4	−1.43	−1.32	−2.06
	(100)	2237.2	−1.89	−1.90	−0.32
	(001)	2366.6	−1.49	−1.85	−0.50

Chapter 5

The Barrier to linearity

5.1 Introduction

The Potential Energy Surface (PES) is the major factor determining the accuracy of the ro-vibrational spectra of water; as previously discussed in section 1.4. In order to improve upon the accuracy of the PES we must take into account all the physically significant factors. We have previously discussed the effects of including the BODC, section 1.2.1, and the relativistic correction, chapter 4. In this chapter we will discuss the further inclusion of a correction to the barrier to linearity in water. Where we define the barrier to be B = V(R_π, R_π, π) - V(R_e, R_e, θ_e), where for the model used in this work θ_e = 1.82 radians, the equilibrium OH separation, R_e = 1.81 a_o and the saddle point at linearity occurs for R_π=1.76 a_o.

Many authors have discussed that the barrier to linearity for water is not yet well determined. The barrier has been calculated repeatedly in electronic structure computations using both perturbational [9, 35, 93] and variational [55, 118] techniques. Even in variational approaches which improved upon perturbative techniques, the potential does not have the correct behaviour at linearity. Even though spectroscopic techniques and *ab initio* electronic structure studies are becoming increasingly more accurate, the barrier height is still not well determined [7, 35, 52, 73, 78, 81, 92, 102]

Császár *et al* [34] investigated the convergence of the *ab initio* prediction to the one-

and n-particle limits. They tested the inversion barrier of ammonia, water, isocyanic acid, and the torsional barrier to ethane.

Their explicit *ab initio* results were obtained using large basis sets, electron correlational treatments as extensive MP5, full coupled cluster method CCSDT and Bruekner doubles theory including perturbational corrections for both triple and quadruple. Subsequently, basis set and electron correlation extrapolation schemes were invoked to gauge any further variations in arriving at the *ab initio* limit. They accounted for the relative shifts in energy due to the Born-Oppenheimer diagonal correction (BODC), the relativistic correction and the core correlation. Their findings were that while most of the effects are modelled very well by the electronic structure calculations by Partridge and Schwenke [102] the inclusion of higher momentum functions in the basis set has a significant effect on the energy levels. This shows that the *ab initio* potential by Partridge and Schwenke (PS) [102] is not yet converged with basis set size. This lack of convergence results in lowering the barrier to linearity and hence the bending band origins which accounts for the errors found in the bending modes. Császár *et al* water results showed that the inversion barrier is 6 times larger than that of ammonia and that the barrier to linearity in water is the hardest to define. Császár *et al* calculated barrier height was 11046 ± 70 cm^{-1} and their work showed the importance of the relativistic correction and that the correlated energy showed slow convergence.

Further work on the barrier to linearity for water was done by Tarczay *et al* [139]. They performed high quality *ab initio* quantum chemical methods, including high order coupled cluster (CC) and many-body perturbation (MP) theory, explicitly correlated (linear R12) techniques and full configuration interaction (FCI) benchmarks, with basis sets ranging from [O/H][3s2p1d/2s1p] to [8s7p6d5f4g3h2i/7s6p5d4f3g2h] which were employed to obtain the best possible value for the barrier to linearity. They also included small corrections due to one- and two-particle relativistic terms, core correlation effects, and the diagonal Born-Oppenheimer correction (BODC). They, like Császár *et al* experienced convergence problems with respect to basis set size in the Partridge and Schwenke [102]

ab initio potential. Their final value for the barrier height was 11127 ± 35 cm^{-1}. This value for the height of the water barrier is unlikely to be improved upon using conventional electronic structure calculation methodology [82].

For the *ab initio* ground state PES due to Partridge and Schwenke [102], the barrier height, from equilibrium to linearity is 11155 cm^{-1} which with allowance for the adiabatic and the relativistic correction, becomes 11192 cm^{-1} . Partridge and Schwenke found it harder to converge the angular part of the potential and thus the *ab initio* potential performs less well for the bending than the stretching modes.

Table 5.1 shows a summary of different predicted barrier heights obtained by various authors. This table summarises the huge variation and large errors in predicted results and therefore emphasises the difficulty in calculating this barrier height for water.

In the previous chapter the effects of the relativistic correction were discussed. We showed how the relativistic correction raised the barrier height by 50 cm^{-1} , improved the stretching fundamentals while making the bending fundamentals and overtones significantly worse. The frequencies of the overtones are very sensitive to the barrier to linearity. Unfortunately to-date there is little available spectroscopic data for the higher bending overtones. The $5\nu_2$ and $6\nu_2$ band origins have recently been accurately measured [114, 178] and a few levels involving 7 quanta of bend have been assigned [115, 117]. As there is such limited data, the assignment of the water spectra relies on reliable predictions of the bending overtones for higher quanta, and rotationally excited states with high K_a [105]. The high K_a states are also very sensitive to the treatment of the bending overtones and so improvement is needed in the treatment of this co-ordinate.

As there is an not only an absence of fully converged *ab initio* potentials and but also an absence of higher bending overtone data we have attempted an intermediate course. In this chapter we discuss augmenting the full potential (*ab initio* plus the BODC and relativistic correction) with a correction to the bending potential. It will be shown that this further augmentation improves the predictions of the vibrational levels by an order of magnitude and is a good starting point for future spectroscopic analysis.

5.2 Calculations

Again for the calculations in this chapter we test the various PESs mainly for the $H_2^{16}O$ isotopomer and otherwise for HDO, HTO, T_2O and D_2O. The experimental values were again taken from the Hitran database [126], but at the time of this work more experimental data was available from other sources [116, 115, 118, 178]. Additional rotationally excited levels were provided by Flaud *et al* [44] and Polyansky *et al* [106]. For the experimental data that is available standard deviations were calculated from the observed values minus the calculated values. These standard deviations were computed for all available J=0 levels σ_{vib} and for J=20 vibrational ground state energy levels σ_{rot}.

The calculations were performed using the DVR3D program suite [142] discussed in section 2.10 and previously optimised basis sets [107] discussed in section 2.10.5.

The potential used was the potential set up in the last chapter 4, i.e. the Born-Oppenheimer potential due to Partridge and Schwenke [102] augmented by the BODC (Born-Oppenheimer diagonal correction) [176] and the relativistic correction, chapter 4

Here results are, mainly, presented for the hydrogenic masses as half way between nuclear and atomic mass as discussed in section, 1.2.1.

Many different corrected potentials were tested and these are summarised in table 5.2 and figure 5.1.

To define these potentials $\Delta V(\theta)$ we used several different criterion. We only studied potentials which only depend on the HOH bond angle, θ. We define the barrier height to linearity as $B = V(R_\pi, R_\pi, \pi) - V(R_e, R_e, \theta_e)$, the correction to this barrier height as $\Delta B = \Delta V(\pi) - \Delta V(\theta_e)$ and $\Delta V(\theta_e) = 0$. For the model used $\theta_e = 1.82$ radians and the OH equilibrium separation is $R_e = 1.81 a_o$. The saddle point at linearity is at $R_\pi = 1.76 a_o$. The third criterion states

$$\left.\frac{\partial \Delta V}{\partial \theta}\right|_{\theta=\pi} = 0, \tag{5.1}$$

this criterion was introduced during the study as there is insufficient experimental data

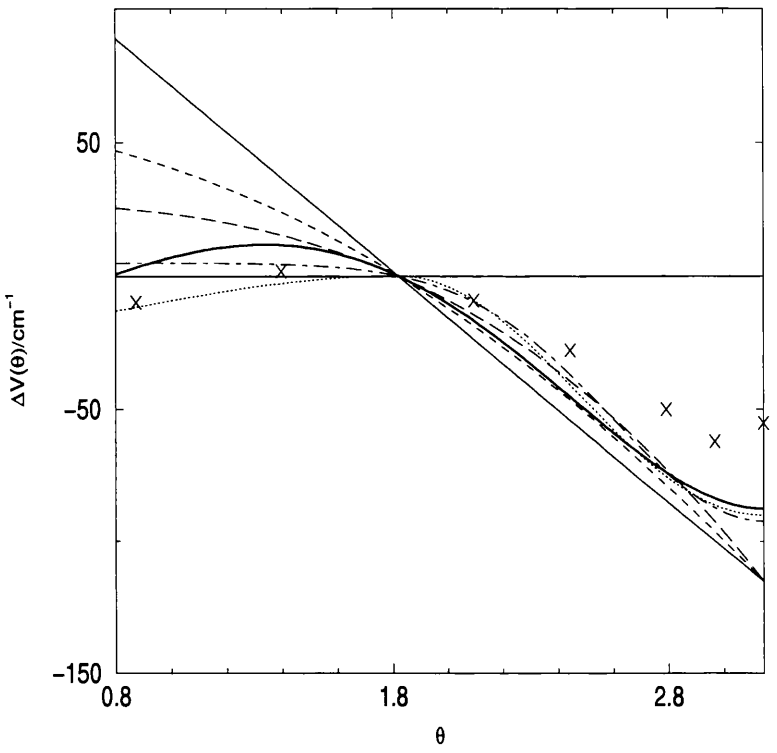

Figure 5.1: Functions, $\Delta V(\theta)$, used to model the correction to the barrier height. Solid line, linear function; dashed line, quadratic function; long dashed line, cubic function; dot-dashed line, Gaussian function; dotted line, sine function. The dark solid line is the final function. x denotes errors estimated by extrapolation from their cc-pV5Z basis by Partridge and Schwenke.

as $\theta -> \pi$ so it is necessary to force the function to have a zero derivative at π.

Initially, for $H_2^{16}O$, a linear function in θ was included in the potential. This is shown in figure 5.1 and table 5.2. The difference in the predicted barrier height by Tarczay *et al* [139] and the barrier height of our overall potential gave us an initial estimate as to how high the correction to the barrier height must be. We therefore started our calculations with a value of ΔB set to 65 cm^{-1} , i.e. 11127 - 11192 cm^{-1} . This correction to the barrier height was successively altered, for all functions, to find the optimum value of ΔB to within $\pm$ 5 cm^{-1} . For the linear function the optimum height of the barrier was $\Delta B = -115$ cm^{-1} . Including this function greatly improved the standard deviation for the vibrational energy levels σ_{vib} while making the results for the rotations, σ_{rot}, slightly worse.

In the paper by Partridge and Schwenke [102] they discuss convergence errors as a function of bond angle. They assume that the energies converge logarithmically and extrapolate the energies to the complete basis set (CBS) limit for the three largest basis sets used. This extrapolation, value minus the energy estimate, gives an approximation of the convergence error in the bending modes. These points are also plotted in figure 5.1. They give an indication of the shape of the correction function that we are looking for, they therefore acted as a guideline to different functions.

The next function to be tested was the quadratic function in θ, which also had an optimum correction to the barrier height of $\Delta B = -115$ cm^{-1} . While still further reducing the errors in the bending modes for the vibrations, this function also significantly reduces the overall error for the rotational energy levels, σ_{rot}. It is instructive to ask why the quadratic function is a better correction to the error for rotations. This is because the correction for $\theta \leq \theta_e$ is a lot smaller and therefore the quadratic function does not over correct in this region. The improved effect of the quadratic function and the shape of the convergence error points suggested that a cubic function may correct better for the errors in the potential. The cubic function improved both the standard deviation for the vibrational energy levels, σ_{vib}, and the rotational energy levels σ_{rot} . The improved predictions for

the rotational energy levels results from the shallower gradient of this function at θ_e.

The experimental data that we have for testing our value of ΔB is not directly sensitive to the value of the potential at $\theta = \pi$, it was therefore considered necessary to force the function to have a zero derivative at $\theta = \pi$, equation 5.1 . With this criterion and the shape of Partridge and Schwenke's convergence points, the obvious choice was a sine or a Gaussian function. The Gaussian function slightly improved the vibrations for a barrier height of $\Delta B = -97$ cm^{-1} .

The sine function which achieved the best results was a two parameter fit. The first parameter is ΔB and the second defines the points at which the curve crosses the $\theta = 0$ axis. The second parameter was chosen to optimise the gradient of the curve at $\theta \leq \theta_e$. The optimum value of ΔB for the sine function is 90 cm^{-1} which is smaller than for the other functions. If, however, the steepest gradient on the curve is extrapolated with a straight line, the barrier height would be in agreement with the previous functions, at around -115 cm^{-1} . These results are good for vibrations and less good for rotations, because the gradient of the curve is too shallow at less than θ_e .

Many other functions were tried and tested and the shape of the function and its overall effect on the motions of the water molecule became well understood so the final function could be chosen.

The final function is also a two parameter fit; again the first parameter is ΔB and the second defines where the curve crosses the $\theta = 0$ axis, again to optimise the gradient at $\theta \leq \theta_e$. The cubic function had the best standard deviation for the rotations and so this second parameter was varied so that the gradient for the final function for just less than θ_e was similar to that of the sine function.

The final function optimised σ_{vib} and σ_{rot} for the water molecule. The final correction to the barrier, ΔB, was found to be -87 cm^{-1} optimised to the nearest wavenumber. If this barrier height is changed by 5 cm^{-1} either side, the overall standard deviation for the vibrations is significantly changed. This prediction of the overall barrier height is therefore much more accurately defined than any other predictions in table 5.1. Confidence in this

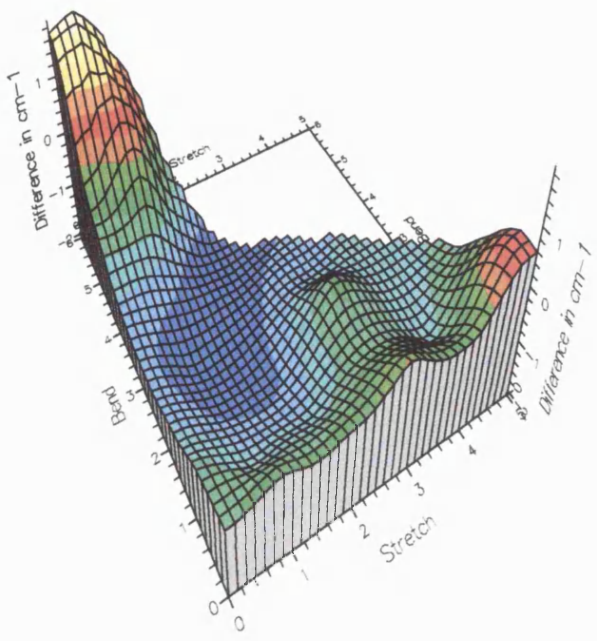

Figure 5.2: Vibrational calculations on Partridge and Schwenke's *ab initio* PES augmented by the Adiabatic Correction, Relativistic Correction and Correction Function. A 3D representation of how Calcs-Obs varies, with quanta of stretch and quanta of bend for J=0.

value is given by the observation that our preliminary studies arrived at the same value despite using less accurate versions of the starting potential.

Table 5.3 shows the overall effect of including this correction to the barrier height on the vibrational energy levels. The results show clearly how the barrier corrects for the errors in the bending modes. As used in the last chapter, we represent these changes in figures 4.5 and 5.2. Figure 4.5 shows how our original potential, PS *ab initio* adiabatic and relativistic, has extremely large errors in the bending modes. Notably, in figure 5.2 the errors, especially in the bending modes, are very much improved.

The J=20 rotational energy levels for the ground vibrational state are shown in Table 5.4, with and without the correction to the barrier. For higher vibrational states there is a shortage of experimental data for high K_a. Table 5.4 shows the overall improvement of

the results with the included barrier, yet the errors still increase with K_a.

Table 5.5 shows how this final function, when added to the PS *ab initio* adiabatic and relativistic correction, effects the overall vibrational levels for other isotopomers of water. We can see clearly that again the effect is very similar and vastly improves the large error in the bending modes for all isotopomers. However as discussed by Zobov *et al* [176] and earlier in section, 1.2.1 the errors for HDO and HTO are larger than for H_2O, D_2O and T_2O which suggests there is still a residual non-Born-Oppenheimer problem.

5.3 Discussion and Conclusion

These results confirm that the Partridge and Schwenke *ab initio* potential, augmented by the adiabatic and relativistic correction, is not as yet well-converged.

The correction shows that the potential needs further correction on the bending modes, without significantly affecting the stretching modes. In this way a careful choice of correcting function can improve the overall results for ro-vibrational motion of the water molecule.

The main error with the underlying potential is in the bending modes. It would therefore seem implicit that correcting for these errors will improve the overall standard deviations for the ro-vibrational motion. Unfortunately the system is more complicated as stretching and bending motions are never entirely independent. This complication means that the final function was a subtle balance of improving the bends without significantly altering the stretches.

The final correction function is similar in shape, although 50 percent larger, than the basis set truncation error found by Partridge and Schwenke as part of their *ab initio* study. This function will act as a guide to how future *ab initio* surfaces should be improved, although these studies would automatically include bend-stretch coupling.

In table 5.3 it shows that some of the pure stretching states are made a little worse, with the inclusion of the correction function, however the overall standard deviation is significantly improved and the errors are made a lot more uniform. The fact that the

errors are now more uniform in the bending and stretching modes makes the extrapolation of this potential much better.

Tables 5.4 shows that this correcting function also greatly improves the results for the rotational motion. These tables and figure 5.3 show there is still a gradual increase in error with increased K_a. The corrected potential therefore is a good starting point for a fitted potential, this will be discussed in the next chapter.

Table 5.1 shows that our prediction of the barrier to linearity is 11105±5 cm^{-1} which is in good agreement with other authors. This prediction falls within the errors of the two most recent studies by Császár *et al* , 11046 ± 70 cm^{-1} and Tarczay *et al* , 11127 ± 35 cm^{-1} . Our prediction, however, has a much smaller error and so is significantly more accurate.

This overall potential has recently been used by Zobov *et al* [177], from which they created a water line-list and assigned water spectra in 21400-25000 cm^{-1} region. This would not have been possible with a less accurate potential.

Since publication of these results Valeev *et al* [159] improved upon previous *ab initio* calculations on the barrier to linearity in water. These high quality computational methods used conventional (MP2) and explicitly correlated second order Møller Plesset energies (MP2-R12/A) to arrive at a new *ab initio* prediction for this barrier height. They used basis functions with high orbital quantum numbers (g- and h-), when previous calculations had only used up to f-.

Their final estimate of the MP2 contribution to the barrier is -363 cm^{-1} which is much lower than previous theoretical predictions. The overall estimate for the barrier they found to be 11113 ± 10 cm^{-1} which is in excellent agreement with the above empirical result of 11105 ± 5 cm^{-1} .

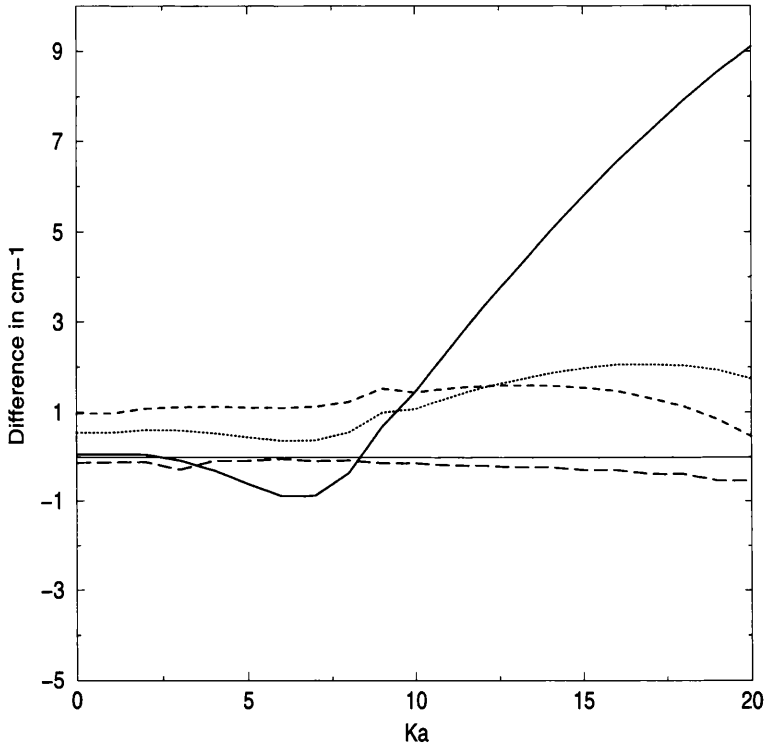

Figure 5.3: A graph to show Obs - Calcs for J=20 with increasing K_a. Dotted line, *ab initio* ; dashed line,*ab initio* + adiabatic; solid line, *ab initio* + adiabatic + relativistic; long-dashed line, *ab initio* + adiabatic + relativistic + correction.

Table 5.1: A comparison of predicted barriers to linearity for water ($H_2^{16}O$ when adiabatic effects are considered).

	Year	Barrier Height	Comments
Carter and Handy [25]	**1987**	11493 cm^{-1}	Spectroscopic Empirical
Jensen [75]	**1989**	11246 cm^{-1}	Spectroscopic Empirical
Polyansky *et al* [109]	**1996**	10966 cm^{-1}	Spectroscopic Empirical
Partridge and Schwenke (PS) [102]	**1997**	11155 cm^{-1}	*ab initio*
Partridge and Schwenke [102]	**1997**	11128 cm^{-1}	Spectroscopic Empirical
PS, adiabatic, relativistic	**1998**	11192 cm^{-1}	*ab initio*
Császár *et al* [34]	**1998**	11046 $\pm$ 70 cm^{-1}	Extrapolated *ab initio*
Lanquetin *et al* [87]	**1999**	11154 cm^{-1}	Effective Hamiltonian
Tarczay *et al* [139]	**1999**	11127 $\pm$ 35 cm^{-1}	High accuracy *ab initio*
This work [W.2]	**1999**	11105 $\pm$ 5 cm^{-1}	Corrected *ab initio*
Baer *et al* [5]	**2000**	11050 $\pm$ 80 cm^{-1}	High accuracy *ab initio*
Valeev *et al* [159]	**2000**	11113 $\pm$ 10 cm^{-1}	High accuracy *ab initio*

Table 5.3: Band origins, in cm^{-1} , for the $H_2^{16}O$, even parity only. Results calculated using (a) Born-Oppenheimer of Partridge and Schwenke, (b) with adiabatic and relativistic corrections added and (c) with the addition of our final angular correction, given as observed − calculated.

	Obs	a	b	c
(010)	1594.75	−2.65	−3.44	−.10
(020)	3151.63	−5.12	−6.86	−.07
(100)	3657.05	−3.49	−0.62	−.85
(030)	4666.80	−7.53	−10.43	.04
(110)	5235.00	−6.20	−4.13	−1.06
(040)	6134.03	−9.90	−14.26	.26
(120)	6775.10	−8.64	−7.50	−1.06
(200)	7201.54	−6.38	−0.70	−1.28
(002)	7445.07	−4.89	0.70	−.86
(050)	7542.39	−12.39	−18.70	.57
(130)	8273.98	−11.06	−11.07	−1.08
(210)	8761.59	−9.07	−4.18	−1.50
(060)	8870.54	−14.87	−23.98	1.39
(012)	9000.14	−7.50	−2.57	−1.01
(220)	10284.37	−11.39	−7.41	−1.50
(022)	10524.3	−7.5	−3.4	1.30
(300)	10599.69	−8.20	−0.19	−.96
(102)	10868.88	−8.81	−0.33	−1.66
(310)	12139.2	−10.9	−3.3	−1.24
(112)	12407.64	−11.53	−4.38	−1.85
(240)	13205.1	−16.0	−14.5	−1.42

Table 5.3: continued.

	Obs	a	b	c
(042)	13453.7	−14.8	−13.0	−1.40
(320)	13640.8	−13.0	−6.4	−.79
(170)	13661.3	−19.7	−27.6	.45
(202)	13828.28	−9.43	1.58	−.06
(122)	13910.90	−13.82	−6.99	−1.91
(400)	14221.16	−12.00	−0.71	−1.97
(004)	14537.51	−9.18	2.0	−.97
(330)	15108.24	−15.11	−9.21	−1.26
(212)	15344.50	−12.02	−1.89	−.19
(410)	15742.80	−14.60	−4.11	−2.12
(222)	16825.23	−12.25	−3.36	1.79
(302)	16898.4	−10.6	2.3	1.30
(420)	17227.70	−16.36	−6.86	−1.68
(104)	17458.30	−13.38	0.56	−1.06
(500)	17748.07	−13.06	0.96	−1.46
(312)	18392.98	−12.28	−0.14	1.85
	σ_{vib}	10.63	8.48	1.25

Table 5.2: Different functions, $\Delta V(\theta)$, used to correct the angular potential. Also given are the standard deviation of the vibrational modes, σ_{vib}, the standard deviation of the rotational levels, σ_{rot}, and the correction to the barrier height, ΔB.

	$\Delta V(\theta)$	$\sigma_{vib}/\mathrm{cm}^{-1}$	$\sigma_{rot}/\mathrm{cm}^{-1}$	$\Delta B/\mathrm{cm}^{-1}$
	0	8.5	4.5	[11192][a]
linear	$\frac{\Delta B(\theta-\theta_e)}{\pi-\theta_e}$	4.8	5.9	−115
quadratic	$\frac{\Delta B(\theta^2-\theta_e^2)}{\pi^2-\theta_e^2}$	3.5	2.4	−115
cubic	$\frac{\Delta B(\theta^3-\theta_e^3)}{\pi^3-\theta_e^3}$	3.0	0.4	−115
Gaussian	$\Delta B\left(\exp\left(\frac{-\pi(\theta-\pi)^2}{\theta_e}\right)-\exp\left(\frac{-\pi(\theta_e-\pi)^2}{\theta_e}\right)\right)$	2.0	1.6	−97
sine[b]	$E\sin^2\left(\frac{\pi(\theta-\theta_e)}{2\theta_e}\right)\ \ \theta\le\theta_e$ $\Delta B\sin^2\left(\frac{\pi(\theta-\theta_e)}{2(\pi-\theta_e)}\right)\ \ \theta\ge\theta_e$	3.7	1.5	−90
final[c]	$F\frac{(\theta^3-\theta_e^3)}{(\theta_e^3-\pi^3)}+G\frac{(\theta^5-\theta_e^5)}{(\theta_e^5-\pi^5)}-$ $(\Delta B+F+G)\frac{(\theta^2-\theta_e^2)}{(\theta_e^2-\pi^2)}$	1.3	0.3	−87.5 (11192-87.5 ≈ 11105)

[a] Actual barrier height,B, when $\Delta V(\theta)=0$

[b] $E=-22\ \mathrm{cm}^{-1}$.

[c] $F=879.7\mathrm{cm}^{-1}$, $G=-381.1\mathrm{cm}^{-1}$.

Table 5.4: Rotational term values, in cm^{-1}, for the vibrational ground state of $H_2{}^{16}O$. Results calculated using (a) Born-Oppenheimer of Partridge and Schwenke, (b) with adiabatic and relativistic corrections added and (c) with the addition of our final angular correction, given as observed − calculated.

	Obs	a	b	c
20_{020}	4048.252	−0.53	0.30	.19
20_{120}	4048.252	−0.53	0.30	.19
20_{119}	4412.317	−0.57	0.33	.22
20_{219}	4412.317	−0.57	0.33	.22
20_{218}	4738.624	−0.66	0.23	.26
20_{318}	4738.636	−0.66	0.23	.26
20_{317}	5031.796	−0.80	0.04	.28
20_{417}	5031.977	−0.79	0.04	.28
20_{416}	5292.096	−0.99	−0.31	.32
20_{516}	5294.035	−0.95	−0.21	.32
20_{515}	5513.266	−1.26	−0.99	.40
20_{615}	5527.046	−1.08	−0.45	.35
20_{614}	5680.787	−1.69	−2.06	.44
20_{714}	5739.232	−1.12	−0.44	.36
20_{713}	5812.074	−1.70	−2.07	.45
20_{813}	5947.327	−1.00	0.05	.37
20_{812}	5966.827	−1.27	−1.70	.39
20_{912}	6167.909	−0.62	1.00	.51
20_{911}	6170.964	−0.73	0.79	.45
20_{1011}	6407.084	−0.59	1.70	.29

Table 5.4: continued.

	Obs	a	b	c
20_{1010}	6407.446	−0.60	1.68	.29
20_{1110}	6664.138	−0.40	2.55	.23
20_{119}	6664.172	−0.40	2.55	.24
20_{129}	6935.425	−0.24	3.39	.20
20_{128}	6935.428	−0.24	3.39	.20
20_{138}	7217.560	−0.13	4.15	.15
20_{137}	7217.560	−0.13	4.15	.15
20_{147}	7507.575	−0.03	4.91	.10
20_{146}	7507.575	−0.03	4.91	.10
20_{156}	7802.700	−0.02	5.61	.05
20_{155}	7802.700	−0.02	5.61	.05
20_{165}	8100.292	−0.05	6.30	.00
20_{164}	8100.292	−0.05	6.30	.00
20_{174}	8397.625	−0.00	6.91	−.10
20_{173}	8397.625	−0.00	6.91	−.10
20_{183}	8691.916	−0.06	7.51	−.17
20_{182}	8691.916	−0.06	7.51	−.17
20_{192}	8979.854	−0.21	8.03	−.30
20_{191}	8979.854	−0.21	8.03	−.30
20_{201}	9257.408	−0.42	8.49	−.48
20_{200}	9257.408	−0.42	8.49	−.48

Table 5.5: Band origins, in cm^{-1} for 4 isotopomers in water calculated using (a)Born-Oppenheimer of Partridge and Schwenke, (b) with adiabatic and relativistic corrections added and (c) with the addition of our final angular correction, given as observed − calculated.

		Obs	a	b	c
D_2O	(010)	1178.38	−1.82	−2.54	−0.14
	(020)	2336.84	−3.49	−5.10	−0.16
	(100)	2671.65	−2.44	−0.50	−0.57
	(001)	2787.72	−2.12	−0.50	−0.25
	(030)	3474.32	−5.09	−7.47	−0.12
	(011)	3956.03	−3.33	−1.91	−0.32
	(031)	6235.08	−6.79	−6.90	−0.55
	(210)	6452.98	−6.62	−3.51	−1.26
	(111)	6533.24	−5.72	−2.36	−0.82
	(121)	7672.92	−7.46	−4.82	−0.96
HDO	(010)	1403.48	−2.30	−3.24	−0.34
	(100)	2723.68	−2.23	−0.43	−0.50
	(020)	2782.01	−4.31	−6.13	−0.53
	(001)	3707.46	−2.94	−0.12	−0.71
	(111)	4099.95	−5.47	−6.26	−0.82
	(030)	4145.48	−6.48	−6.95	−0.89
	(011)	5089.54	−5.19	−3.25	−1.01
	(200)	5363.82	−4.31	−0.44	−1.04
	(101)	6415.46	−5.77	−1.60	−1.45
	(021)	6451.90	−7.07	−5.52	−1.39

Table 5.5: continued.

		Obs	a	b	c
	(210)	6746.91	−7.97	−5.54	−2.52
	(002)	7250.52	−5.56	0.06	−1.12
HTO	(010)	1332.5	−2.13	−3.02	−0.27
	(100)	2299.8	−1.81	−0.15	−0.42
	(001)	3716.6	−3.13	−0.49	−0.82
T_2O	(010)	995.4	−1.43	−1.32	−0.08
	(100)	2237.2	−1.89	−1.90	−0.31
	(001)	2366.6	−1.49	−1.85	−0.65

Table 5.6: Band origins, in cm^{-1} for the $H_2^{16}O$, even parity only. Results calculated using Born-Oppenheimer of Partridge and Schwenke,with adiabatic and relativistic corrections added and the addition of our final angular correction, given as observed − calculated for nuclear, middle and atomic masses

	Obs	Nuclear	Middle	Atomic
(010)	1594.75	−.30	−.10	.09
(020)	3151.63	−.44	−.07	.31
(100)	3657.05	−1.30	−.85	−.39
(030)	4666.80	−.51	.04	.59
(110)	5235.00	−1.70	−1.06	−.40
(040)	6134.03	−.44	.27	.97
(120)	6775.10	−1.90	−1.06	−.23
(200)	7201.54	−2.09	−1.28	−.34
(002)	7445.07	−1.72	−.86	.07
(050)	7542.39	−.26	.58	1.41
(130)	8273.98	−2.06	−1.08	−.07
(210)	8761.59	−2.49	−1.50	−.37
(060)	8870.54	.47	1.40	2.32
(012)	9000.14	−2.06	−1.01	.09
(220)	10284.37	−2.66	−1.50	−.19
(022)	10524.3	.07	1.30	2.58
(300)	10599.69	−2.25	−.96	.24
(102)	10868.88	−2.88	−1.66	−.27
(310)	12139.2	−2.61	−1.24	.23
(112)	12407.64	−3.24	−1.85	−.27

Table 5.6: continued.

	Obs	Nuclear	Middle	Atomic
(240)	13205.1	−2.90	−1.42	.20
(042)	13453.7	−2.93	−1.40	.20
(320)	13640.8	−2.32	−.79	.85
(170)	13661.3	−1.06	.45	1.99
(202)	13828.28	−2.90	−.06	.25
(122)	13910.90	−3.46	−1.91	−.15
(400)	14221.16	−3.70	−1.97	−.31
(004)	14537.51	−2.55	−.97	.85
(330)	15108.24	−2.96	−1.26	.55
(212)	15344.50	−3.07	−.20	.43
(410)	15742.80	−3.94	−2.12	−.20
(222)	16825.23	−.29	1.79	3.61
(302)	16898.4	.49	1.30	4.30
(420)	17227.70	−3.64	−1.68	.43
(104)	17458.30	−4.11	−1.06	−.05
(500)	17748.07	−3.71	−1.46	.42
(312)	18392.98	−.52	1.85	3.60

Chapter 6

Empirical Potential Energy Surface (PES)

As previously discussed the potential energy surface (PES) is the major factor determining the accuracy of the rotation-vibration spectra of water. In section 1.4 it was shown that even the best empirical potential by Partridge and Schwenke (PS) [102] does not achieve spectroscopic accuracy. The overall *ab initio* potential of PS augmented by the BODC [176], the relativistic correction, section 4, and the correction to the barrier, section 5, as presented in this thesis was considered to be a good starting point for the new empirical potential energy surface discussed in this chapter.

6.1 Calculations

For many years empirically fitted potentials were modifications of the *ab initio* potentials. If, however, the potential can be divided into various physical contributions, each component can be modified individually giving a better fit to the observed data [71, 88]. Another method is to simply scale the *ab initio* potential by a constant factor to improve the overall agreement with experiment [17, 65, 72]; this modifies the energies while leaving the stationary points unchanged. The concept of morphing multiplies the co-ordinates by scaling factors i.e. changes the stationary position geometry while leaving the energetics

unchanged. The idea of morphing was first introduced by Bowman *et al* [13, 14, 50] in 1991 for the HCO and the HCN molecule. Bowman *et al* morphed the co-ordinates and then did subsequent energy scaling. A more refined method is presented by Meuwly and Hutson [95] in 1999 for Ne-HF where they morph their potential at the same time as energy scaling. The method used here closely follows their work.

In theory the morphing process should adjust the PES by a small amount to improve the agreement with experiment. It is important, for example, to keep the equilibrium values r_e and θ_e fairly constant for water so that the rotational levels will not change wildly. In principle the morphing process is just a question of choosing the appropriate parameters and performing a least-squares fitting calculation.

It was considered that a two-step morphing calculation would be done on the PS *ab initio* potential, augmented by the BODC, the relativistic correction and the correction to the barrier height. In the previous chapter when correcting the discrepancy in the barrier to linearity, a function of θ only was used. In this chapter we consider that the error in the predictions of the barrier to linearity $(V_\pi, R_\pi, \pi) - V(R_e, R_e, \theta_e)$ may be improved by multiplicative functions which also depends on r_1 and r_2, as stretching and bending motions are never entirely independent. This was the first step of the two-step morphing process. The second step morphs the entire *ab initio* potential V_{ai}.

The new empirical potential V_{emp} was chosen to be

$$V_{emp} = M_f^{(2)}(r_1, r_2, \theta)(V_{PS} + \Delta V_{ad} + \Delta V_{rel} + M_f^{(1)}(r_1, r_2, \theta)\Delta B) \tag{6.1}$$

Where V_{PS} is the Partridge and Schwenke *ab initio* PES [102], ΔV_{ad} is the BODC (Born-Oppenheimer Diagonal Correction) by Zobov *et al* [176], ΔV_{rel} is the relativistic correction, in chapter 4, and ΔB is the correction to the barrier height, discussed in previous chapter 5. $M_f^{(1)}$ and $M_f^{(2)}$ are the morphing functions using the symmetrised displacement co-ordinates with the Jensen functional form [75] for the angular part, which has a zero derivative at π given by

$$S_1 = \frac{r_1 + r_2}{2} - r_e \tag{6.2}$$

$$S_2 = \cos(\theta) - \cos(\theta_e) \tag{6.3}$$

$$S_3 = \frac{r_1 - r_2}{2}. \tag{6.4}$$

It is possible to rewrite expression 6.1 so that there are two independent morphing functions multiplying different parts of the potential. However, it was feared that this form would lead to strongly correlated fits, that is to say that the iteration process may diverge the results or produce large errors.

This functional form of the morphing function was expressed as a simple power series, given in equation 6.5. $\mathrm{M}_f^{(2)}$, the overall morphing function, is written as

$$M_f^{(2)} = \sum_{i,j,k} c_{i,j,k} S_1^i S_2^j S_3^k. \tag{6.5}$$

$\mathrm{M}_f^{(1)}$ is very similar except that the correction to the barrier height is chosen as the first parameter in the fitting process. Although the correction to the barrier height ΔB was optimised in the previous chapter, this further morphing may alter the optimisation slightly and so it is included in the morphing function as parameter c_1.

$$M_f^{(1)} = c_1 + \sum_{i,j,k} c_{i,j,k} S_1^i S_2^j S_3^k \tag{6.6}$$

The parameters of the two morphing functions $\mathrm{M}_f^{(1)}$ and $\mathrm{M}_f^{(2)}$ were optimised independently, as the two functions are highly correlated. The correction to the barrier height ΔB depends strongly on θ, and so $M_f^{(1)}$ mainly improved the bending modes, while $\mathrm{M}_f^{(2)}$ had a much greater effect on the stretching states. It was initially thought that the correct order for optimising the parameters would be to start with $\mathrm{M}_f^{(1)}$, fix these parameters and then optimise the parameters for $\mathrm{M}_f^{(2)}$. In practice the procedure was a lot more complicated. With increased accuracy of the empirical potential, either the error in the bending modes

or the stretching states would dominate and thus either $M_f^{(1)}$ or $M_f^{(2)}$, respectively, would have to be re-optimised. After considerable manipulation it was found that the only parameter of $M_f^{(1)}$ to have a noticeable effect on the overall standard deviation was that of the barrier height. However, for further, more accurate fits, the fitting routine written for this work, FIT (see appendix B), will almost certainly utilise this function.

The fitting procedure involves adding and removing parameters so that the solution becomes increasingly more accurate. The standard deviation which was optimised in this fitting process was the difference between the overall calculated energy levels and the observed energy levels. Very recently Tennyson *et al* [152] produced a very accurate database of the observed ro-vibrational energy levels for water. A major advantage of this list is that it incorporates all the previously published experimental data into one list. This work also establishes which levels are correctly assigned, by comparison with theoretical linelists, when there was, previously, more than one assignment in the literature. Some of the energy levels have been given reassignments, which is important for pattern recognition, as discussed later. These levels, also, all have an error attached which becomes important as the calculated results get closer to the observed values. These observed energy levels were therefore used in the fitting process. In fact, without this new catalogue of energy levels, the accuracy of the empirical fits would be limited as the parameters would be falsely forced to incorrect levels.

Initial nuclear motion calculations were the same as those used in the previous chapter using the DVR3D programme suite, section 2.10. Values of the basis set parameters (NEVAL, NPNT2, NALF, MAX3D, RE1, DISS1, WE2), section 2.10.5, were taken from Nic Fulton's thesis [45]. Convergence tests in this work showed that the number of NPNT1 and NPNT2 points (the number of DVR points for r_1 and r_2) needed to be increased to 28 for convergence up to 18000 cm^{-1} . The analytical derivatives for the fitting routine were calculated using XPECT3 (section 2.10.3 and appendix A). The fitting routines used were LSQFIT and FIT, discussed in appendix B. All results are presented for the hydrogenic masses as half-way between the nuclear and the atomic mass as discussed in section 1.2.1.

To begin with, parameters were fitted for J=0, even parity, up to 18500 cm^{-1} as this is computationally very rapid i.e. CPU around 10 minutes on the FUJI VP300 Fujitsu machine in Manchester. Patterns in the observed minus the calculated levels gave insight into which further parameters should be included/removed. To a good approximation, for increased quanta of symmetric stretch, bend, asymmetric stretch (v_1,v_2,v_3) and combinations of all three, higher orders of S_1, S_2 and S_3, respectively, are required in the fit. The patterns found in the fitting process confirmed many reassigned levels by Tennyson *et al* [152]. All the observed energy levels only accurate to the nearest whole number of wavenumbers, or estimates of levels in Tennyson *et al* [152] were removed from the fitting process. These removed levels are summarised in table 6.1.

Convergence testing at this point showed that levels with high quanta of symmetric stretch were un-converged. Therefore, the number of radial grid points was increased from 21 to 28 and angular grid points from 30 to 40, increasing the CPU time to around 15 minutes.

Table 6.2 shows these initial 15 overall morphing parameters i.e. $M_f^{(2)}$, for J=0 even parity only, vibrational energy levels. The correction to the barrier height, i.e. c_1, was in this case found to be 82.5 cm^{-1} and the barrier to linearity to be 11109.5 $\pm$ 5 cm^{-1}.

In table 6.3 we compare the vibrational energy levels obtained with these parameters with the Partridge and Schwenke results for their empirical fit. This table shows that although their results are more accurate for lower vibrational energies they extrapolate far worse for energies above 16000 cm^{-1} . In Partridge and Schwenke's paper [102], vibrational energy levels up to 16000 cm^{-1} only, were published and the (060) vibrational level was not included, which has a large error. It can also be seen from this table that our overall standard deviation is half that of Partridge and Schwenke's.

When odd parity vibrational levels were calculated using the parameters given in table 6.2, the standard deviation for the odd levels was far worse than with even-only levels. The largest deviations of the calculated from the observed was for levels with non-zero quanta of asymmetric stretch. Calculations of rotational levels with these parameters in

table 6.2 were also worse than the results with V_{ai} before fitting.

In 1996 Xie and Yan [174] produced a spectroscopically-determined potential energy surface for $H_2^{16}O$ for vibrational calculations only which produced a standard deviation of 1.1 up to 21221 cm^{-1} . In 1997 Schryber *et al* [127] discussed using Xie and Yan's potential energy surface for rotations and reported that for high K_a values, their spectroscopically-determined PES produced very large errors of around 28-30 cm^{-1} . In order that this work shouldn't suffer from the same problem, parameters were then fitted to J=0 even, J=0 odd levels and J=2 even levels and checked for J=10 and J=20. These new parameters are given in table 6.4 which and are similar to those in table 6.2 but with minor alterations and 3 additional levels.

Table 6.5 shows the new set of even and odd parity levels for the new parameters given in table 6.4. It can be seen that the overall standard deviation, σ_{vib} is 0.22, compared with Partridge and Schwenke's empirical fit where σ_{vib} is 0.24. Both are an order of magnitude better than the result obtained with V_{ai}, of $\sigma_{vib} = 1.12$.

Results for the A_1 symmetry for J=2 are given in table 6.6 as observed minus calculated. This table shows that the J=2 even parity levels are predicted to the same accuracy as those found using Partridge and Schwenke's empirical potential energy surface. Similar results were obtained for the A_2, B_1 and B_2 symmetries. Result for the A_1 symmetry for J=10 are presented in table 6.7 for the vibrational fundamentals of $H_2^{16}O$. These results are compared to the results using the *ab initio* PES, V_{ai}. There is a general overall improvement in the standard deviation from 0.43 to 0.34 however the predictions for the (010) levels are further from the observed values; this would suggest that further work needs to be done in optimising the barrier height for this PES.

Table 6.8 shows how the predictions for the D_2O and T_2O isotopomers of water are improved by the empirical potential defined above. This table shows that observed-calculated results are marginally worse than they are for $H_2^{16}O$, which is to be expected as the fitting procedure was done purely with this isotopomer. Additional fitting calculations would further improve the errors for each individual isotopomer.

6.2 Conclusions

The empirical potential energy surface, V_{emp}, presented here vastly improves the overall standard deviation for both vibrational and $J \leq 5$ rotational energy levels as compared with the *ab initio* potential energy surface, V_{ai}, introduced in previous chapters. Table 6.5 shows the improvement in the predictions for the vibrational energy levels to be of an accuracy marginally better than the accuracy obtained with Partridge and Schwenke's empirical surface. Table 6.6 shows that this potential also predicts the J=2 rotational energy levels to the same accuracy as Partridge and Schwenke's potential energy surface. Table 6.8 shows that this empirical surface improves the predictions for the isotopomers of water.

In summary this surface is as accurate as Partridge and Schwenke's is for $J \leq 5$ but is less accurate for higher values of J. So in many respects this empirical potential energy surface is no better than Partridge and Schwenke's potential energy surface, however only 18 parameters are needed to give an overall improvement in both the vibrational and rotational energy levels. There is therefore room for improvement of this empirical surface, reducing the overall difference between experimental levels and theoretical levels. In order to improve, further, on the accuracy of the above empirical potential, large scale calculations involving many more rotational levels would be needed. The next step is to run calculations for $J \leq 5$ inclusive in order to improve the rotational energy level calculations.

Further improvement to this surface maybe found by considering mass effects to partially account for non-adiabatic behaviour, see section 1.2.1.

This empirical surface also gives a new estimate for the barrier height to linearity, 11109.5 ± 5 which is within the error bars of our previous calculation in chapter 5 and agrees with the two most recent predictions by Valeev *et al* [159] (11113 ± 10 cm^{-1}) and Baer *et al* [5] (11050 ± 80 cm^{-1}).

Even		Odd	
(022)	10521.8	(051)	11242.8
(240)	13205.	(061)	12586.
(042)	13453.6	(141)	13256.2
(320)	13640.7	(151)	14648.2
(170)	13661.	(241)	16546.3
(132)	15377.7	(043)	16967.5
(340)	16534.3	(053)	18350.3
(142)	16796.0	(133)	18758.6
(420)	16823.	(341)	19679.1
(500)	16898.4	(063)	19721.
(222)	17227.3	(421)	19863.3
(104)	17748.1	(223)	20442.3
(430)	18271.	(431)	21312.
(600)	19781.	(115)	22513.
(402)	20533.6	(611)	23940.

Table 6.1: Vibrational energy levels from Tennyson *et al* [152] removed from the fitting procedure

i	j	k	$c_{i,j,k}$	i	j	k	$c_{i,j,k}$
0	0	0	999831.602	0	2	0	−202.473
1	1	0	18459.850	0	3	0	−1380.016
1	0	1	12883.966	0	4	0	1477.356
2	0	0	−6917.189	0	1	1	8441.950
3	0	0	13932.557	2	1	0	−31824.653
0	0	2	−4027.303	2	0	1	−7547.532
0	0	3	−7184.089	1	2	0	−826.654
4	0	0	−2901.917				

Table 6.2: Initial coefficients of $M_f^{(1)}$ for $H_2^{16}O$. Units are consistent with bond lengths in a_0 and bond angle in radians for energies in μE_h.

Table 6.3: Band origins, in cm^{-1}, for $H_2^{16}O$. Results calculated as observed, (a) Values from Tennyson *et al* [152], minus calculated, (b) Partridge and Schwenke's empirical potential, (c) V_{emp} for this work

	Obs[a]	b	c
(010)	1594.746	−0.03	−0.03
(020)	3151.630	0.01	0.05
(100)	3657.053	0.01	−0.11
(030)	4666.790	0.00	0.11
(110)	5234.978	−0.06	−0.20
(040)	6134.015	−0.02	0.14
(120)	6775.093	−0.02	−0.12
(200)	7201.540	−0.01	0.02
(002)	7445.045	−0.07	0.03
(050)	7542.437	−0.07	0.17
(130)	8273.976	−0.08	−0.09
(210)	8761.582	−0.09	−0.12
(060)	8869.954	−0.63	−0.18
(012)	9000.136	0.03	0.07
(220)	10284.367	0.01	−0.03
(300)	10599.686	−0.01	0.08
(102)	10868.876	−0.04	0.11
(230)	11767.390	−0.14	−0.10
(032)	12007.776	−0.14	−0.13
(310)	12139.315	−0.06	−0.11
(112)	12407.662	−0.01	0.06
(400)	13828.277	0.11	0.05

Table 6.3: continued.

	Obs[a]	b	c
(122)	13910.896	0.09	0.08
(202)	14221.161	0.03	0.20
(004)	14537.504	0.10	0.12
(330)	15108.239	0.08	0.12
(410)	15344.503	0.10	−0.18
(212)	15742.795	0.02	0.03
(302)	17458.354	0.43	−0.04
(510)	18392.974	1.02	0.18
	σ_{vib}	0.24	0.12

i	j	k	$c_{i,j,k}$	i	j	k	$c_{i,j,k}$
0	0	0	999831.602	0	3	0	−1380.016
1	1	0	18459.850	0	4	0	1477.356
1	0	1	12600.000	0	1	1	8441.949
2	0	0	−6917.189	0	2	1	−31824.651
3	0	0	13932.557	2	0	1	−7547.532
0	0	2	−4027.303	1	2	0	−826.654
0	0	3	−7184.089	0	2	1	−150.000
4	0	0	−2901.917	1	1	1	750.000
0	2	0	−202.473	0	3	2	−300.000

Table 6.4: Final coefficients of $M_f^{(1)}$ for $H_2^{16}O$. Units are consistent with bond lengths in a_0 and bond angle in rads for energies in μE_h.

Table 6.5: Band origins, in cm^{-1}, for the $H_2^{16}O$. Results calculated as observed, (a) Values from Tennyson *et al* [152], minus calculated, (b) *ab initio* potential V_{ai}, (c) Partridge and Schwenke's empirical potential, (d) V_{emp} for this work

ν_3 even	Obs[a]	b	c	d
(010)	1594.746	−0.10	−0.03	−0.02
(020)	3151.630	−0.07	0.01	0.06
(100)	3657.053	−0.85	0.01	−0.10
(030)	4666.790	0.04	0.00	0.11
(110)	5234.978	−1.06	−0.06	−0.18
(040)	6134.015	0.26	−0.02	0.15
(120)	6775.093	−1.06	−0.02	−0.09
(200)	7201.540	−1.28	−0.01	0.06
(002)	7445.045	−.86	−0.07	0.07
(050)	7542.437	0.57	−0.07	0.19
(130)	8273.976	−1.08	−0.08	−0.06
(210)	8761.582	−1.50	−0.09	−0.07
(060)	8869.954	0.80	−0.63	−0.16
(012)	9000.136	−1.01	0.03	0.12
(220)	10284.367	−1.50	0.01	0.04
(300)	10599.686	−0.96	−0.01	0.17
(102)	10868.876	−1.66	−0.04	0.16
(230)	11767.390	−1.69	−0.14	−0.02
(032)	12007.776	−1.52	−0.14	−0.03
(310)	12139.315	−1.24	−0.06	0.01
(112)	12407.662	−1.85	−0.01	0.12
(400)	13828.277	−0.06	0.11	0.23

Table 6.5: continued.

	Obs[a]	b	c	d
(122)	13910.896	−1.91	0.09	0.17
(202)	14221.161	−1.97	0.03	0.28
(004)	14537.504	−0.97	0.10	0.22
(330)	15108.239	−1.26	0.08	0.29
(410)	15344.503	−0.19	0.10	0.03
(212)	15742.795	−2.12	0.02	0.13
(302)	17458.354	−1.06	0.43	0.12
(510)	18392.974	1.85	1.02	0.48
ν_3 odd	Obs[a]	b	c	d
(001)	3755.929	−0.36	−0.02	0.02
(011)	5331.265	−0.46	0.05	0.04
(021)	6871.520	−0.60	0.03	0.02
(101)	7249.818	−0.79	−0.04	−0.09
(031)	8373.853	−0.74	−0.04	−0.02
(111)	8806.999	−0.97	−0.04	−0.16
(041)	9833.585	−0.73	−0.03	0.05
(121)	10328.731	−1.00	0.06	−0.06
(201)	10613.354	−0.73	−0.05	−0.03
(003)	11032.406	−0.95	−0.04	−0.01
(131)	11813.207	−1.17	−0.03	−0.09
(211)	12151.26	−0.89	−0.07	−0.18
(013)	12565.00	−1.16	0.01	−0.03
(221)	13652.66	−0.73	0.20	0.13
(301)	13830.94	−0.00	0.09	0.15
(023)	14066.19	−1.42	−0.01	−0.09

Table 6.5: continued.

	Obs[a]	b	c	d
(103)	14318.81	−1.11	0.04	−0.34
(231)	15119.03	−1.01	−0.01	−0.03
(311)	15347.96	−0.06	0.11	−0.05
(033)	15534.71	−1.74	−0.10	−0.21
(113)	15832.77	−1.26	0.06	−0.45
(321)	16821.64	0.50	0.55	0.73
(203)	16898.84	1.32	0.54	0.27
(123)	17312.54	−1.19	0.30	−0.31
(401)	17495.53	−0.61	0.26	−0.68
(331)	18265.82	0.05	0.11	0.63
(213)	18393.31	1.63	0.83	0.27
	σ_{vib}	1.12	0.24	0.22

Table 6.6: A_1 symmetry for J=2, for the $H_2^{16}O$. Results calculated as observed, (a) Values from Tennyson *et al* [152], minus calculated, (b) Partridge and Schwenke's empirical potential, (c) V_{emp} for this work

	Obs[a]	b	c
(000)	70.091	−0.001	0.006
(000)	136.164	−0.002	−0.010
(010)	1664.965	−0.031	−0.012
(010)	1743.486	−0.030	−0.062
(020)	3221.961	0.005	0.073
(020)	3317.211	0.004	−0.025
(100)	3725.942	0.012	−0.092
(100)	3789.969	0.008	−0.121
(001)	3833.577	−0.020	0.014
(030)	4737.202	0.003	0.131
(030)	4856.216	0.007	−0.034
(110)	5304.009	−0.060	−0.172
(110)	5379.940	−0.058	−0.233
(011)	5411.411	0.054	0.027
(040)	6204.444	−0.013	0.175
(040)	6359.782	0.017	−0.089
(120)	6844.235	−0.017	−0.080
(120)	6936.077	−0.017	−0.199
(021)	6955.086	0.027	−0.016
(200)	7269.313	−0.014	0.064
(200)	7331.623	−0.018	0.003
(002)	7513.430	−0.067	0.085

Table 6.6: continued.

	Obs[a]	b	c
(002)	7571.935	−0.056	0.020
(050)	7829.251	0.010	−0.261
(130)	8343.182	−0.077	−0.046
(031)	8462.463	−0.040	−0.092
(210)	8829.530	−0.083	−0.056
(111)	8885.207	−0.043	−0.179
(210)	8902.698	−0.079	−0.152
(012)	9068.751	0.032	0.144
(012)	9137.254	0.034	0.011
(041)	9929.713	−0.038	−0.056
(220)	10352.424	0.012	0.052
(121)	10410.232	0.050	−0.095
(220)	10440.106	0.008	−0.103
(300)	10666.478	−0.009	0.189
(201)	10687.629	−0.049	−0.031
(300)	10725.483	−0.014	0.097
(102)	10935.820	−0.040	0.170
(102)	10993.881	−0.035	0.103
(003)	11106.583	−0.045	−0.016
(230)	11835.483	−0.149	−0.016
(131)	11899.408	−0.049	−0.157
(230)	11944.100	−0.124	−0.267
(032)	12076.843	−0.124	0.018
(032)	12175.861	−0.143	−0.332
(310)	12206.348	−0.054	0.037

Table 6.6: continued.

	Obs[a]	b	c
(211)	12227.881	−0.090	−0.197
(310)	12275.676	−0.056	−0.131
(112)	12474.850	−0.010	0.142
(112)	12543.052	−0.003	0.024
(013)	12641.205	−0.029	−0.046
(042)	13648.122	−0.241	−0.564
(320)	13707.906	0.106	0.389
(221)	13732.386	−0.031	0.009
(320)	13791.018	0.164	0.071
(301)	13903.869	0.047	0.121
(400)	13950.761	0.108	0.107
(122)	13978.260	0.084	0.195
(122)	14059.518	0.088	0.019
(023)	14144.993	−0.086	−0.133
(202)	14286.801	0.024	0.285
(202)	14343.827	0.029	0.218
(103)	14391.614	−0.008	−0.350
(004)	14604.182	0.095	0.266
(241)	16636.535	−0.928	0.105
(321)	16898.386	−0.161	0.680
(401)	16971.460	0.059	0.246
(500)	17023.132	0.605	0.036
(222)	17293.421	0.151	0.207
(222)	17372.653	0.199	0.064
(123)	17389.611	−0.849	−0.422

Table 6.6: continued.

	Obs[a]	b	c
(302)	17522.885	0.254	−0.001
(203)	17566.223	−0.152	−0.673
(302)	17578.514	0.267	−0.137
(104)	17813.223	0.087	0.021
(104)	17865.615	0.133	−0.091
	σ_{vib}	0.18	0.19

Table 6.7: Rotational term values for J=10, in cm^{-1}, for the fundamentals of $H_2^{16}O$. Results calculated as observed, (a) Values from Tennyson *et al* [152], minus calculated, (b) V_{ai} defined in this work (c) V_{emp} defined in this work

J	K_a	K_c	(v_1,v_2,v_3)	Obs[a]	b	c
10	0	10	(000)	1114.5323	0.06	0.04
10	2	8	(000)	1437.9687	0.11	0.10
10	4	6	(000)	1616.4532	0.14	0.14
10	6	4	(000)	1875.4620	0.07	−0.00
10	8	2	(000)	2254.2847	0.01	−0.14
10	10	0	(000)	2701.8888	−0.07	−0.32
10	0	10	(010)	2705.0968	−0.69	0.02
10	2	8	(010)	3058.3986	0.01	0.11
10	4	6	(010)	3253.7382	0.01	0.11
10	6	4	(010)	3565.0037	−0.16	−0.20
10	8	2	(010)	3997.5086	−0.31	−0.51
10	10	0	(010)	4497.1929	0.47	−0.86
10	0	10	(100)	4750.3621	−0.76	−0.07
10	2	8	(100)	5069.0883	−0.70	−0.00
10	4	6	(100)	5246.8003	−0.64	−0.03
10	6	4	(100)	5497.2153	−0.70	−0.20
10	8	2	(100)	5865.6049	−0.78	−0.51
10	10	0	(100)	6264.7457	−0.80	−0.78
10	1	10	(001)	4852.7552	−0.28	0.05
10	3	8	(001)	5175.9551	−0.24	0.09
10	5	6	(001)	5434.4839	−0.24	0.01

Table 6.7: continued.

J	K_a	K_c	(v_1,v_2,v_3)	Obs[a]	b	c
10	7	4	(001)	5748.6614	−0.18	−0.28
10	9	2	(001)	6139.3236	−0.12	−0.61
				σ_{vib}	0.43	0.34

Table 6.8: Band origins, in cm^{-1} for 2 symmetric isotopomers in water calculated using (a) V_{ai} in this work and (b) V_{emp} in this work.

		Obs	a	b
D_2O	(010)	1178.38	−0.14	−0.02
	(020)	2336.84	−0.16	0.13
	(100)	2671.65	−0.57	−0.19
	(001)	2787.72	−0.25	−0.17
	(030)	3474.32	−0.12	0.33
	(011)	3956.03	−0.32	−0.01
	(031)	6235.08	−0.55	0.20
	(210)	6452.98	−1.26	−0.36
	(111)	6533.24	−0.82	−0.34
	(121)	7672.92	−0.96	−0.27
T_2O	(010)	995.4	−0.08	0.07
	(100)	2237.2	−0.31	−0.07
	(001)	2366.6	−0.65	−0.06

Bibliography

[1] F. Allard, P. H. Hauschildt, S. Miller, J. Tennyson, Astrophys. J. **39** (1994) 426

[2] R. D. Amos, I. L. Alberts, J. S. Andrews, S. M. Colwell, N. C. Handy, D. Jayatilaka, P. J. Knowles, R. Kobayashi, K. E. Laidig, G. Laming, A. M. Lee, P. E. Maslen, C. W. Murray, J. E. Rice, E. D. Simandiras, A. J. Stone, M. D. Su, D. J. Towers, The Cambridge Analytic Derivatives Package Issue 6, Cambridge (1995)

[3] A. M. Arthurs, A. Dalgarno, Proc. R. Socs. London, Ser. A, **256** (1960) 540

[4] Z. Bačić, J. C. Light, Ann. Phys. Chem.**40** (1989) 469

[5] R. Baer, Chem. Phys. Letts. **324** (2000) 101

[6] K. Balasubramanian, Relativistic effects in Chemistry, Part A: Theory and techniques and Part B:Applications, Wiley, New York (1997)

[7] R. J. Bartlett, S. J. Cole, G. D. Purvis, W. C. Ermler, H. C. Hsieh, I Shavitt, J. Chem. Phys. **87** (1987) 6579

[8] R. J. Bartlett, I. Shavitt, G. D. Purvis, J. Chem. Phys. **71** (1979) 281

[9] W. S. Benedict, N. Gailar, E. K. Plyler, J. Chem. Phys. **24** (1956) 1139

[10] P. F. Bernath, Chem. Soc. Rev. **25** (1996) 111

[11] M. Born, K. Huang, Dynamical Theory of Crystal Lattices, Oxford University Press: New York, App VIII, (1954)

[12] M. Born, R. J. Oppenheimer, Ann. Rev. Phys. **84** (1927) 457

[13] J. M. Bowman, B. Gazdy, J. Chem. Phys. **94** (1991) 816

[14] J. M. Bowman, B. Gazdy, Chem. Phys. Letts. **200** (1992) 311

[15] J. M. Brown, J. T. Hougen, K-P. Huber, J. W. C. Johns, I. Kopp, H. Lebfrebvre-Brion, A Merer, D. Ramsay, J. Rostos, R. Zare, J. Molec. Spec. **55** (1975) 500

[16] M. E. Brown, C. D. Koresko, G. A. Blake, Astrophys. J. Letts. **508** (1998) L175

[17] F. B. Brown, D. G. Truhlar, Chem. Phys. Letts **117** (1985) 307

[18] M. G. Bucknell, N. C. Handy, S. F. Boys, Molec. Phys. **28** (1974) 759

[19] P. R. Bunker, Ann. Rev. Phys. Chem. **34** (1983) 59

[20] P. R. Bunker, R. E. Moss, J. Molec. Spec. **80** (1980) 217

[21] C. Camy-Peyret, J. -M. Flaud, J. -Y. Mandin, J. -P. Chevillard, J. Molec. Spec. **113** (1985) 208

[22] M. Carleer, A. Jenouvreier, A. -C. Vandeele, P. F. Bernath, M. F. Méienne, R. Colin, N. F. Zobov, O. L. Polyansky, J. Tennyson, J. Chem. Phys. **111** (1999) 2444

[23] G. D. Carney, L. L. Sprandel, C. W. Kern, Adv. Chem. Phys. **37** (1978) 305

[24] S. Carter, N. C. Handy, Comput. Phys. Rep **5** (1986) 115

[25] S. Carter, N. C. Handy, J. Chem. Phys. **87** (1987) 4294

[26] J. Cernicharo, E. Gonzalez-Alfonso, J. Alcolea, R. Bachiller, D. John ApJ **432** 1994 L59

[27] A. Cheung, D. M. Rank, C. H. Townes, D. D. Thornton, W. J. Welch, Nature **221** (1969) 626

[28] M. S. Child, L. Halonen, Adv. Chem. Phys. **57** (1994) 1

[29] M. S. Child, R. T. Lawton, Faraday Disc. Chem. Soc. 71 (1981) 273 ; Chem. Phys. Letts. **87** (1982) 217

[30] S. E. Choi, J. C. Light, J. Chem. Phys. **97** (1992) 7031

[31] E. U. Condon, G. H. Shortley, The Theory of Atomic Spectra,Cambridge University Press, Cambridge (1935)

[32] L. H. Coudert, J. Molec. Spec. **181** (1997) 246

[33] R. D. Cowan, D. C. Griffin, J. Opt. Soc. Am. **66** (1976) 1010.

[34] A. G. Császár, W. C. Allen, H. F. Schaefer, J. Chem. Phys. **108** (1998) 9751

[35] A. G. Császár, I. M. Mills., Spectro. Acta A **53** (1997) 1101

[36] A. S. Dickinson, P. R. Certain, J. Chem. Phys. **49** (1968) 4204

[37] B. M. Dinelli, C. R. Le Sueur, J. Tennyson, R. D. Amos, Chem. Phys. Letts, **232** (1995) 295

[38] T. H. Dunning Jr., J. Chem. Phys. **90** (1989) 1007

[39] C. Eckart, Phys. Rev., **47** (1935) 552

[40] S. T. Epstein, The Variation Method in Quantum Chemistry, Academic Press. New York.

[41] M. P. Esplin, R. B. Wattson, M. L. Hoke, L. S. Rothman, J. Quant. Spectro. Radiative. Transf. **60** (1998) 711

[42] J. -M. Flaud, C. Camy-Peyret, A. Bykov, O. Naumenko, T. Petrova, A. Scherbakov, L. Sinitsa, J. Molec. Spec. **183** (1997) 300

[43] J. -M. Flaud, C. Camy-Peyret, A. Bykov, O. Naumenko, T. Petrova, A. Scherbakov, L. Sinitsa, J. Molec. Spec. **185** (1997) 211

[44] J. -M. Flaud, C. Camy-Peyret, J. P. Maillard, Molec. Phys. **32** (1976) 499

[45] N. Fulton, PhD Thesis, University College London, London (1997)

[46] W. Gabriel, E. A. Reinsch, P. Rosmus, S. Carter, N. C. Handy, J. Chem. Phys. **99** (1993) 897

[47] C. Galus, L'eau est soluble dans le Soleil, Le Monde, July 24, (1997) pg 1

[48] R. R. Gamache, L. S. Rothman, J. Quant. Spec. Radiative. Transfr. **48** (1992) 519

[49] J. S. Garing, R. A. McClatchey, Appl. Opt. **12** (1973) 2525

[50] B. Gazdy, J. M. Bowman, J. Chem. Phys. **95** (1991) 6309

[51] P. D. Gensheimer, R. Mauersberger, T. L. Wilson, A&A **314** (1996) 281

[52] W. H. Green, A. Willetts, D. Jayatilaka, N. C. Handy, Chem. Phys. Letts. 169 (1990) 127; W. Gabrieel , E. Reinsch, P. Rosmus, S. Carter, N. Handy, J. Chem. Phys. **99** (1993) 897

[53] D. N. B. Hall. PhD Thesis, Harvard University, USA (1970)

[54] L. Halonen, Adv. Chem. Phys. **104** (1998) 41

[55] L. Halonen, T. Carrington Jr., J. Chem. Phys. **88** (1988) 4171

[56] N. C. Handy, Y. Yamaguchi, H. F. Schaefer III, J. Chem. Phys. **84** (1986) 4481

[57] N. C. Handy, A. M. Lee, Chem. Phys. Letts. **252** (1996) 425

[58] D. O. Harris, G. G. Engerholm, W. Gwinn, J. Chem. Phys. **43** (1965) 1515

[59] J. B. Hearnshaw, The Analysis of Starlight: One Hundred and Fifty Years of Astrononmical Spectroscopy, Cambridge University Press, Cambridge (1986)

[60] H. Hellmann, Einführung in die Quantenchemie. Franz Deutiche, Leipzig (1937)

[61] J. R. Henderson, C. R. Le Sueur and J. Tennyson, Comp. Phys. Comm. **75** (1993) 379

[62] J. R. Henderson, S. Miller, J. Tennyson, J. Chem. Soc. Faraday Trans. **86** (1990) 1963

[63] P. Hennig, W. P. Kramer, G. H. F. Diercksen, G. Strey, Theoret. Chim. Acta, **47** (1978) 233

[64] G. Herzberg, Molecular Spectra and Molecular Structure, Malabar, Florida (1945)

[65] K. Higgins, F.-M. Tao, W. Klemperer, J. Chem. Phys. **109** (1998) 3048

[66] K. Hinkle, T. G. Barnes, ApJ **227** (1979) 923

[67] T. -S. Ho, T. Hollebeck. H. Rabitz, L. B. Harding and G. Schatz, J. Chem. Phys, **105** (1996) 10472

[68] A. R. Hoy, P. R. Bunker, J. Molec. Spec. **52** (1983) 439

[69] A. R. Hoy, P. R. Bunker, J. Molec. Spec. **74** (1979) 1

[70] A. R. Hoy, I. M. Mills, G. Strey, Molec. Phys. **24** (1972) 1265

[71] J. M. Hutson, A. Ernesti, M. M. Law, C. F. Roche, R. J. Wheatley, J. Chem. Phys. **105** (1996) 9130

[72] G. Jansen, J. Chem. Phys. **105** (1996) 89

[73] F. Jensen, Chem. Phys. Letts. **261** (1995) 1155

[74] F. Jensen, Introduction to Computational Chemistry, Wiley, Chichester (1999)

[75] P. Jensen, J. Molec. Spec. **133** (1989) 438

[76] P. Jensen, S. A. Tashkun, V. G. Tyuterev, J. Molec. Spec. **168** (1994) 271

[77] B. R. Johnson, W. P. Reinhardt, J. Chem. Phys. **85** (1986) 4538

[78] U. G. Jørgensen, P. Jensen, J. Molec. Spec. **161** (1993) 219 ; P. Jensen, J. Molec Spec. **133** (1989) 438

[79] G. S. Kedziora, I. Shavitt, J. Chem. Phys. **109** (1997) 5547

[80] W. D. Klopper, J. Comput. Chem. **18** (1997) 20.

[81] H. G. Kjaergaard, B. R. Henry, H. Wei, S. Lefebvre, T. Carrington, O. S. Mortensen, M. L. Sage, J. Chem. Phys. **100** (1994) 6228

[82] P. J. Knowles, private communication (1998) ; A. G. Császár, private communication (1999)

[83] P. J. Knowles, G. J. Sexton, N. C. Handy, Chem. Phys. Letts. **79** (1979) 202

[84] W. P. Kraemer, B. O. Roos, P. E. M. Siegbahn. Chem. Phys. **69** (1982) 305

[85] B. Krohn, W. Ermler, C. W. Kern, J. Chem. Phys. **60** (1974) 22

[86] H. W. Kroto, Molecular Rotation Spectra, John Wiley and Sons, London (1975)

[87] R. Lanquetin, L. H. Coudert, C. Camy-Peyret, J. Molec. Spec. **195** (1999) 54

[88] R. J. Le. Roy, C. Bissonette, T. H. Wu, A. K Dham, W. J. Meath, Faraday Disc. **97** (1994) 81

[89] J. C. Light, I. P. Hamilton, J. V. Lill, J. Chem. Phys. **82** (1985) 1400

[90] J. K. L. MacDonald, Phys. Rev. **43** (1933) 830

[91] J. -Y. Mandin, J. -P. Chevillard, C. Camy-Peyret, J. -M. Flaud, J. Molec. Spec., **116** (1986) 167

[92] J. M. L. Martin, J. P. François, R. Gijbels, J. Chem. Phys. **95** (1991) 8374

[93] A. B. McCoy, E. Silbert III, J. Chem. Phys. **92** (1990) 1893

[94] R. McWeeny, Methods of Molecular Quantum Mechanics, 2nd edition, Academic Press, London (1989)

[95] M. Meuwly, J. M. Hutson, J. Chem. Phys. **110** (1999) 8338

[96] S. Miller, J. Tennyson, H. R. A. Jones, A. J. Longmore in U. G. Jørgensen, Lecture Notes in Physics Vol. 428, Molecules in the Stellar Environment, Springer-Verlag, Berlin (1994)

[97] P. M. Morse, Phys. Rev. **34** (1929) 57

[98] M. J. Mumma, H. A. Weaver, H. P. Larson, D. S. Davis, M. Williams, Science **232** (1986) 1523

[99] J. N. Murrell, S. Carter, S. C. Farantos, P. Huxley, A. J. C. Varandas, Molecular Potential Energy Functions, Wiley, Chichester (1984)

[100] NATO AGARD (Advisory Group for Aerospace Research and Development), 1993, Advisory Report No. 287, Terminology and Assessment Methods of Solid Propellant Rocket Exhaust Signatures, Propulsion and Energetics Panel, Working Group 21 (Brussels: NATO)

[101] O. Naumenko, A. Campargue, J. Molec. Spec. **199** (2000) 59

[102] H. Partridge, D. W. Schwenke, J. Chem. Phys. **106** (1997) 4618

[103] J. C. Pearson, T. Anderson, E. Herbst, F. C. Delucia, P. Helminger, Astrophys. J, 379 (1991) L41. T. Amano, F. Scappini, Chem. Phys. Letts, **182** (1991) 93

[104] S. A. Perera, R. J. Bartlett, Chem. Phys. Letts. **216** (1993) 606.

[105] O. L. Polyansky, J. Molec. Spec. **112** (1985) 79

[106] O. L. Polyansky, J. R. Busler, B. Guo, K. -Q. Zhang, P. F. Bernath, J. Molec Spec. **176** (1996) 305

[107] O. L. Polyansky, P. Jensen, J. Tennyson, J. Chem. Phys. **101** (1994) 7651

[108] O. L. Polyansky, P. Jensen, J. Tennyson, J. Molec. Spec **178** (1996) 184

[109] O. L. Polyansky, P. Jensen, J. Tennyson, J Chem. Phys. **105** (1996) 6490

[110] O. L. Polyansky, J. Tennyson, J. Molec. Spec. **154** (1992) 246

[111] O. L. Polyansky, J. Tennyson, J. Chem. Phys. **306** (1999) 5056

[112] O. L. Polyansky, J. Tennyson, P. F. Bernath, J. Molec. Spec. **186** (1997) 213

[113] O. L. Polyansky, J. Tennyson, N. F. Zobov. Spectro. Acta. **55A** (1999) 659

[114] O. L. Polyansky, N. F. Zobov, J. Tennyson, J. A. Lotoski, P . Bernath, J. Molec. Spec. **184** (1997) 35

[115] O. L. Polyansky, N. F. Zobov, S. Viti, J. Tennyson, J. Molec. Spec. **189** (1998) 291

[116] O. L. Polyansky, N. F. Zobov, S. Viti, J. Tennyson, P. F. Bernath, L. Wallace, Science **277** (1997) 346

[117] O. L. Polyansky, N. F. Zobov, S. Viti, J. Tennyson, P. F. Bernath, L. Wallace, J. Molec. Spec. **186** (1997) 422

[118] O. L. Polyansky, N. F. Zobov, S. Viti, J. Tennyson, P. F. Bernath, L. Wallace, ApJ **489** (1997) L205

[119] H. M. Quiney, H. Skanne, I. P. Grant, Chem. Phys. Letts **290** (1998) 473

[120] R. Radau, Ann. Sci. Ecole Normale Superior **5** (1868) 311

[121] V. Ramanathan, A. M. Vogelmann, Ambio **26** (1997) 38

[122] Lord Rayleigh, Theory of Sounds, Vol 1, Section 88, Macmillan, London, (1937), reprinted Dover, New York)

[123] W. Ritz, Reine Angew Math., **135** (1908) 1

[124] B. J. Rosenberg, W. C. Ermler, I. Shavitt, J. Chem. Phys. **65** (1976) 4072

[125] L. S. Rothman, R. R. Gamache, R. H. Tipping, C. P. Rinsland, M. A. H. Smith, D. C. Benner, V. Malathy Devi, J. -M. Flaud, C. Camy-Peyret, A. Perrin, A. Goldman,

S. T. Massie, L. R. Brown, R. A. Toth, The Hitran Molecular Database: Editions of 1991 and 1992.

[126] L. S. Rothman, C. P. Rinsland, A. Goldman, S. T. Massie, D. Edwards, J. -M. Flaud, A. Perrin, C. Camy-Peyret, V Dana, J. -Y. Mandin, J. Schroeder, A McCann, R. R. Gamache, R. Wattson, K. Yoshino, K. Chance, K. Jucks, L. Brown, V. Nemtchinov, P. Varanasi, J. Quant. Spec. Radiative Transf. **60** (1998) 665.

[127] J. H. Schryber, O. L. Polyansky, P. Jensen, J. Tennyson, J. Molec. Spec. **185** (1997) 234

[128] W. A. Schutte, A. G. G. M. Tielens, D. C. B. Whittet, A. Boogert, P. de Graauw Ehrenfreund, T. Prusti, E. F. Van Dishoek, P. Wesselins, Astronomy & Astrophysics **315** (1996) L333

[129] D. W. Schwenke, Chem. Phys. Letts., **189** (1992) 91

[130] D. W. Schwenke, J. Phys. Chem. **100** (1996) 2867

[131] D. W. Schwenke, J. Molec. Spec. **190** (1998) 397

[132] D. W. Schwenke, H. Partridge, J. Chem. Phys. **113** (2000) 16

[133] G. J. Sexton, N. C. Handy, Molec. Phys. **51** (1984) 1321

[134] J. F. Stanton, J. Gauss, W. J. Lauderdale, J. D. Watts, R. J. Bartlett, ACES II. The package also contains modified versions of the MOLECULE Gaussian integral program of J. Almlof, P. R. Taylor, the ABACUS integral derivative program written by T. Helgaker, H. Jensen, P. Jorgensen, P. R. Taylor, and the PROPS property evaluation integral code of P. Taylor.

[135] A. H. Stroud, D. Secrest, Gaussian Quadrature Formulas , Prentice-Hall, London (1966)

[136] B. T. Sutcliffe, J. Tennyson, Int. J. Quant. Chem. **29** (1991) 183

[137] B. T. Sutcliffe, Current Aspects of Quantum Chemistry (R. Carbo ed.), Studies in Theoretical Chemistry, Vol.21, pp.99 Elsivier (1982)

[138] A. Szabo, N. Ostlund, Modern Quantum Chemistry, Macmillan, New York (1982)

[139] G. Tarczay, A. G. Császár, W. D. Klopper, V. Szalay, W. C. Allen, H. F. Schaefer, J Chem. Phys. **110** (1999) 11971

[140] J. Tennyson, Comput. Phys. Rep, **4** (1986) 1

[141] J. Tennyson, Comp. Phys. Comms. **42** (1986) 257

[142] J. Tennyson, J. R. Henderson, N. G. Fulton, Comp. Phys. Comms. **86** (1995) 175

[143] J. Tennyson, S. Miller, Comp. Phys. Comms. **55** (1989) 149

[144] J. Tennyson, S. Miller, J. R. Henderson Methods in Computational Chemistry, Vol 4, Molecular Vibrations, New York 1992

[145] J. Tennyson, S. Miller, C. R. Le Sueur, Comp. Phys. Comms. **75** (1993) 339

[146] J. Tennyson, O. L. Polyansky, Contemp, Phys, **39** (1998) 283

[147] J. Tennyson, B. T. Sutcliffe, J. Chem. Phys. **77** (1982) 4061

[148] J. Tennyson, B. T. Sutcliffe, J. Chem. Phys. **46**(1982) 97

[149] J. Tennyson, B. T. Sutcliffe, J. Molec. Spec. **101** (1983) 71

[150] J. Tennyson, B. T. Sutcliffe, Int. Quantum Chem. **42** (1992) 941

[151] J. Tennyson, B. T. Sutcliffe, Molec. Phys. **58** (1986) 1067

[152] J. Tennyson, N. F. Zobov, R. Williamson, O. L. Polyansky, P. F. Bernath, J. Phys. Chem. Ref. Data, in press

[153] R. A. Toth, J. Opt. Soc. Am. **8** (1991) 2236

[154] R. A. Toth, J. Molec. Spec. **190** (1998) 379

[155] R. A. Toth, J. Molec. Spec. **194** (1999) 28

[156] R. A. Toth, Applied Optics **33** (1994)

[157] R. A. Toth, J. Molec. Spec. **166** (1994) 176

[158] T. Tsuji, K. Ohnaka, Elementary Processes in Dense Plasmas, Addison-Wesley, Reading, (1995)

[159] E. F. Valeev, A. G. Császár, W. C. Allen, H. F. Schaefer III, J. Chem. Phys. 114 (2001) 2875

[160] E. F. Van Dishoek, C. Wright, J. Cernicharo, E. Gonzalez-Alfonso, T. de Graauw, F. Helmich, B. Vandenbussche, Astrophys. J. Letts. **503** (1998) L173

[161] J. H. Van Vleck, Phys. Rev. **33** (1929) 467

[162] A. J. C. Varandas, J. Chem. Phys. **105** (1996) 9

[163] L. Visscher, K. G. Dyall, J. Chem. Phys. **104** (1996) 9040.

[164] S. Viti, PhD Thesis, University College London, London (1997)

[165] S. Viti, O. L. Polyansky, J. Tennyson, Astron. Soc. of the Pacific Conference Series **154** (1998) 718

[166] S. Viti, J. Tennyson, O. L. Polyansky, Proc. Royal Astron. Soc. **287** (1997) 79

[167] L. Wallace, P. F. Bernath, W. Livingston, K. Hinkle, J. R. Busler, B. Guo, K. -Q. Zhang, Science **268** (1995) 1155

[168] L. Wallace, W. Livingston, K. Hinkle, P. F. Bernath, Astrophys. J. Suppl. Ser., **106** (1996) 165

[169] L. Wallace, W. Livingston, Natl. Solar Observ. Tech. Rep. 92-001, National Optical Astronomy Observatories, Tucson, AZ, 1992

[170] J. K. G. Watson, Molec. Phys. **15** (1968) 479

[171] R. B. Wattson, L. S. Rothman, J. Quant. Spec. Radiative. Transf. **48** (1992) 763

[172] R. J. Whitehead, N. C. Handy, J. Molec. Spec. **59** (1976) 459

[173] H. Worden, R. Beer, C. P. Rinsland J. Geophys. Res., **102** (1997) 1287

[174] D. Xie, G. Yan, Chem. Phys. Letts **248** (1996) 409

[175] N. F. Zobov, D. Belmiloud, O. L. Polyansky, J. Tennyson. J. Chem. Phys., **133** (2000) 1546

[176] N. F. Zobov, O. L. Polyansky, C. R. Le Sueur, J. Tennyson, Chem. Phys. Letts. **260** (1996) 381

[177] N. F. Zobov, O. L. Polyansky, J. Tennyson, S. Shirin, R. Nassar, T. Hirao, T. Imajo, P. F. Bernath, L. Wallace, Astrophys. J., **530** (2000) 994

[178] N. F. Zobov, O. L. Polyansky, J. Tennyson, J. A. Lotoski, P. Colarusso, K. -Q. Zhang, P. F. Bernath, J. Molec. Spec. **193** (1999) 118

[179] J. Zuniga, A. Bastida, A. Requena, J. Chem. Soc., Faraday Trans **93** (1997) 1681

6.3 Publications on the work in this Thesis

[W.1] A. Csaszar, J. Kain, O. Polyansky, N. Zobov, J. Tennyson, Chem. Phys. Letts. 293 (1998) 317

[W.2] J. Kain, O. Polyansky, J. Tennyson, Chem. Phys. Letts. 317 (2000) 365

Appendix A

Program structure of the modified DVR3D program suite for fitting calculations

Figure A.1 gives an outline of how **DVR3D/ROTLEV/XPECT3** and **FIT** work in conjunction with each other to produce an empirically fitted potential energy surface to calculated ro-vibrational energy levels compared with experiment. In summary **DVR3D** calculates the wavefunctions on stream **iwave** for the vibrational motion which can be passed directly to **XPECT3** or via **ROTLEV** for rotational motion. **XPECT3** then calculates the expectation values for the different parameters for different calculated energy levels. As the Hellmann-Feynman theory holds for linear fits, the expectation values are just the derivatives of the parameters for the calculated energy levels. These derivatives are passed to program **FIT** by stream **ifit**. **FIT** itself finds the differences between the (new) calculated energy levels and the observed ones available for different symmetries and different rotations. These energy differences are then past to **LSQFIT** which performs a least-square fit and returns the new parameters. The new parameters are then passed back to **DVR3D** on stream **iout**.

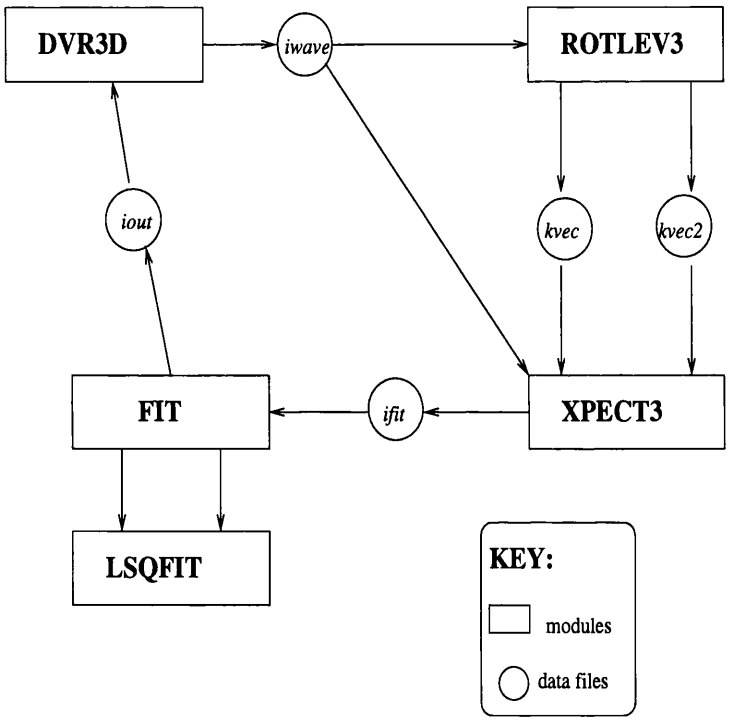

Figure A.1: Structure and data flow for the modified **DVR3D** program suite for iterative empirical fitting. Scratch disk files used by individual modules are not shown.

A.1 Modifications to DVR3D

An overview of how to operate the **DVR3D** program suite can be found in Tennyson *et al* [142]. A summary of the **DVR3D** program suite is covered in section 2.10.

Minor modifications were made to **DVR3D** so that it automatically reads in the new parameters on stream **iout** from **FIT**. This is so that iterations do not have to be done manually by the user. For an empirical fit the morphing function multiplies the entire potential, therefore it is necessary to call the potential and then multiply by the parameters and their functional form.

SUBROUTINE POTV be supplied by the user in the form

(V,R1,R2,XCOS,JT,PV).

V	Value of the potential
R1, R2, XCOS	The position geometry
JT	JT = 1, include parameter
	JT = 0, remove parameter
CV(nprop)	CV(nprop) = array of parameters

Modifications to the input cards for DVR3D

Card:3 NCOORD,NPROPIN,NPRTformat(3i5)

NCOORD[3]	the number of vibrational co-ordinates of the problem:
	2 for an atom - rigid diatom system
	3 for a full triatomic
NPROPIN	is the number of parameters to be read for a morphing of the entire PES
NPRT	is the number of parameters to be read for a morphing of the correction to the barrier

A.2 Modifications to ROTLEV3B

Minor modifications were made so that **XPECT3** could read streams **kvec** and **kvec2**. The modifications were main found in SUBROUTINE DSREAD for the reading of the wavefunctions.

The operation by the user should remain unchanged.

A.3 XPECT3 - Program Use

XPECT3 computes expectation values for a set of arbitrary (scalar) properties defined by subroutine PROP. The expectation values can be either diagonal or off-diagonal (transitional); the states are defined by the the bra and ket input files. These files are produced either by **DVR3D**, stream **iwave**, or **ROTLEV3/3B**, stream **kvec** or **kvec2**. They contain most of the data necessary to characterise the run. This data must be consistent which means that runs creating the bra and ket files must have identical input for cards 5-9 in **DVR3D**, otherwise an error condition will result. To generate diagonal (or off diagonal for the same quantum numbers) expectation values no bra file is required.

XPECT3has the option to put the data on an output file for further processing. For example if analytic derivatives are computed using the Hellmann-Feynman theorem then **ifit** can be used to pass the derivatives to **FIT**. **XPECT3** requires the user to supply subroutine PROP, which defines the units used, usually atomic units.

A.3.1 Card input for XPECT3

The user must supply the following four lines of input on card:

Card 1: NAMELIST/PRT/

ZDIAG[T]	= T, diagonal expectation values calculated using ket wavefunctions only.
	= F, off-diagonal calculation using either bra and ket functions.

ZPRINT[F]	= T supplies extra print out for debugging purposes.
ZTRA[T]	= T writes property data to stream ITRA.
ZSTART[F]	= T initiates the output file for the property data.
	= F writes data to the end of existing file on stream ITRA.
IKET[11]	input stream from **DVR3D/ROTLEV3/3B** for the ket
	(formatted) in atomic units.
IBRA[0]	= 0 input from ket file only in atomic units.
	> 0 input stream for the Bra (unformatted).
	N.B NPNT must be the same for the bra and ket
ITRA[13]	output stream for property data (if ZTRA= T)
ZFORM[F]	= T then the output file ITRA is formatted.
IEZERO[57]	input stream from DVR3D
IJ1PARA[58]	I/O stream from DVR3D
	For J=0 writes derivatives of parameters for EZERO
	For J≠0 reads derivatives of parameters for EZERO
IFIT[12]	= J,S1,IE,EW,EH format(I2,1x,A2,I4,3X,2f10.3)
	DER(N,IE)(*)
J	= Angular Momentum
S1	= Symmetry (A1,A2,B1,B2)
IE	= Number of energy level
EW	= Calculated energy level in wavenumbers
EH	= Calculated energy level in hartrees
DER(N,IE)	= Derivatives
N	= number of properties

Card 2: TITLE format(9A8)

A 72 character title.

Card 3: LPOT,NPROP,NV1,NV2 format(6I5)

LPOT	highest value of λ in the Legendre expansion of properties. (implies LPOT+1+MOD(LPOT,2) point Gauss-Legendre integration is used for the θ coordinate).
NPROP[0]	number of properties to be considered must be consistent with subroutine PROP. must also be less than MXPROP(100)
NV1[all]	number of ket eigenfunctions considered.
NV2[all]	number of bra eigenfunctions considered (ignored if IBRA=0).

Card 4: (IPROP(i),i=1,nprop) format(20I5)

IPROP	is an array of NPROP pointers which can be optionally used by subroutine PROP to identify which properties have been requested. If card left blank, IPROP(i) defaults to i.

SUBROUTINE PROP	CALL PROP(der,R1,R2,X,nprop,nprt)
DER(N,IE)	are the derivatives
R1,R2,X	is the geometry
NPROP	is the number of functions for overall morphing
NPRT	is the number of functions for the barrier morphing

A.4 FIT - Program Use

Program **FIT** is given in Appendix B. **FIT** calculates the differences in energies between the experimental levels and the calculated levels, with respective derivatives in order to

pass to the least squares fitting routine **LSQFIT**, also given in Appendix B. It takes the derivatives of the parameters with respect to calculated energy levels from **XPECT3** from stream **ifit**.

A.4.1 Card input for FIT

Card 1: NAMELIST/PRT/

ZMORPH[T]	= Morph 1, IPARA[32]
ZMORPH[F]	= Morph 2, IPARA[38]
ZPARA[T]	= Input parameters in wavenumbers
ZPARA[F]	= Input parameters in microhartrees

Card 2: NDAT, NDATO, NPARA format(3I10)

NDAT	= Number of Calculated Data Points
NDATO	= Number of Experimental Data Points
NPARA	= Number of Parameters. This must be the same as number of parameters (NPROP,NPRT) in XPECT3
IPARA[32/38]	input stream for old parameters Written as JT, CV format(i5,3x,f25.15) JT = 1, include parameter JT = 0, remove parameter CV = new parameter
IOUT[10]	output for new parameters into DVR3D Written as JT, CV format(i5,3x,f25.15) JT = 1, include parameter JT = 0, remove parameter CV = new parameter
IOBS[30]	input stream for observed values. Written as J, S1, IE, E, J, K_a, K_c, v_1,v_2,v_3

	J = Angular Momentum
	S1 = Symmetry (A_1,A_2,B_1,B_2)
	IE = Number of energy level
	E = Calculated Energy (wavenumbers)
	K_a, K_c projection of J on to the A,C axis respectively
	v_1,v_2,v_3, symmetric stretch, bend, asymmetric stretch
ICALC[33]	input stream from **XPECT3** containing calculated energies and derivatives for the number of parameters.

Appendix B

Fortran routines for FIT and LSQFIT

B.1 Program FIT

```
      implicit double precision(a-h,o-y),logical(z)

      allocatable::eobs(:),ecalc(:),ecalcw(:)
      allocatable::dcon(:,:),eobshar(:),ezobs(:),cvp(:)
      allocatable::cvol(:),er(:),der(:,:),jfit(:)
      allocatable::j1(:),j21(:),n1(:),n21(:),i1(:)
      allocatable::jz1(:),jz2(:),jz3(:),iz1(:),iz2(:),iz3(:)
      allocatable::ediff(:),se(:),np(:),cv(:)
      allocatable::ediffw(:),xediffw(:)
      character*2,allocatable,dimension(:)::s1,s21
      integer:: npara,ndato,ndat,jcount,jcount2,count3

      namelist/prt/zmorph,zpara

      data iout/10/,IOBS/30/,ICALC/33/
      data zmorph/.true./,zpara/.true./

c     zpara = true when the parameters are in wavenumbers
c     zpara = false when the parameters are in microhartrees
c     zmorph = true morph1
c     zmorph = false morph2
c     ndat = number of data points
c     npara  = number of parameters
c     J = rotational const
c     S = symmetry
c     N = number
c     eobs = observed energy level
c     ecalc = calculated energy level

      open(unit=iout,status='new',form='formatted')
      open(unit=91,status='new',form='formatted')
      write(6,201)
 201  format(1h1,5x,'Spectroscopic Fitting Routine 18/02/00',/)
      write(6,200)
 200  format(/)

      read(5,prt)
      if (zmorph) then
         ipara=32
         write(6,*) 'Morphing of the overall potential chosen'
```

```
      else
         ipara=38
         write(6,*) 'Morphing of the barrier correction only'
      end if
      write(6,200)
      if (zpara) then
         write(6,*) 'Parameters read in Wavenumbers '
      else
         write(6,*) 'Parameters read in Mircohartrees '
      end if

      read(5,108) ndat,ndato,npara
108   format(3I10)
      write(6,200)
      write(6,*) 'Number of parameters ', npara
      write(6,200)
      write(6,*) 'Number of Calculated Data points is ',ndat
      write(6,200)
      write(6,*) 'Number of Observed Data points is ',ndato
      write(6,200)

      allocate(eobs(ndato),ecalc(ndat),ecalcw(ndat))
      allocate(ediff(ndato),ediffw(ndato),xediffw(ndato))
      allocate(jfit(npara),i1(npara),cvp(npara))
      allocate(se(npara),cv(npara),np(npara))
      allocate(j1(ndat),j21(ndato),n1(ndat))
      allocate(jz1(ndato),jz2(ndato),jz3(ndato))
      allocate(iz1(ndato),iz2(ndato),iz3(ndato))
      allocate(n21(ndato),s1(ndat),s21(ndato))

      k = 0
      do i=1,npara
         read(ipara,*) jfit(i),cv(i)
         if(jfit(i) .eq. 1) then
         write(6,112)
112      format(/5x,'jfit(i)       cv(i)',/)
         write(6,106) jfit(i),cv(i)
         k = k + 1
         np(k) = i
         write(6,*) 'np(k) ',np(k)
         end if
      end do

      npf = k

      allocate(cvol(npara),er(npara))
      allocate(dcon(jcount3,npf+1),der(ndat,npf))

         write(6,113) npf
113      format(/5x,'Number of included parameters',I5)

         do i=1,npara
            cvol(i) = cv(i)
         end do


      sdsq=0.0d0
      sdsqw = 0.0d0
      jcount = 0
      jcount2 = 0
      jcount3 = 0
```

```
      rewind icalc
      do i=1,ndat
        read(icalc,*) j1(i),s1(i),n1(i),ecalcw(i),ecalc(i)
         do m=1,npf
            read(icalc,*) der(i,m)
         end do
         rewind iobs
         do j=1,ndato
           read(iobs,*) j21(j), s21(j),n21(j),eobs(j),jz1(j),
    $ jz2(j),jz3(j),iz1(j),iz2(j),iz3(j)
            if(j21(j).eq.j1(i).and.n1(i).eq.n21(j) .and. s21(j)
    $ .eq. s1(i))then
               xediffw(j) = eobs(j) - ecalcw(i)
               if (abs(xediffw(j)).lt.5d0 .and. xediffw(j).lt.3.5d0)
    $   then
               write(91,22) j21(j),s21(j),n21(j),eobs(j),ecalcw(i),
    $ jz1(j), jz2(j),jz3(j),iz1(j),iz2(j),iz3(j), xediffw(j)
22             format(I2,2x,A2,1x,I3,2x,f10.4,2x,f10.4,2x,I2,2x,I2,2x,
    $ I2,2x,I2,2x,I2,2x,I2,f20.12)
               jcount2 = jcount2 + 1
               end if
            end if
         end do
      end do

      write(6,*) 'jcount2', jcount2
      open(unit=25,status='new',form='formatted')

      rewind 91
      rewind 25
      do j=1,jcount2
         read(91,22) j21(j),s21(j),n21(j),eobs(j),ecalcw(j),
    $ jz1(j),jz2(j),jz3(j),iz1(j),iz2(j),iz3(j),xediffw(j)
         if (eobs(j).eq.eobs(j-1).and.abs(xediffw(j)).lt.
    $  abs(xediffw(j-1))) then
         goto 23
         end if
         if (eobs(j).eq.eobs(j-1).and.abs(xediffw(j)).gt.
    $  abs(xediffw(j-1))) then
         goto 20
         end if
         if (eobs(j).eq.eobs(j-2).and.abs(xediffw(j)).lt.
    $  abs(xediffw(j-1))) then
         goto 23
         end if
         if (eobs(j).eq.eobs(j-2).and.abs(xediffw(j)).gt.
    $ abs(xediffw(j-1))) then
         goto 20
         end if
         if (ecalcw(j).eq.ecalcw(j-1).and.abs(xediffw(j)).lt.
    $  abs(xediffw(j-1))) then
         goto 23
         end if
         if (ecalcw(j).eq.ecalcw(j-1).and.abs(xediffw(j)).gt.
    $  abs(xediffw(j-1))) then
         goto 20
         end if
         if (ecalcw(j).eq.ecalcw(j-2).and.abs(xediffw(j)).lt.
    $  abs(xediffw(j-1))) then
         goto 23
         end if
         if (ecalcw(j).eq.ecalcw(j-2).and.abs(xediffw(j)).gt.
```

```
     $  abs(xediffw(j-1))) then
           goto 20
           end if
           if (eobs(j).eq.eobs(j-2).and.abs(xediffw(j)).gt.
     $ abs(xediffw(j-1))) then
           goto 20
           end if
           if (eobs(j).ne.eobs(j-1)) then
              write(25,22) j21(j),s21(j),n21(j),eobs(j),ecalcw(j),
     $ jz1(j),jz2(j),jz3(j),iz1(j),iz2(j),iz3(j),xediffw(j)
           jcount3= jcount3 +1
           goto 20
           end if
 23        continue
           write(25,22) j21(j),s21(j),n21(j),eobs(j),ecalcw(j),
     $ jz1(j),jz2(j),jz3(j),iz1(j),iz2(j),iz3(j),xediffw(j)
           jcount3 = jcount3 +1
 20         continue
          end do

          open(unit=25,status='new',form='formatted')
          open(unit=99,status='new',form='formatted')
          open(unit=109,status='new',form='formatted')

          write(6,*) 'jcount3 ', jcount3
          allocate(eobshar(jcount2),ezobs(jcount2))

          rewind 34
 10       do i=1,ndat
             read(34,*) j1(i),s1(i),n1(i),ecalcw(i),ecalc(i)
     write(6,*) j1(i),s1(i),n1(i),ecalcw(i),ecalc(i)
             open(unit=88,status='new',form='formatted')
     do m=1,npf
                read(34,*) der(i,m)
                write(6,*) 'der(i,ifit(m))',der(i,m)
                dcon(i,m) = der(i,m)
                write(88,*) dcon(i,m)
                write(99,220) dcon(i,m)
 220            format(f20.12)
                write(6,*) 'dcon(i,m) ',dcon(i,m)
     end do
   rewind 25
   do j=1,jcount3
      read(25,22) j21(j),s21(j),n21(j),ezobs(j),ecalcw(j),
     $  jz1(j),jz2(j),jz3(j),iz1(j),iz2(j),iz3(j),xediffw(j)
      eobshar(j) = ezobs(j) / 219474.63
      if(j21(j).eq.j1(i).and.n1(i).eq.n21(j) .and. s21(j)
     $ .eq. s1(i))then
                ediff(j)= eobshar(j) - ecalc(i)
c               write(6,*) 'ediff ',ediff(j)
                ediffw(j) = ezobs(j) - ecalcw(i)
                jcount = jcount +1
                sdsq=sdsq+ediff(j)**2
                sdsqw = sdsq*219474.63
                write(6,1200) j21(j),jz1(j),jz2(j),jz3(j),
     $ iz1(j),iz2(j),iz3(j),s21(j),n21(j),ezobs(j),ecalcw(i),
     $ ediffw(j)
                ecalc(j) = ecalc(i)
                rewind 88
                do m=1,npf
                   read(88,*) dcon(j,m)
c                  write(6,*) 'dcon(j,m) ',dcon(j,m)
```

```
                  write(109,220) dcon(j,m)
               end do
               close(unit=88,status='delete')
            end if
         end do
      end do

190   continue

p=0

   if (npf.eq.ndato.or.npf.gt.ndato) then
      write(6,*) 'UNDERDETERMINED: STOP'
      stop
   end if

  sd=dsqrt(sdsq/(jcount3))
       sdw = sd* 219474.63
       write(6,160) sd
       write(6,161) sdw

       call lsqfit(dcon,npf,npara,jcount3,ediff,se,np,cv)

       do i=1,npf
          cv(np(i))=cv(np(i))+ediff(i)
          write(6,*) 'cv(np(i) ',cv(np(i))
          write(45,*) cv(np(i))
          er(i)=se(i)
          write(6,*) 'er(i) ',er(i)
       end do


       rewind 45
       do k=1,npara
          if (jfit(k) .ne. 0) then
               read(45,*) cvp(k)
            else
               cvp(np(k))=0.00d0
          end if
       end do

      write(6,104) (jfit(j),cvol(j),cvp(j),j=1,npara)
      write(6,106) (jfit(j),cvp(j),j=1,npara)
      write(iout,106) (jfit(j),cvp(j),j=1,npara)
c     if (abs(cvol(j)-cv(j)) .lt. 1d-06) stop

 11   format(e20.5)
 16   format(e20.8)
 100  format(f20.5,2i5)
 101  format(20X,f15.9)
 102  format(i5)
 103  format(f20.9,i5)
 104  format(i5,3x,f25.15,3x,f25.15)
 105  format(i5,3f10.5,3e15.8)
 106  format(i5,3x,f25.15)
 110  format(I3,A2,2x,I3,8x,f11.5)
 306  format(I3,A2,I4,3X,f10.3,3x,f10.7,6(2X,E13.6)/
     $    (17x,5(2x,e13.6)))
 308  format(I2,1x,A2,I4,3X,f10.3,3x,f10.7,6(2X,E13.6)/
     $    (17x,5(2x,e13.6)))
 1100 format(I2,1x,A2,I4,3X,f12.9,3x,f12.9,3x,f12.9,
     $   6(2X,E13.6)/(17x,5(2x,e13.6)))
```

```
1200   format(I2,1x,3I1,2x,"(",3I1,")",3x,A2,I4,3X,f15.6,3x,
    $   f15.6,3x,f15.6)

109    format(/5x,'j1        s1        n1        eobs
    $  ecalc            ediff      props',/)

160    format(/,1x,'standard deviation = ',e15.9,/)
161    format(/,1x,'standard deviation = ',e15.9,/)
       deallocate(eobs,ecalc)
       deallocate(jfit,i1)
       deallocate(dcon,der)
       deallocate(j1,j21,n1)
       deallocate(n21,s1,s21)
       deallocate(eobshar)
       deallocate(cvol,er)

       stop
       end
```

B.2 Program LSQFIT

```
      subroutine lsqfit(dcon,nvar,npara,lines,v,se,jfit,cv)
      implicit double precision(a-h,o-z)
      dimension sr(nvar+1),dcon(lines,nvar+1)
      dimension co(nvar+1,nvar+1)
      dimension a(nvar+3,nvar+3),b(nvar+2,nvar+2)
      dimension r(nvar+2,nvar+3),x(nvar+3),dnf(nvar+3)
      dimension v(lines),se(nvar),jfit(npara),cv(npara)
      logical lg, lg1

      iout=6
      x=0.
      a=0.
      r=0.
      b=0.
      co=0.

      write(6,*) 'lines', lines
      write(6,*) 'mvar ', nvar

      open(unit=109,form='formatted')

      rewind 109
      do i=1,lines
         do j=1,nvar
            dcon(i,j) = 0.0d0
            read(109,*) pony
            dcon(i,j) = pony
            write(6,*) 'dcon(i,j) ',dcon(i,j)
         end do
      end do


     lg=nvar.eq.lines
     lg1= nvar.eq.1
     write(iout,1000)
     n1 = nvar+1
     do k=1,lines
        dcon(k,n1)=v(k)
     end do

     do m=1,n1
```

```
            z1 = 0.0d0
            do k=1,lines
               z1=dcon(k,m)*dcon(k,m)+z1
            end do
                write(iout,*) z1
                dnf(m)=1.0/dsqrt(z1)
                write(iout,*) 'dnf(m) ',dnf(m)

                do k=1,lines
                   dcon(k,m) = dcon(k,m)*dnf(m)
                   write(itou,*) 'dcon(k,m) ',dcon(k,m)
                end do
         end do

         z0 =1.0/dnf(n1)
         write(iout,*) 'z0 ',z0
         if (lg1) goto 5
         write(iout,1001)

 5       do i=1,nvar
            a(i,i)=1.0
            n2 = i+1
            do k=n2,n1
               z2 = 0
               do l=1,lines
                  z2=dcon(l,i)*dcon(l,k)+z2
               end do
               a(i,k)=z2
               a(k,i)=z2
            end do
         end do

         if (lg1) goto 38
         write(iout,3002)
         write(iout,3000)((a(ii,jj),ii=1,4),jj=1,4)

         fnorm=0.
         do i=2,nvar
            n2 = i-1
            do k=i,nvar
               z2 = a(n2,k)
               snz2=z2
               fnorm=snz2*snz2+fnorm
            end do
         end do

         fnorm=2.*fnorm+float(nvar)

c     cholesky procedure, triangular matrix

         det=1.0

         do m=1,nvar
            n2=m-1
            do j=m,n1
               z2=0.
               if (m.eq.1) goto 12
               do k=1,n2
                  z2=r(k,m)*r(k,j)*z2
               end do
 12            z2=a(m,j)-z2
               if (j.ne.m) goto 14
```

```
                det=det*z2
                if ((z2-1d-31).gt.0.) goto 13
                write(iout,1002)z2
                if (z2.le.0.) stop
 13             r(m,m)=dsqrt(z2)
                goto 15
 14             r(m,j)=z2/r(m,m)
 15             continue
              end do
            end do
            z2=det/fnorm
            write(iout,1003)det
            write(iout,1004)fnorm
            write(iout,1005)z2
            write(iout,3003)
            z2=0.
            z3=0.
            m=nvar
 17         x(m)=(r(m,n1)-z2)/r(m,m)
            v(m)=x(m)*dnf(m)*z0
            z3=x(m)*a(m,n1)+z3
            if(m.eq.1)goto 19
            z2=0.
            do j=m,nvar
               z2=r(m,j)*x(j)+z2
            end do
            m=m-1
            goto 17

 19         write(iout,1006)
            srq=0.
            do i=1,nvar
               z2=0.
               do k=1,nvar
                  z2=a(i,k)*x(k)+z2
               end do
               z2=z2-a(i,n1)
               write(iout,1010)z2
               snz2=1.e08*z2
               srq=snz2*snz2+srq
            end do

            eps=dsqrt(srq)*(fnorm/float(nvar-1))**
     1       (float(nvar-1)/2.)/det
            eps=1.e-08*eps
            write(iout,1007)eps

            if(lg) goto 23
 22         z3=(1d0-z3)*z1/float(lines-nvar)
            write(iout,1008)z3
            if (z3.lt.0.)z3=0.
            sigma=dsqrt(z3)
            write(iout,1009)
            if(lg1) goto 39
c  cholesky procedure, inverse matrx
 23         k=n1
 24         i=k
            k=k-1
            b(k,k)=0.
            write(48,4001)k,k,b(k,k)
 25         n2=i
            i=i-1
```

```
         z2=0.
         if(i.eq.nvar) goto 27
         do n=n2,nvar
            z2=r(i,n)*b(n,k)+z2
         end do
         do n=n2,nvar
            z3=r(i,n)*b(n,k)+z2
         end do
         b(i,k)=-z2/r(i,i)
 27      continue
         if(i.eq.k) then
            write(48,2001)i,r(i,i)
            write(48,4001)i,k,b(i,k)
         end if
            write(48,4001)i,k,b(i,k)
            b(k,i)=b(i,k)
            write(48,4001)k,i,b(k,i)

         if(i.gt.1) goto 25
         if(k.gt.1) goto 24

c     check of inversion and square roots of diagonal elements

            zdiag=0.
            zoff=0.

            do i=1,nvar
               z2=b(i,i)
               write(48,4001)i,i,z2
               if(z2.lt.0.0) then
                  write(iout,3100)
                  z2=dabs(z2)
               end if
               sr(i)=dsqrt(z2)
               z2=dnf(i)
               if (lg) goto 28
               se(i)=z2*sr(i)*sigma
               if(sr(i).eq.0.)then
                  write(iout,3200)i
                  sr(i)=1.
               end if
 28            sr(i)=1./sr(i)
               do k=i,nvar
                  zcheck=0
                  do l=1,nvar
                     zcheck=zcheck+a(i,l)*b(l,k)
                  end do
                  if (i.eq.k) goto 30
                  zabs=dabs(zcheck)
                  if(zoff.gt.zabs) goto 31
                  zoff=zabs
                  goto 31
 30               continue
                  zabs=dabs(zcheck-1d0)
                  if (zdiag.gt.zabs) goto 31
 31               continue
                end do
            end do

            if(lg) goto 37
            write(iout,1010)(v(m),se(m),m=1,nvar)
 33         write(iout,1011)
```

```
         write(iout,1012)zdiag
         write(iout,1013)zoff
         write(iout,1014)
         do i=1,nvar
            do k=1,i
               z2=b(i,k)
               co(i,k)=z2*sr(i)*sr(k)
            end do
            write(iout,1015)(co(i,k),k=1,i)
         end do

         do i=1,nvar
            do k=1,i
               test=abs(co(i,k))
               if(test.gt.0.950.and.test.lt.0.9999)then
                  write(iout,1030)jfit(i),jfit(k),co(i,k)
               end if
            end do
         end do
 36      return
c
c
c special cases - nvar=line=1 not permitted

 37      write(iout,1016)
         write(iout,1017)(v(m),m=1,nvar)
         goto 33

 38      v(1)=a(1,2)*dnf(1)*z0
         z3=a(1,2)*a(1,2)
         goto 22

 39      z2=dnf(1)
         se(1)=z2*sigma
         write(iout,1010)v(1),se(1)
         goto 36

 1000    format(40H,Normalisation of equations of condition)
 1001    format(/,36H Characteristics of normal equations)
 1002    format(21H Near singular matrix, d12.1,/)
 1003    format(10x,12H Determinant,D14.4)
 1004    format(10x,12H Norm       ,E14.4)
 1005    format(10x,12H Det/Norm   ,D14.4)
 1006    format(/,18H Sum Defect Vector)
 1007    format(16H Redheffer error,E12.4,/)
 1008    format(9H Variance        ,D12.4,/)
 1009    format(30H Solution with standard errors)
 1010    format(10X,D15.7,E14.3)
 1011    format(/,24H Check of inverse matrix)
 1012    format(10x, 25H largest deviation from 1,E10.2,/)
 1013    format(10x, 25H largest deviation from 0,E10.2,/)
 1014    format(10x, 25H Correlation coefficients,/)
 1015    format(3x,16f7.3)
 1016    format(9H Solution)
 1017    format(10x,D15.7)
 1030    format(1x, '***Correlation between ',i3,'and ',i3,
     1   ' = ',f7.3,'***')
 2000    format(1x,'z2 =',e11.4,/)
 2001    format(1x,i2,2x,'r=',e11.4,/)
 3002    format('a matrix')
 3000    format(4(e12.4,1x))
 3003    format('r matrix')                                              610
```

```
3004    format('x vector')                                                  620
3005    format('b matrix')                                                  630
3100    format('**** z2 lower than zero ****')                              840
3200    format('**** sr(',i2,') = 0.0  then set to 1.')                     930
4001    format('b(',i3,',',i3,')=',e11.4)

        end
```